CHARACTERIZATION OF WIRE-BASED Z-PINCHES FOR EFFICIENT ENERGY COUPLING

By

JIGYASA BATRA

PHYS01201304001

Bhabha Atomic Research Centre, Mumbai

A thesis submitted to the

Board of Studies in Physical Sciences

In partial fulfillment of requirements

for the Degree of

DOCTOR OF PHILOSOPHY

of

HOMI BHABHA NATIONAL INSTITUTE

November, 2020

Homi Bhabha National Institute

Recommendation of the Viva Voce Committee

As members of the viva voce committee, we certify that we have read the dissertation prepared by Smt. Jigyasa Batra entitled **"Characterization of wire-based Z-pinches for efficient energy coupling"** and recommend that it may be accepted as fulfilled the thesis requirement for the award of Degree of Doctor of Philosophy.

Sr No	Composition	Name	Signature with date
1.	**Chairman**	Prof. S. Krishnagopal	K. S[illegible] 14/9/21
2.	**Convener** (Guide)	Prof. K. D. Joshi	Kanhaiya Datt 14.9.2021
3.	**External Examiner**	Prof. S. R. Mohanty	Smruti Ranjan Mohanty 14/09/21
4.	**Member**	Prof. J. A. Chakera	[illegible] 14/9/21
5.	**Member**	Prof. S. Ghorui	Srikumar Ghorui 14/09/21
6.	**Member**	Prof. A. Roy	Amitava R[illegible] 14/09/21

Final approval and acceptance of this thesis is contingent upon the candidate's submission of final copies of the thesis to HBNI.

I hereby certify that I have read this thesis prepared under my direction and recommend that it may be accepted as fulfilling the thesis requirement.

Date 14.9.2021
Place: Mumbai

Kanhaiya Datt

Dr. K.D. Joshi
(Guide)

STATEMENT BY AUTHOR

This dissertation has been submitted in partial fulfillment of requirements for an advanced degree at Homi Bhabha National Institute (HBNI) and is deposited in the Library to be made available to borrowers under rules of the HBNI.

Brief quotations from this dissertation are allowable without special permission, provided that accurate acknowledgement of source is made. Requests for permission for extended quotation from or reproduction of this manuscript in whole or in part may be granted by the Competent Authority of HBNI when in his or her judgment the proposed use of the material is in the interests of scholarship. In all other instances, however, permission must be obtained from the author.

Jigyasa
Jigyasa Batra
14/09/2021

DECLARATION

I, hereby declare that the investigation presented in the thesis has been carried out by me. The work is original and has not been submitted earlier as a whole or in part for a degree / diploma at this or any other Institution / University.

Jigyasa

Jigyasa Batra

14/09/2021

List of Publications arising from the thesis

Journal

1. "Low and high energy deuterium ions emission in a 4.7 kJ plasma focus device and its variation with gas filling pressure", Jigyasa Batra, Ashutosh Jaiswar, Rohit Srivastava, Ram Niranjan, R.K. Rout and T.C Kaushik, *Indian J. Pure Ap. Phy.*, **2014,** *52*, 246-250.
2. "Experimental Investigations on Specific Energy Deposition and Burst Characteristics in Electrically Exploded Single Copper Wires", Jigyasa Batra, Ashutosh C. Jaiswar, Rajashri R. Valvi, and T. C. Kaushik, *IEEE Trans. Plasma Sci.*, **2019,** *47, 1*, 596–602.
3. "Experimental and Numerical Analysis of Post Burst Dynamics in Electrically Exploding Single Copper Wire", Jigyasa Batra, Alok K. Saxena, Ashutosh C. Jaiswar, Rajashri R. Valvi, and T. C. Kaushik, *IEEE Trans. Plasma Sci.*, **2020**, *48, 6,* 2187-2194.
4. "Experimental study to investigate effect of thermophysical properties of various metals on electrical explosion of wire in air and vacuum", Jigyasa Batra, Alok K. Saxena, Ashutosh C. Jaiswar, Rajashri R. Valvi, K.D. Joshi and T.C. Kaushik; *IEEE Trans. Plasma Sci.*, **2021**, *49*, *9*, 2866-2877. doi: 10.1109/TPS.2021.3099899.

Conferences

1. "Laser Interferometery for Temporal Electron Density Measurement of Electrically Exploding Wire Plasmas" Jigyasa Batra, Ashutosh Jaiswar, Alok Saxena, T.C. Kaushik and S.C. Gupta; *28th PSSI National Symposium on Plasma Science & Technology*, Bhubaneswar, India, December 3-6, **2013**, 230-231.

2. “Experimental analysis of energy deposition in single exploding wire of various diameters and capacitor bank energies”, Jigyasa Batra, Ashutosh Jaiswar, Rajshree R. Valvi and T.C. Kaushik, *30th National Symposium on Plasma Science & Technology*, Kolkata, India, December 1-4, **2015**,181.
3. “Experimental Study of Single Exploding Wire Behavior in Air and Vacuum”, Jigyasa Batra, Ashutosh C. Jaiswar and T.C. Kaushik, *10th International Conference on Inertial Fusion Sciences and Applications,* Saint Malo, France, September 11-15, **2017**, 297.
4. “Experimental Study on Critical Length of Electrically Exploding Wire”, Jigyasa Batra, Ashutosh C. Jaiswar and T.C. Kaushik, *32rd National Symposium on Plasma Science & Technology,* Gandhinagar, India, November 7-10, **2017**, 284.
5. “Development of X-Pinch System with Slow Rising (0.1kA/ns) Current Source”, S. C. Andola, Jigyasa Batra, A.C. Jaiswar and T. C. Kaushik, *33rd National Symposium on Plasma Science & Technology,* New Delhi, India, December 4-7, **2018**, 82.

Report

1. “Interferometer for Electron Density Measurement in Exploding Wire plasmas”, Jigyasa Batra, Ashutosh Jaiswar and T.C Kaushik, BARC/2016/E/018, BARC Report, **2016**, 1-31.

Dedicated
To
My Family

ACKNOWLEDGEMENTS

I express my deep sense of gratitude to my guide Prof. K. D. Joshi for his invaluable guidance, constant encouragement and moral support for completing the research work and writing of this thesis. I would like to express my sincere gratitude to Prof. T.C. Kaushik for the continuous support of my Ph.D study and research, for his patience, motivation, enthusiasm, and immense knowledge. I owe him a lot for imparting the knowledge of pulsed power as well as providing me an opportunity to work on Electrically Exploding Wires. Special thanks to the current members of my doctoral committee Dr. S. Krishnagopal, Dr. Amitava Roy, Dr. J. A. Chakera, Dr. Srikumar Ghorui and to the former members Dr. A. Sinha, Dr. N. K. Gupta, Dr. K. C. Mittal, Dr. P. A. Naik, and Dr. S. C. Gupta for their critical comments and suggestions at various stages of this work. With profoundest gratitude and greatest humility, I would like to extend my gratefulness and deepest appreciation to Dr. Alok K. Saxena for his incredible contribution in shaping my research work of thesis. His unflinching support, encouragement, advice, constructive criticism, his truly scientific intuition, dynamism and wisdom has exceptionally inspired me and enriched my growth as a researcher. My special thanks to Mr. A. C. Jaiswar, Mr. A. M. Rawool, and Mrs. Rajashree R. Valvi who provided necessary technical help for carrying out the experimental work. I am also thankful to my colleague Mr. Sanjay C. Andola for his contribution and valuable discussions in X-pinches.

I owe my gratitude to my husband, Mr. Ravish Batra for his continuous support. I am fully indebted to my family especially to my parents in laws, Mrs. Sudha Batra and Mr. Jagdish Batra, for bountiful support in my endeavor and extending encouragement throughout the work and also in my difficult times. I am forever grateful to my mother, Mrs. Krishna Devi, whose foresight and values paved the way for needed substantive support.

CONTENTS

		Page No.
SUMMARY		**v**
LIST OF FIGURES		**vii**
LIST OF TABLES		**Xii**
CHAPTER 1	**INTRODUCTION**	**1**
	1.1 Z-pinches………………………………………………………………..	**1**
	1.2 Electrically Exploding Wire…………………………………………	**4**
	1.3 General Electrical Characteristics……………………………………	**5**
	1.4 Historical Overview and Present Status……………………………	**8**
	1.5 Motivation……………………………………………………………	**17**
	1.6 Plan of Thesis………………………………………………………...	**22**
CHAPTER 2	**DIAGNOSTICS FOR ELECTRICALLY EXPLODING WIRES**	**25**
	2.1 Electrical Diagnostics…………………………………………………	**25**
	2.1.1 Voltage Measurement…………………………………………	**25**
	2.1.1.1 Spark Gaps…………………………………………..	**26**
	2.1.1.2 Electro-optic Methods……………………………….	**26**
	2.1.1.3 Voltage Dividers…………………………………….	**27**
	2.1.1.3.1 Description of Resistive Voltage Divider Employed………………………………..	**29**
	2.1.2 Current Measurements……………………………………......	**29**
	2.1.2.1 Current Viewing Resistor (CVR)……………….…...	**29**
	2.1.2.2 Fast Current Transformer…………………….……...	**30**

2.1.2.3 Faraday Effect………………………………………. **30**

2.1.2.4 Rogowski Coil and Magnetic Pick up Coil………… **30**

2.1.2.4.1 Description of Rogowski coil Employed……………………………….. **31**

2.1.3 Estimation of Energy Deposition…………………………….. **35**

2.2 X-rays Diagnostics……………………………………………………. **37**

2.3 Laser Interferometer for Electron Density Estimation……………….. **40**

2.3.1 Experimental Results using Streak Mode of Camera………. **44**

2.3.2 Spatial and Temporal Profile of Electron Density in EEW using Frame Mode of Camera……………………………….. **46**

2.4 Faraday Cup…………………………………………………....... **50**

CHAPTER 3 DESCRIPTION OF EXPERIMENTAL SET-UP AND NUMERICAL SCHEME **53**

3.1 Experimental Set-up…………………………………………...... **53**

3.1.1 Details of Load……………………………………….…...... **56**

3.1.2 Experimental Chamber……………………………………….. **57**

3.2 1-D Magnetohydrodynamic Numerical Scheme………………….…... **57**

CHAPTER 4 BURST CHARACTERISTICS AND POST BURST DYNAMICS OF COPPER WIRE EXPLOSION IN AIR **61**

4.1 Effect of Coating, Diameter and Rate of rise of current……………… **63**

4.2 Experimental Observation and Analysis of a Post Burst Feature…….. **70**

4.2.1 Experimental Observations and Analysis…………………...... **70**

4.2.2 Numerical Observations and Analysis……………………....... **74**

4.2.2.1 Pre-burst Regime…………………………………… **75**

4.2.2.2 Post-burst Regime………………………………….. **77**

4.3 Results of Electron density Measurement using Laser Interferometer……………………………………………………… **80**

CHAPTER 5 EXPERIMENTAL INVESTIGATIONS ON EFFECT OF MATERIAL PROPERTIES ON EEW CHARACTERISTICS IN AIR AND VACUUM 85

5.1 Effect of Electrical and Thermophysical Properties of Metal……….. **87**

5.1.1 Electrical Explosion in Air…………………………………… **88**

5.1.1.1 Non-refractory Metals………………………………. **89**

5.1.1.2 Refractory Metals and Palladium………………...... **94**

5.1.2 Electrical Explosion in Vacuum……………………………… **96**

5.1.2.1 Non-refractory Metals……………………….. **97**

5.1.2.2 Refractory Metals and Palladium…………….. **101**

5.1.3 Comparative Analysis of Overall Aspects of Effect of

Material in Air and Vacuum……………………………… **102**

5.2 Summary…………………………………………………….. **105**

CHAPTER 6 EFFECT OF EEW CONFIGURATION INCLUDING X-PINCHES ON EMISSION OF X-RAYS **107**

6.1 Wire Configurations……………………………………………. **107**

6.2 X-rays Detection Methodology………………………………… **111**

6.3 Experimental Results and Analysis…………………………….. **111**

6.4 Effect of Insulation Coating on X-rays yield of X-pinches…….. **115**

6.5 Summary and Conclusion………………………………………. **117**

CHAPTER 7 CONCLUSION AND FUTURE SCOPE OF STUDIES **119**

7.1 Conclusion……………………………………………………… **119**

7.2 Future Scope of Studies………………………………………… **124**

REFERENCES **126**

Summary

Studies pertaining to characterization of electrically exploding wires (EEW) behavior are indispensable due to their utilization in diversified applications of wire-based Z-pinches. Single wire is the basic element of all wire-based Z-pinches. Therefore, understanding of mechanisms involved in single exploding wire plasma is imperative. Exploding wire process is a short duration (nanoseconds to microseconds) phenomenon of dynamic nature in space as well as in time and the mechanisms involved are interdependent on various experimental parameters like current rate, surrounding medium, wire material and its dimensions etc.. Thus, a comprehensive phenomenology has not yet been emerged due to its complicated and intercorrelated behavior with experimental parameters varying over a wide range. Present work includes the characterization of single exploding wire plasmas for varying experimental parameters like diameter, insulating coating, and current rate using a pulsed power system of moderate current rates (~25-90 A/ns). Effect of material is also studied with respect to two surrounding mediums (air and vacuum) separately for current rate of ~90 A/ns. Thesis work focuses especially on those aspects which are reported rarely and not considered in detail to explore the wire dynamics in earlier published works. This work also includes the study on effect of various envisaged configurations of wires as load including typical X-pinches on radiation emission in X-rays range using the present compact and easily configurable pulsed power system of moderate current rates. Experimental study has been carried out using various diagnostics like electrical (voltage and current measurements), optical (Laser Interferometer and streak camera) and X-rays PIN diodes. Laser interferometer and Faraday Cup have also been developed for measurements of electron density and ions flux in pulsed plasmas. Results of experiments carried out for copper wires explosion in air also provide evidence that action

integral; which is generally taken as constant for specific metal; also varies with respect to thickness of wire and current rate. 1 D Magnetohydrodynamics numerical simulations have also been carried out to find the possible reason of a distinct post burst feature observed in our experiments under specific conditions. Consequential role of density fronts in explosion process for appearance of a pause of short duration (1-2 ns) after burst is analyzed and discussed in detail. Effect of initial resistivity and enthalpy of atomization on behavior of EEW in air of different metals is reported first time in this thesis. Contribution of speed of sound in diverting energy deposition in different metals while changing surrounding medium from air to vacuum is also reported first time. Though metals from three different groups show distinct behavior and dependency on electrical and thermophysical properties in vacuum but if the behavior of deposited energy with speed of sound is considered then all metals show a similar trend except W. Present range of circuit parameters find relevance in applications like nano particle generation, sharpening of voltage pulse using opening switches, explosive initiators, shock waves studies, pulsed radiation source in extreme U.V and also in high energy density physics. This study is useful for optimization of experimental parameters for efficient coupling of electrical energy in exploding wire plasmas.

List of Figures

1.1	General implementation schemes of Z-pinches using EEW (a) Single Wire, (b) X-Pinches, (c) Cylindrical wire Array and (d) Plasma column shows radial pressure due to Lorentz force because of axial current density and azimuthal magnetic field.	**3**
1.2	Basic schematic of capacitor bank discharge circuit for EEW as load	**6**
1.3	Typical current, rate of change of current and voltage profiles in single exploding wire; these are experimental profiles for 20 mm long copper wire explosion in air whose diameter is 185 μm.	**7**
1.4	Voltage profiles showing appearance of dwell; this voltage profile is experimentally observed for 20 mm long copper wire of with diameter of 58 μm with charging voltage of 11 kV.	**8**
2.1	Basic Schematic of Resistive voltage divider	**28**
2.2	Schematic of a) Rogowski Coil structure, b) Area of a single turn loop with direction of magnetic field, c) Rogowski coil along with integrator	**32**
2.3	Typical Voltage profiles before and after subtracting inductive contribution for wire of 233 μm diameter at charging voltage of 11 kV.	**36**
2.4	Temporal profiles of a) rate of change of current; b) Resistive voltage c) Current and d) Energy deposited for a specific shot of copper exploding wire in air at 11 kV. Wire is of diameter 185 μm with insulation coating on it making overall diameter of 233 μm and length is of 20 mm.	**37**
2.5	(a) Transmission curves for different filters in energy range of 100 eV-10 keV; (b) Spectral sensitivity of Si PIN diode used for present study.	**38**
2.6	(a) Photograph of present system for X-pinch with PIN diode flange from inside chamber, (b) Top view of PIN diode flange with metal enclosure of PIN diode, (c)	

	Side view for Pin diode Flange	**39**
2.7	(a) Schematic of Mach Zehnder Laser Interferometer with two possible positions of detectors where interference can be observed, however only one detector is used; (b) Photograph of interferometer in our lab for EEW system for explosion in air.	**41**
2.8	Schematic of experimental arrangements for discharging capacitor through load and synchronizing this event with streak camera	**43**
2.9	Interferogram of spark gap plasma	**43**
2.10	Interferogram for exploding wire plasmas	**45**
2.11	(a) Three-dimensional view of expanding plasma indicating concentric cylinders of different electron densities, (b) Schematic of fringes in interferogram and corresponding top view of concentric circles of electron density of exploding wire plasma.	**47**
2.12	Schematic of Faraday Cup and biasing circuit	**51**
2.13	Temporal Ions flux measurement with pressure	**52**
3.1	(a) Schematic of Experimental set-up and (b) equivalent electrical circuit	**54**
3.2	Photograph of Experimental Set-up	**55**
3.3	(a) Single Wire and (b) X-pinch Load between anode and cathode within squirrel cage geometry	**55**
3.4	Axi-symmetric 1-D mesh scheme used for exploding wire simulations.	**58**
4.1	(a) Specific energy deposited up to burst versus charging voltage in the case of 100 μm bare wire, 122 μm coated wire, and 136 μm (see text) coated wire, (b) Specific energy deposition up to burst versus diameter of wire at different charging voltages.	**66**
4.2	Difference between 'time of burst' expected theoretically using action integral of copper [33] and experimentally measured values versus diameter at different charging voltages ranging from 11–40 kV.	**68**

4.3 Time of burst versus charging voltage for relatively thin wires (20, 58, and 81 μm). **69**

4.4 Typical profiles of voltage across the wire for specific diameter of 58 µm at variable charging voltages. **71**

4.5 Typical profiles of voltage across the wire for varying wire diameters at charging voltage of 40 kV. **72**

4.6 Experimental and simulated profiles of voltage and current for wire of diameter 58µm exploded at a charging voltage of 35 kV. Five-time steps t_1 to t_5 are marked for detailed analysis **75**

4.7 Pre-burst behavior: Radial profiles mass density, resistivity, current density and Lorentz force acting on different meshes at three different time instances i.e. near to start of vaporization (t_1 = 46 ns), before voltage peak (t_2= 60 ns), and at voltage peak (63.4 ns). **76**

4.8 Post-burst behavior: Radial profiles mass density, electrical resistivity of different meshes at three different time instances i.e. at voltage peak (63.4 ns), just after the peak (t_4 =66.5 ns) and at pause (t_5= 70 ns). **77**

4.9 Radial profiles of mass density for wires of diameters 20 µm, 58 µm, 81 µm and 233 µm at 40 kV in upper graph. An expanded view of corresponding resistivity profiles is shown in lower graph. **79**

4.10 Specific power vs. specific energy. **79**

4.11 (a) Interferogram captured for exposure time of 14 ns till time of kink and (b) Inferred Electron density profile. **81**

4.12 (a) Interferogram captured for exposure time of 14 ns till time of kink, (b) Electron density profile inferred corresponding to interferogram in (a). **81**

4.13 (a) Interferogram captured for exposure time of 14 ns just after time of kink, (b) Electron density profile inferred corresponding to interferogram in (a). **82**

4.14	(a) Interferogram captured for exposure time of 14 ns just after kink, (b) Electron density profile inferred corresponding to interferogram in (a).	**82**
5.1	(a) Typical voltage profiles of all six metals in air, (b) Expanded Illustration of Current and Voltage profiles with indication of time instants of melting & burst for copper wire.	**90**
5.2	Dependence of overheating on initial resistivity of non-refractory metals considered	**91**
5.3	Radial expansion of light emitted and Streak photographs of optical emission from EEW in air a) Copper, b) Gold, c) Aluminium, d) Tungsten, e) Palladium and (f) Titanium with sweep speed of 100 ns/cm.	**93**
5.4	Comparison of experimentally observed overheating factor with (a) initial resistivity and (b) Enthalpy of atomisation in Pd, Ti and W for EEW in air.	**94**
5.5	Voltage profiles of a) Pd, refractory metals: b) Ti& c) W and non-refractory metals: d) Al e) Cu f) Au in vacuum.	**97**
5.6	Comparison of experimentally observed overheating factor with a) Initial Resistivity and b) enthalpy of atomisation for all metal wires electrically exploded in vacuum	**99**
5.7	Radial expansion of light emitted and Streak photographs of optical emission from EEW in vacuum a) Gold, b) Aluminium, c) Copper, d) Tungsten, e) Palladium and (f) Titanium with sweep speed of 100 ns/cm; minimum spectral sensitivity of photocathode in camera used is 20 mA/W. Sensitivity of camera is kept same for all metal wires using same neutral density filter of optical density 0.5 in front of focussing lens.	**100**
5.8	Comparison of experimentally observed overheating factor with speed of sound in all metals in both mediums	**105**
6.1	Schematic of various wire configurations	**109**
6.2	PIN diode signals along with dI/dt signals for different configurations mentioned in	

each graph. **112**

6.3 dI/dt and PIN diode signals with different filters as mentioned in inset for X-pinches of two W wires **115**

6.4 Rate of change of current and two PIN diode signals observed in oscilloscope for X-pinch of two coated wires of W. Pin diode signals are truncated due to saturation of voltage range in oscilloscope. **117**

List of Tables

2.1	Energy Range of X-rays for Transmission using foil filters	**37**
4.1	Effect of diameter and charging voltages on experimental characteristics (Time of burst, Specific Energy deposited and its rate along with observance of kink).	**71**
4.2	Range of electron densities measured over the length of wire near wire axis at fixed radii (2 μm and 5 μm) before and after instant of kink.	**81**
5.1	Material properties of wires under investigation	**86**
5.2	Observed experimental parameters for electrical explosion of wires in air.	**87**
5.3	Observed experimental parameters for electrical explosion of various metal wires in Vacuum	**96**
6.1	Details of experimental circuit parameters and PIN diode signals	**111**
6.2	X-rays yield estimated using different types of X-pinches.	**114**

Chapter 1

Introduction

Electrical explosion of wires has long been the topic of research interest for its application in different configurations to achieve plasma confinement by Z-pinches. Therefore, this chapter begins with a general introduction of Z-pinches. Then, introduction of Electrically Exploding Wires (EEW) is given along with discussion on significance of EEW in diversified applications. General electrical characteristics of EEW are also described. A short historical overview on the experimental and theoretical works performed by the researchers across the world on exploration of possible mechanisms is described later. Complexity in EEW mechanism due to interrelated circuit parameters is discussed afterwards. Then, present status is elucidated. Finally, the chapter concludes by discussing the motivation behind the present research work followed by discussion on scope for thesis work.

1.1 Z-pinches

Z-pinches also known as Zeta pinches is a distinctive configuration to achieve confinement of plasma by magnetic forces, and is a topic of interest for plasma as well as pulse power research community. It is a plasma confinement system in which current is driven through a plasma column in axial direction thus generating azimuthal magnetic field around this column which tends to confine plasma in radial direction by Lorentz force. Z-pinches can be achieved using various implementation schemes which includes fibre pinch, gas puff Z-pinch, vacuum spark, capillary discharge and plasma focus devices etc. [1]. Fiber Pinches became more popular in 1980's motivated for achieving thermonuclear fusion conditions in deuterated polyethylene fibers with diameters in range of 20-200 micron and lengths in range of 1-5 cm. Fiber based pinches; being of dielectric in nature; differ from other pinches based on metal wires and gas puffs and were found to be more stable to MHD perturbations with currents of 250 kA to 640 kA and rise time of 100 ns [1] lead to neutrons yield of around 10^{10} neutrons. In gas puff Z-pinches, a supersonic gas jet is made to flow using an injection nozzle in cathode directed towards anode. This gas column is ionized by voltage applied between anode and cathode or it can be preionized. Linear mass density of gas can be adjusted by controlling gas flow rate for efficient implosion by compression depending upon the atomic number of gas used. Afterwards, annular gas puffs became more popular for enhancing the implosion velocity and increase the X-rays yield but development of wire array has set aside this technology for being relatively more efficient for conversion of electrical energy to implosion kinetic energy and finally to X-rays radiation. Vacuum spark is also based on compression of plasma column by its own magnetic field. These are generated in a vacuum capillary with the high voltage pulses and were found to be useful for formation of hot spots at different points along its length. These have been used as pulsed X-rays source for flash radiography.

In plasma Focus device, special arrangements of electrodes are made in a vacuum chamber for making conditions favorable for generating the current sheath along the surface of an insulator which is overlaid over anode electrode. This current sheath is moved along the insulator surface due to the force produced by electric and magnetic field, and finally results to the stagnation of plasma column when plasma sheath reaches at the top of anode. Radial compression of plasma column occurs at the axis resulting in pinching due to Lorentz force. After disruption of pinch, ions or electrons are accelerated in axial direction. Plasma focus device is generally used as good pulsed source of ions and soft X-rays. If deuterium gas is used then plasma focus device can be used as source of pulsed neutrons also. Single wire explosion is also an attractive option for Z-pinches for being simple and of low fabrication cost. Other examples of wire-based Z-pinches include cylindrical wire arrays and X-pinches.

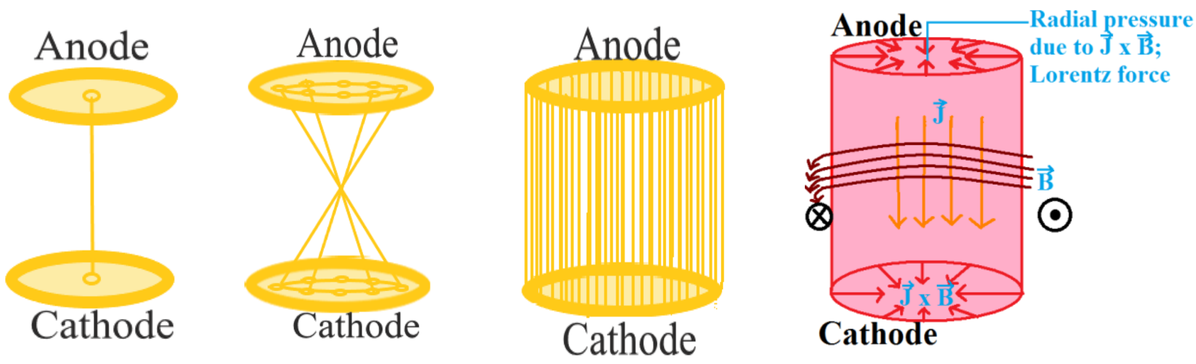

Fig.1.1: General implementation schemes of Z-pinches using EEW (a) Single Wire, (b) X-Pinches, (c) Cylindrical wire Array and (d) radial pressure on plasma column due to Lorentz force because of axial current density (J) and azimuthal magnetic field.

In single wire (Fig.1.1 (a)), only a single wire is mounted between electrodes as the load of a circuit and in cylindrical wire array, wires are mounted in cylindrical periphery as shown in Fig. 1.1 (c).

In X-pinches, these are made up of two or more wires crossing at one point in form of X and its schematic is shown in (Fig.1.1 (b)).

In Z-pinches, two pressures namely thermal and magnetic pressures oppose each other and govern the confinement. Bennett first in 1934 [2] and later in 1955 [3] described the condition required for radial pressure balance in a static Z-pinch by a relation which correlates the experimental parameters. According to this relation, compression can be achieved in a uniform plasma column of radius r, electron density n with electron temperature T_e & ion temperature of T_i if a current greater than I is passed through this column to generate sufficient magnetic pressure for its compression. These parameters are related by following equation:

$$8 \cdot \pi \cdot (n \cdot \pi . r^2) \cdot k_b \cdot (T_i + Z \cdot T_e) = \mu_o \cdot I^2 \quad (1.1)$$

Here k_b is the Boltzmann constant and Z represents the ionization state of atoms.

1.2 Electrically Exploding Wire

Electrically Exploding Wire (EEW) comprises a process in which a high current density (10^6-10^{10} A/cm^2) is created in thin (diameter ~ few 10-100 microns) wires which melt, vaporize and finally result in plasma over a time duration varying from nanoseconds to microseconds in an explosive and complex manner.

EEWs has been the subject of interest since its inception because of their intriguing properties of being pulsed source of radiation with wide spectrum of wavelengths from infrared to hard X-rays (depending upon circuit parameters) and capability of generating matter at extreme conditions of temperature (eVs to keVs) and pressures (≥ Mbars). As a pulsed radiation source for desirable wavelength spectrum with pre-decided circuit parameters, EEWs has proven useful for atomic florescence spectroscopy [4], optical pumping of lasers [5], lithography [6]-[7], nanoscopy [8], X-rays microscopy and X-rays photoelectron spectroscopy etc. [7].

EEWs configurations like X-pinches and wire arrays have also gained significant attention due to their use in diversified applications. X-pinches are capable of producing predetermined point source of size of ~0.5-20 µm of X-rays with energy in the range of 1-10 keV [9] thus relevant for applications like X-ray point projection radiography of plasmas [10], biological samples [11], [12], and also for studying high-speed events like pinch plasmas [13].

Multiple wire array initially suggested by Stallings et al. [14]; for efficient energy coupling from high power low inductance pulsed power generator has been a breakthrough for generation of intense X-rays [15], [16] using EEWs. Subsequent, rapid development of pulsed-power technology led to numerous suggestions [17], [18] at Sandia National Laboratory for the use of cylindrical wire array Z-pinches for inertial confinement fusion (ICF). This idea was also pursued at laboratories like at Physics International [19] and Kurchatov Institute for Atomic

Energy [20]. It has been reported that the efficiency for emission of radiation is strongly affected by development of instabilities and residual mass left in cores of wires [21]. Distribution of electrical energy deposited across each single wire affects residual mass left in core [21], [22]. These facts suggest that the dynamics of single EEW has significant contribution in wire based EEW arrays.

1.3 General Electrical Characteristics

High current densities are normally created in wire by using capacitor or capacitor bank-based pulse power sources capable of generating currents of amplitude reaching from 10 to 100s of kA with rise time ranging from nanoseconds to microseconds. Rise time of current in such systems is decided by inductance of circuit. A single capacitor or a bank of capacitors is charged using a high voltage DC power supply and is discharged through spark gap using a trigger circuit at pre decided charging voltage. Schematic of capacitor discharge circuit for wire in load is shown in Fig. 1.2. In most of these systems, resistance of the circuit is kept small and current follows the underdamped sinusoidal oscillations. Therefore, the peak current (I_{peak}) flowing through the circuit; with inductance L; due to discharge of the capacitor having capacitance; C and charged to voltage $V_{ch.}$ is given by following expression:

$$I_{peak} = V_{ch.} \cdot \sqrt{\frac{k.C}{L}} \tag{1.2}$$

Where k; ($k = e^{-(\frac{RT}{4L})}$); is voltage reversal factor which takes into account of resistance (R) of circuit and is estimated by taking the average of ratios of consecutive alternate peaks (second to first peak, third to second, and so on).

The time period T of the oscillatory discharge of RLC circuit with underdamped condition is decided by total inductance and capacitance of the circuit and can be approximated as:

$$T = \frac{1}{2 \cdot \pi \cdot \sqrt{LC}} \tag{1.3}$$

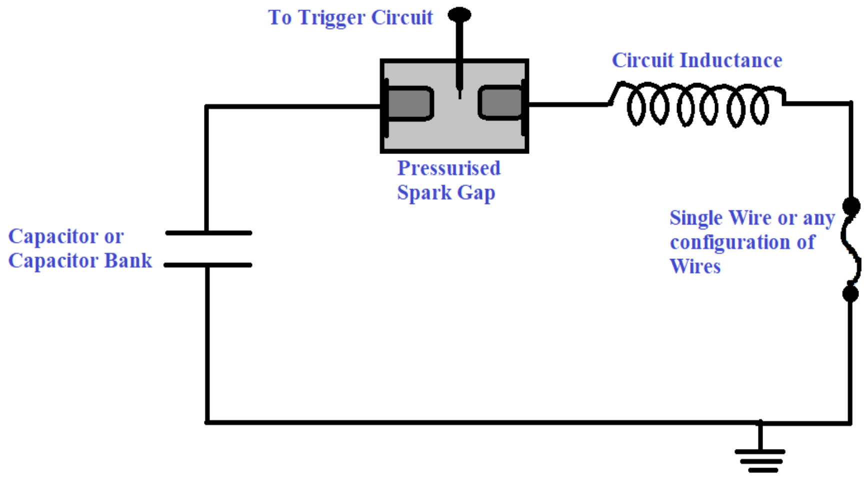

Fig. 1.2: Basic schematic of capacitor bank discharge circuit for EEW as load

General electrical characteristics of EEWs are observed by measuring the temporal profiles of current flowing in the circuit and voltage across the wire. Since, there is significant change in resistance of wire during explosion process, which is reflected in current and rate of change of current thus also in the voltage as shown in Fig. 1.3. Initially, Tucker and Toth [23] and later Lebedev [24], explained that instants of phase transition stages (till melting and melting to burst) can also be marked in the temporal profiles of voltage across exploding wires as shown in Fig. 1.3.

In the beginning of exploding wire process, ohmic heating leads to melting of metal with an increase in resistance and hence in voltage. After melting is finished at t_m (Fig.1.3), rapid increase in resistance (and sharp decrease in current (Fig.1.3)) and hence in voltage appears representing the stage of melting to vaporization. Dynamics of this stage is complicated and has always been the subject of investigations. Formation of parallel conducting channels [25], [26], expansion of explosion products [26]-[28], change in resistance of metal with temperature [29], and also development of instabilities [30], [31] are major factors which influence specific energy deposition. The time instant at which peak in voltage occurs is known as time of burst 't_B' (Fig.1.3). This time of burst is also indicated by sharp dip in rate of change of current (dI/dt) as shown in Fig.1.3. Voltage is maximum at time of burst and specific energy deposition till this time is crucial parameter for utilization in various applications.

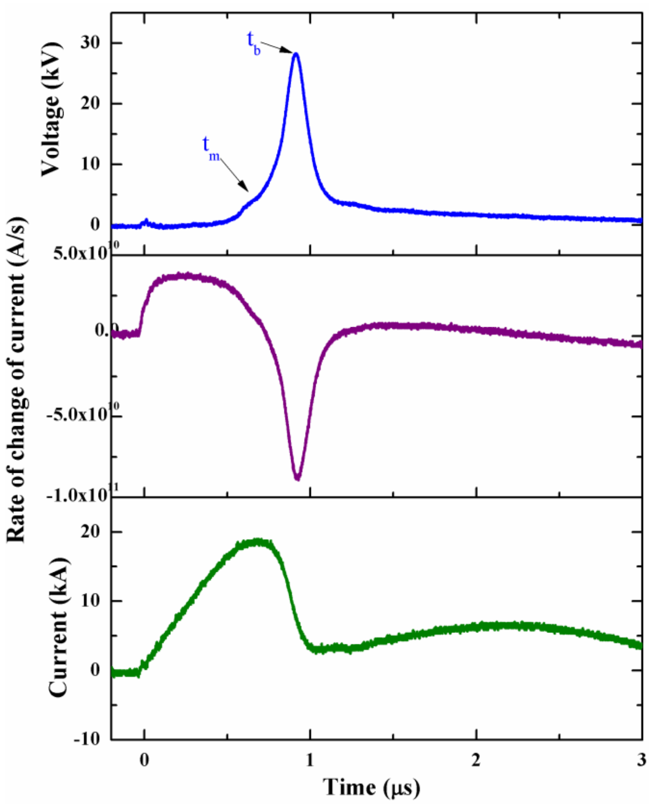

Fig 1.3: Typical current, rate of change of current and voltage profiles in single exploding wire; these are experimental profiles for 20 mm long copper wire explosion in air whose diameter is 185 µm.

After burst, breakdown is initiated which is also termed as restriking [32] or arc discharge [33]. If capacitor energy is completely utilized in explosion then oscillations stops just after the current and voltage becomes zero and this is known as the condition for matched explosion [33]. In some cases of EEWs, oscillations due to restriking or breakdown does not start immediately after the burst but initiates after a time gap (nanoseconds to microseconds); this time gap in which voltage remains stagnant or current is zero is known as dwell time. Appearance of dwell is conditional for the cases when wire explosions are slow. In dwell time period, confined metal vapor expands and reaches to a pressure at which gap between electrodes satisfies the condition for breakdown to initiate. Typical voltage profile for EEW with dwell is shown in Fig. 1.4.

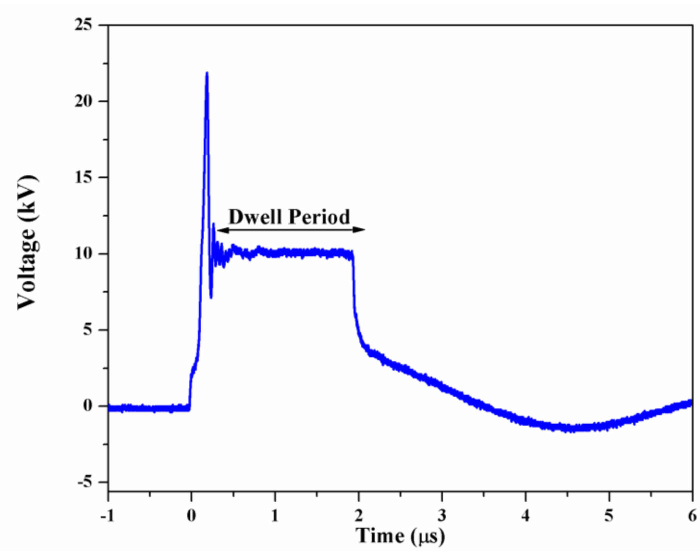

Fig. 1.4: Voltage profiles showing appearance of dwell; this voltage profile is experimentally observed for 20 mm long copper wire of with diameter of 58 µm with charging voltage of 11 kV.

1.4 Historical Overview and Present Status

Many theories have been proposed to unfold exploding mechanisms of single exploding wire since its discovery but still comprehensive phenomenology is yet to emerge. Among these, a few theoretical as well as experimental works are discussed which are of substantial importance in understanding the explosion process in EEW.

After the inventive experiment of Van Marum in 1784 with reference cited therein [34], initial experiments were conducted to use this method of EEWs for various applications like thin film deposition, spectroscopy and as pulsed source of high temperature plasma etc. [34]. After realisation of this fact that these pulsed plasma discharges are efficient way to heat and confine high temperature plasma, it was visualized as a promising way to generate required conditions for thermonuclear fusion. This possibility of being utilized for thermonuclear fusion found its way in first systematic analytic result given by Bennett [2]. This was the beginning of modern Z-pinch era which started with an equilibrium equation, known as Bennett relation [2], [3]. Further improvements were done in 1957 by Pease [35] and Braginskii [36] for taking into account radiation losses in cases where it becomes significant. Both of these authors independently; predicted the limiting current required for Z-pinch in equilibrium considering bremsstrahlung losses to balance joule's heating.

In 1950s, researchers; with references cited there in [20]; suggested that deuterium tritium-based Z-pinches could be utilized for producing fusion power. But soon it was realised that magnetohydrodynamic instabilities (having microsecond time scale) disrupt plasma confinement. Unfortunately, these magneto-hydrodynamic instabilities were unavoidable thereby making it impossible to achieve required typical minimum plasma radius and maximum confinement time for thermonuclear fusion using Z-pinches [20], [36]. Thus, scientific community lost interest in Z-pinches as fusion configurations. However, development in this field still continued in 1960's considering the fact that these could be used as efficient source of UV, XUV, and X-rays pulses [37], [38].

The experiments carried out after middle of twentieth century, were focussed to understand possible mechanisms in the process of EEWs. Primary experimental investigations [38]-[41] were focused on voltage and current measurements, electrical conductivity at large current density (10^6-10^7 A/cm^2), estimation of energy deposited, temperature measurement, shock waves studies, and analysis of spectrum emitted in the process of EEW. Initial theories proposed are well documented in four volumes by Chace et al. [38]-[42]. Chace and Levine [43] in 1960 gave criterion of classification of EEW into slow explosion, fast explosion and explosive ablation based upon energy density and rate of energy density. Kleen; with references cited there in [34]; gave some experimental evidences about occurrence of unduloids using rotating camera and Wrana; with references cited there in [34]; further commented that decreasing conductivity is due to presence of metal vapours. This work along with record of research works till that time is well documented by Mcgrawth [34] in 1966 in a document “Exploding Wire Research”. Chace et al. [44] reported evidence pointing to a condition of extreme super heating of the liquid followed by sudden explosive vaporization; which he termed as “Transplosion”. Super heating, by definition, implies heating of a liquid beyond its boiling point under induced conditions. Transplosion term is further referred to “Phase explosion” in a test of electrically exploding conductors by Martynyuk [45] for explosive boiling in liquid under pulsed heating conditions at a rate exceeding 10^8 K/s. Explosive boiling or phase explosion, by definition, is a stage when superheated metastable liquid undergoes an explosive liquid to vapor phase transition with massive homogeneous nucleation of vapor bubbles into a stable two-phase states. This happens near critical temperature of liquid. If; by any means; rate of temperature rise with time of a liquid is rapid enough that liquid vapor transition phase equilibrium does not follow binodal curve then this transition shifts towards spinodal curve and liquid becomes superheated at that pressure. At near critical temperature, the bubble nucleation process occurs homogeneously everywhere in the substance. The rate of bubble nucleation and vapor sphere growth rate increases exponentially. The increasing nucleation prevents the system from going to the spinodal. When the bubble radius reaches the critical size, it continues to expand and eventually explodes resulting a mixture of gas and droplets which is termed as explosive boiling or phase explosion. At the beginning, explosive boiling phenomenon was used by Martynyuk [45] to calculate the critical temperature of metals.

Investigations proceeded further towards unseen opportunities of exploding wire-based pinches with advancement in instrumentation technology and development in pulsed power engineering. After the development of fast pulsed power generators (Gamble-I and Gamble -II) at the Naval Research Laboratory, intense X rays were observed from exploding single wires of various atomic compositions in 1969 by Shanny & Vitkovitsky as per references cited therein [20] and by Mosher *et al.* [46] in 1973. Stenerhag et al. [47] in 1971 reported their work on effect of wire parameters on X-rays emission. Apart from studies to observe experimental outcomes by varying circuit parameters, the investigations have been also carried out to understand physical mechanisms involved in exploding wire pinch plasma.

Tucker and Toth [23] in 1975 from Sandia National Laboratories published a computer code for predicting behaviour of exploding wires with given circuit parameters. They computed energy required for melting, vaporisation and burst for 23 elements which were found to be in good match with the data available in Handbooks; references cited there in [23]. The burst, was referred to the time at which resistance or voltage in exploding process peaks. This code provided resistivity vs. specific action data for these elements for current density of 10^7 A/cm^2. Specific action; earlier introduced as “Action integral” by “Anderson and Neilson” [48] in 1959; is an empirical constant for a particular metal, and is used to decide the burst time for a given wire diameter and current profile under assumption that wire diameter does not change significantly up to burst. In other way, the diameter of wire which should ideally be chosen to burst at the pre decided burst time; can be calculated *a priori* using action integral (h_b) generally defined as

$$h_b = \int_0^{t_b} j^2 \, dt \tag{1.4}$$

where h_b has units in A^2 s/mm^4, while j is the current density in A/mm^2 and t_b is the time of burst in seconds. It is also referred to as "specific action integral" [49] or "integral of specific current action" [50]. The action integral is a material dependent empirical parameter and generally taken as constant [33], [49]. However, Chemezova *et al.* [50] in 1998 have shown that h_b varies with the rate of energy injection in to the metal [10^{10}–10^{13} J/(g·s)] for current densities in the range of 10^7–10^9 A/cm^2.

Studies related with rapid metal heating and other aspects like change in resistivity of metals with temperature and pressures; have proven to be a boon in understanding physics of EEWs. Lebedev and Savvatimskii [24] in 1984 documented their work about behaviour of metals under pulsed heating at current density of around 10^7 A/cm^2. This work included the effect on specific heat, thermal expansion of metals, and resistivity of liquid state as a function of energy supplied during explosion. They found that the amount of deposited energy could significantly be higher if the volume of expansion of heated liquid is limited than in the case of a free expansion. Tamping and surrounding medium of higher density were possible ways to confine expanding liquid. Lindemuth [51] also gave a computational model in 1985 for optimizing dimensions of Tampers for efficient energy deposition in opening switches. Predictions from this proposed model have shown impact of surrounding medium on free expansion and also upon the characteristics of exploding conductor. They have used resistivity model considering resistivity as function of temperature and density where data for temperature as a function of density and specific energy is taken from SESAME library with reference cited there in [51]. Burgess [32] in 1986; covering wider range of temperatures and densities; has also given an empirical model for electrical resistivity as a function of temperature and volume. This model considered multiphases; solid, liquid, and partially ionized vapor as well as a mixed phase; combination of cold vapor and condensed phase as was expected in the exploding conductors.

A well-recognized theory for phase transition from solid to vapor state through rapid evaporation of metal from the surface of the wire making it progressively thinner, converting into a nonconducting vapor; earlier suggested by Wrana as per reference cited there in [34] and Chace et al. [42]; was affirmed by Bennett [52] in 1965 which reports about occurrence of vaporization wave in all metals at high temperature. This vaporization wave theory is later discussed by Rakhel [53] in 1996. In his work [53], condition required for superheating of liquid is formulated and revisited the theory given by Bennett for vaporization of exploding wires through travel of evaporation wave initiated from surface. One dimensional Magnetohydrodynamic (MHD) model was used in his work for typical regime of exploding wires for current density of around 10^7 A/cm^2 and it was concluded that the process of expansion of the two-phase mixture is very similar to the motion of a wave. Since research on EEW was in comprehensible position till this time for considering different approaches for investigating exploding mechanisms in different time regimes (microsecond and nanosecond EEWs). Fast EEW's; being of more practical significance; were more focussed and studied. Range of these fast EEW's was considered in general for which current densities and heating rate lie in between 10^7 to 10^9 A/cm^2 and 10^{10} to10^{13} J/g-s respectively [54]. EEWs for current densities and heating rate below this range were considered under slow explosions and those above this range have been termed as superfast explosions. Tkachenko et al. [30] in 1999 have used mathematical modelling for fast (microsecond) as well as superfast (nanosecond) regimes to study explosion mechanism as a process of travel of phase transition wave from outer boundary to center of wire. In this model, two new major points were taken into account for necessary improvements in

Bennett model viz. finite thickness of phase transition layer and considering intermediate states of metal to insulator phase transition such as metal-semiconductor-dielectric instead of two states (conducting metal and expanding non-conducting saturated vapor) only. It was concluded from their work that this phase transition wave velocity varies for different time scale regimes of wire explosions and metal–dielectric phase transition takes place without phase transition to a two-phase state in the skin in a nanosecond explosion. Tkachenko et al. [55] in 2004 carried out again theoretical study for exploring this evaporation wave front. Based upon phase equilibrium of vapor supersaturation with liquid core, two cases were considered for electrical explosion viz. spinal mechanism of explosion (SME) and nucleus mechanism of explosion (NME). In case of SME, phase transition from conducting state to vapor state is instantaneous. On the other hand, NME is associated with phase transition wave which travels from surface to axis of wire. However, it was concluded [55] that it is unlikely to be accessible by available experimental techniques. Experimental data obtained for EEW in water were found to be in good agreement with estimated energy deposited within NME limit. In case of EEW in air and vacuum, experimental value of energy deposited is found to be less than that estimated theoretically considering NME. This might be because of the fact that the energy deposition has been terminated by growth of instabilities.

For ensuring the uniform heating in fast exploding wires, Sedoi et al. [54] in 1999 carried out theoretical as well as experimental work to set a criterion for characteristic times required for instabilities (Magnetohydrodynamic instabilities and capillary forces) to develop. Detailed overviews on development of instabilities in Z-pinches along with its other aspects are covered in a review article of Haines [56] in 2011. Theoretical work by Haines and Coppins [57] on instabilities in 1991 brought out importance of some parameters which are omitted while considering ideal MHD instabilities. Later, more careful analysis by Coppins and Culverwell [58] in 1997 concluded that pinch is not stable at early times and thermal instabilities driven by joule heating occur apart from Magnetohydrodynamic instabilities. Oreshkin et al. [31], [59] in 2004 and 2016 have reported about thermal or overheating instabilities which are shown to be responsible for strata formation in EEWs.

A number of experimental studies were also carried out to examine morphology of EEW using imaging techniques. Kalantar et al. [60] in 1993, Guskov et al. [61], and Ivanenkov [62] in 1998 have shown the possibility of cold dense stable core surrounded by plasma corona in exploding wires with the help of optical and X-ray diagnostics. Pikuz et al. [63] in 1999 showed for the first time the details of persistent foam like liquid-vapor structure of the expanded wire core using X-ray backlighting. Experiments also continued for studying dynamics of core. Sinars et al. [64], [65] in 2000 and 2001 reported their work on measurement of expansion rates and study of morphology of core for fast EEWs. Sinars et al. [65] in 2001 performed experiments to measure initial energy deposition in wires with and without insulating coating and reported their observations on expansion rates of dense wire cores for several materials. It was shown in their results that most rapid and uniform expansion occurs for wires in which the initial energy deposited prior to plasma formation is a substantial fraction of energy required to completely vaporize the wire. Conversely, wire materials with less energy deposition relative to the vaporization energy show complex internal structure and the slowest, most non-uniform expansion. Inhomogeneity in energy deposition in exploding wire process depends upon the rate of energy deposition also. If characteristics times required for explosion are more than for the times required for instabilities (mechanical distortions, MHD instabilities, thermal instabilities) to develop, then it results in inhomogeneous energy deposition in exploding wire.

Energy deposited till burst was found to be of significant importance for deciding the use of EEWs in variety of applications. Tkachenko et al. [66] in 2007 have carried out experimental investigations to locate discharge current channels using laser probing for fast electrical explosions in air and vacuum with current rates of 50 A/ns. Two possibilities have been shown for breakdown channels; either through external shunting or through internal breakdowns. Shunting is due to formation of parallel current diversion channels. Later in 2012, Tkachenko et al. [26] have shown using experiments and magnetohydrodynamic simulations, that for Al wire explosion in vacuum the core remains for long time in dense state with temperature higher than critical temperature and liquid to vapor transition occurs only after most of the current is shunted by corona.

Sarkisov et al. [27] in 2007 have used simple thermodynamics calculations instead of the complex MHD simulations to describe fast nanosecond wire explosion taking into account the experimental current wave form and the thermal dependence of metallic resistivity and heat capacity at constant pressure. This work has shown good agreement for voltage profiles of seven different metals up to stage of melting and indicates importance of corona formation in transition stage of melting to burst. Further, fine works by Tkachenko et al. [66] in 2009 and by Romanova et al. [67] in 2015 report about detailed study of distribution of current and discharge channels in the process of explosion of wires of different materials in air as well as in vacuum using schlieren imaging, X-rays and optical shadowgraphy. It was concluded that the different breakdown mechanisms take place depending upon the type of material, whether refractory or non-refractory and surrounding medium. Based upon explosion characteristics, Romanova et al. [67] have classified metals into three categories. Recently, Romanova et al. [68] in 2019 have reported stable tubular structure of explosion products using shadow photography in experiments conducted for copper wire explosion in air at current rate of 50A/ns.

In particular, since it is difficult to estimate current distribution experimentally in different sections of wire while explosion, thus, the prediction of spatial energy deposition is also difficult to determine the internal structures of exploding wire for probing the dynamics involved. Therefore, specific energy deposition till burst is a crucial parameter for various applications; which requires optimization of circuit parameters. In last two decades, many researchers have studied effect of current density [54], current rate [69], [70], polarity [69], [71], surrounding medium [72], material [67] and wire dimensions [73] on behavior of EEWs and energy deposition up to burst. Interdependence amongst these variable experimental parameters and effect of each on explosion mechanism makes it quite complicated to understand the EEW phenomenon in different time scales. Therefore, still there is a wide scope of investigations to understand complex dynamical behavior of EEW to efficiently utilize these in diversified applications as discussed above.

1.5 Motivation

Single exploding wire is basic element of X-pinches, cylindrical wire arrays and any other configuration of wire arrays. It is indispensable to understand the dynamics of single wire explosion which constitute the basic element of every possible configuration of EEWs. As discussed in previous section that experimental parameters are interdependent and decide the explosion mechanisms which makes it crucial to predetermine EEWs behavior for efficient energy coupling.

The work in the thesis focuses on characterizing the behavior of single EEW with respect to variable circuit parameters (dimensions of wire, current rate, surrounding medium and material) especially for those which are reported rarely and not considered in detail to explore the wire dynamics in earlier published works. Since only a few investigations have been reported in literature [74]-[77] on electrical explosion of copper wires in air, initial experiments were conducted to observe the effect of coating on copper wires in air as surrounding medium, then experimental study is carried out to observe the effect of current rate (25-90A/ns) and diameter (20-233μm) of coated wires [73] (with optimized length [78]) on specific energy, specific power, time of burst and action integral.

To consider the rate dependent effects in these experiments, another parameter "specific power averaged over time of burst" obtained by dividing the deposited specific energy to the time taken up to wire burst has been used for comparative analysis. The results of above-mentioned experimental study indicated that if current rate and insulating coating are suitably chosen then thinner wires are better to generate higher specific power averaged over time of burst. Another significant outcome of these experiments is that the action integral is indeed affected by thickness of wire and rate of rise of current as also reported in some theoretical works [50], [79].

To understand the dynamics involved in explosion process, the effect of rate of current rise on time required for burst of wire has been studied. It has been observed that time taken for burst initially decreases with increase in rate of rise of current. However, after a certain threshold value of rate of current rise for a specific diameter, there is no significant decrease in time of burst and rate of decrease almost ceases, which finally leads to nearly constant value of time of burst. Experiments carried out beyond this threshold values have been interestingly found to show some peculiar distinctive kink like behavior in post burst experimental voltage profiles.

This feature which appears to be a pause or transient rise in voltage for a very short duration (~2 ns) while its down fall is marked in repeated shots and analyzed in detail experimentally as well as with numerical simulations [80]. Though such kind of feature have also been found in voltage profiles reported in earlier works [28], [81]; however, the discussion and detailed analysis of this is missing. Numerical analysis indicates that the formation of high-density front and its survival till burst is responsible for observing a pause in post-burst voltage profile. Density front seemed to be formed as a consequence of non-uniform radial expansion of wire during process of explosion. Experimental results emphasize that the averaged specific power (averaged over time of burst) is more important parameter than the specific energy to be deposited. However, this effect is significant for optimum diameters corresponding to particular set of system parameters, as seen experimentally as well as through numerical simulations.

As for a given current rate, mode of explosion for a wire in given surrounding medium depends upon properties of the metal used; hence, the investigation has been extended further on various metal wires to understand the effect of the wire-material on explosion phenomena. In many of the already reported works, though, the researchers [28], [70], [76], [82] have attempted to analyze the effect of wire material on mode of explosion in a specific surrounding medium (either vacuum or any other medium) but the detailed analysis of electrical characteristics and explosion behavior of various metals with respect to the media confining it including vacuum for same set of circuit parameters is rarely reported. It is not only the material properties but the surrounding medium may also play an important role in phase transition occurring during electrical explosion.

Thus, comparative study for behavior of different metals in air and vacuum is of significant importance. In the present study, effect of material on fast EEW (current rate ≈ 85 x

10^9 A/s) in air and vacuum is investigated. Six metals viz. Cu, Au, Al, Ti, Pd and W; representing wide range from low to high atomic numbers and covering each of three groups of metals viz. refractory metals, non-refractory metals and intermediate based on the explosion process [28] are considered. Correlation of energy deposition parameters with initial electrical and thermophysical properties of these metals is experimentally studied for both the mediums. Temporal profiles of self-emitted light are also recorded experimentally to have an insight for probable mechanisms involved.

To best of our knowledge, the effect of EEW material properties (like initial resistivity and enthalpy of atomization) on overheating up to burst (ratio of energy deposited to energy of atomization) for explosion in air is reported for first time in this thesis. In air, refractory and non-refractory metals are seen to exhibit different behavior as inferred from experimental results. However, it is interesting to note that in vacuum, the specific energy deposition in metals from all three groups is influenced by speed of sound in specific metal. Experimental results indicate some unconventional behavior of these metals during explosion especially in vacuum when compared with previously reported such works [83], [84]. Role of speed of sound in a specific metal appears in present study to be more dominating for process of energy diversion when surrounding medium is changed from air to vacuum.

Overall performance of Au is found to be best among all the metals investigated presently in both the media after considering three important parameters i.e. burst current, specific power and overheating factor. However, Ti and W have least values of these parameters in vacuum as well as in air.

To generate X-rays pulse from exploding wire, an experimental study is carried out to observe the effect of various configurations of wires on X-rays emission using PIN diodes as detectors along with available thin foil filters of Be (50μm) for X-rays of energy greater than 1.3 keV, Al (6.5μm) for energies in range of 0.7 keV to 1.7 keV and greater than 2 keV, and Ti (12.5μm) to cover an energy range from 2.8 keV to 5 keV. Out of various configurations of different geometries including single wire, it has been found that wires only in typical X-pinch configuration can yield significant X- rays (>100 mJ for energy >1.3 keV) with current rate of ~0.08 kA/ns which is much slower than generally reported current rates for X-rays emission from X-pinches [85] except those reported in a very few recent studies [86]. Significant X- rays yield has been confirmed for present capacitor bank with X-pinches made up of different metals like Mo, W and Cu. X-pinches made up of two wires, of any of these metals, yield relatively more radiation in respect of energy as well as in intensity than that of X-pinches made up of four wires which seems to be due to lesser mass at crossed point required for compression for present current rising rate. In another experiment to understand the effect of coating on X-rays emission in X-pinches, X-rays emission yield from X-pinches of two 13 μm bare W wires is compared with that from X-pinches made up of two 13 μm wires overlaid with grease or silicone-based lubricant. This study was motivated by results of earlier experimental study [73] for observing the effect of coating on specific energy of single wires. A significant increase in intensity of radiation is observed in energy range of 1.3 keV to 5 keV for grease coated X-pinch configuration due to expected enhanced specific energy deposition in single wires of X-pinches and limited expansion of exploding wires due to coating.

Interesting applications have been one of the reasons to pursue research work on various aspects of single exploding wire in the present thesis. In addition to application in pulse X-rays generation, EEWs with present range of current densities (10^8-10^9 A/cm^2) make them an easily configurable source in laboratories for nanoparticle generation [33], shock wave generation [73] and to study matter at extreme conditions like warm dense matter studies [87]. Requirement of high current density in explosion process of exploding wires and its characteristics of transforming conducting state to non-conducting state at very fast rate (nano seconds to microseconds) makes them beneficial for interrupting large current densities and used in circuit breaking, opening switches [88] and in pulse sharpening of the voltage signal.

Single exploding wire with experimental parameters of present work is also useful as pulsed source for deep UV to visible range. Lebert et al. [6] in 1996 have reported on utilization of pinch plasmas for UV applications. Interaction of ultra violet radiation with organic molecules make pulsed discharges valuable for their major contribution in polymers processing for treatments of food, water, fabrics and other bio medical products [6].

1.6 Plan of Thesis

Present work focuses on systematic study of fast electrically exploding single wires using moderate power generators. The thesis reports investigations on the behaviour of fast electrically exploding wires with variable circuit parameters (current rate, dimension of wires, surrounding medium, material and configuration) and brings out interesting outcomes which are novel and considerable to understand physics of exploding wire process. Experiments are carried out to study the dynamics of single exploding wire with major focus on characteristics influencing specific energy deposition till burst. This study is useful for looking into the mechanisms responsible for optimisation of efficient energy coupling.

Detailed experimental as well as numerical analysis are also done to understand distinct post burst feature observed for copper wire explosion in air. Detailed comparative study on effect of wire material on deposited energy for wires exploded in air and vacuum is also the part of this thesis work. To examine the effect of geometries in wire configurations on X-rays emission, experiments are carried out with various configurations. The X-pinches have been found most suitable for X-rays emission for this capacitor bank of moderate powers. Effect of coating on wires of X-pinches on X-rays emission is also studied.

Laser Interferometer is also developed at laboratory for diagnosing electron density profiles in pulsed plasmas. This interferometer is also used for estimating electron density profiles in single exploding wire.

Chapter 2 covers details about electrical diagnostics used for estimation of energy deposition. This chapter describes methodology used for energy calculations. This chapter also comprises details of PIN detectors used for X-rays yield measurements in X-pinches. Description of Laser Interferometer and Faraday cup (FC); as pulsed plasma diagnostics; developed in laboratory are also included in this chapter.

Chapter-3 presents the details of experimental set-up, charging voltage range, current rates range, load configuration, and other variable parameters like dimensions of wire, wire material used for present study. Details of one dimensional magnetohyrodynamics (1-D MHD) simulations used for analysing experimentally observed distinct post burst feature in copper wire explosion in air are also elaborated in this chapter.

Chapter-4 presents experimental results and discussion on investigations of Specific Energy deposition and burst characteristics in electrically exploded single copper wires in air for variable circuit parameters (current rate, dimensions of wire and insulating coating). This study also provides experimental evidence of variation in specific action integral with current rate for a given material. Appearance of post burst feature of kink in voltage and current profiles for a range of circuit parameters and possible mechanism responsible for it are also discussed. Results and analysis of in-situ electron density measurements are also included. Considerable emphasis has been given on results of numerical simulations for observance of this signature.

Chapter-5 presents results of comparative experimental study to observe the effect of metals with varying thermophysical and electrical properties on electrical explosion in air and in vacuum at current rate of 90A/ns. Experimental results and their analysis are described in detail.

Chapter-6 includes results of experimental study on effect of configurations of exploding wires on X-rays yield. Some new configurations along with single wire and X-pinches are demonstrated. X-pinches; found to be the best configuration for X-rays emission for present range of circuit parameters. Also, the effect of coating has been probed further.

Chapter-7 provides significant outcomes of experimental results and conclusions are made with future scope of present work.

The work is expected to contribute in further understanding and optimization of these systems.

Chapter 2

Diagnostics for Electrically Exploding Wires

The work in the thesis involves studies for characterization of exploding wire to understand the burst dynamics which comprises of exploring the effect of circuit parameters on time of burst, voltage profiles, energy deposition, electron densities and the radiation generated. Thus, diagnostics needed for this study include measurement of current, voltage, electron densities and X-rays energy/ intensity. This chapter discusses the general features along with merits and demerits of relevant diagnostics commonly used for pulsed plasmas in brief and elaborate the details of specific diagnostics used in this work. Electrical diagnostics method used for estimation of energy deposited, and X-rays detector used in present study have been discussed. Laser Interferometer and faraday cup; which are designed and developed during the course of this work for analysis of pulsed plasmas; are also described in detail.

2.1 Electrical Diagnostics

Electrical characteristics of exploding wires are observed by measuring the temporal profiles of current in the circuit and voltage across exploding wires. Pulsed voltages and currents with rise time in range of ns to microsecond can be measured using various methods. Measured current in the circuit and voltage across exploding wires have further been used to estimate the energy deposited in exploding wires.

2.1.1 Voltage Measurement

Commonly used methods for voltage measurement include voltage dividers, spark gaps, and techniques based on electro-optical effects (like Kerr cell and Pockel cell) [82]. Each of these is discussed in brief as follows.

2.1.1.1 Spark Gaps

Metal spheres, generally made up of aluminium or copper, with smooth surfaces and uniform curvature are used in the measurement of peak of impulse voltages. A fixed spark gap distance with known atmospheric conditions of temperature and pressure can be used to measure the voltage by comparing it with calibrated values of breakdown voltage under those conditions. Accuracy in measurement of crest of voltage depends upon the uniformity of electric field between two electrodes and is decided by ratio of gap to the diameter of the sphere. This can be used for voltages with rise time $\geq$ 500 ns [89] but this method cannot be used to reveal information about voltage waveforms [90]. For electrically exploding wires with present experimental set-up, response times required for observing changes in voltage profiles should be around 10 ns.

2.1.1.2 Electro-optic Methods

These methods are based on the principle of electric field induced birefringence in some optical materials. Polarization state of probing light beam is modulated by applying the electric field created by the voltage to be measured. This modulation is registered in a photo detector as intensity variations and further decoded to recover the voltage waveform [89]. The refractive index of the electro-optical transducer varies with applied electric field and change in refractive index ($\Delta\mu$) can be given by following relation.

$$\Delta \mu = \mu_o + a \cdot E + b \cdot E^2 \tag{2.1}$$

Here, μ_o is refractive index of material in the absence of applied electric field, E is applied electric field, ‘a’ and ‘b’ are electro optic coefficients of that material.

Pockel and Kerr cells are based on this principle and used to measure voltage using appropriate electro-optical material and suitable configuration. In Pockel cell, optical properties of medium linearly changes with electric field, i.e corresponds to second term in (2.1) and in Kerr cell, this behavior corresponds to the square of electric field, i.e third term in (2.1). These cells can be employed for measurement of high voltage (up to 100's of kVs) pulses covering wide range of frequencies suitable for observing transient changes with rise times of microseconds to nanoseconds [89]. Though, these electro-optical methods have advantages over electrical methods for being immune to electromagnetic noise and also exhibit higher sensitivity but its arrangement requires extra space along with precise alignment of optical components. If these systems are to be used for nanosecond measurements then it should be a part of pulsed power system to avoid inductances provided by connecting cables which can affect their response times. It is tedious and complicated to couple electro-optic systems with exploding wire load. This also makes experimental set-ups bulkier.

2.1.1.3 Voltage Dividers

Dividers are used to reduce the magnitude of high voltage pulses by electrical means to achieve a value that can be registered in a recording device like oscilloscope. Voltage dividers, contrary to electro-optical methods, can be easily coupled with experimental set-ups and does not require special arrangements in respect of space and alignment. They are simple in design, analysis and also cost effective. Thus, voltage dividers are preferred for present experiments. Voltage dividers can be resistive, capacitive and mix of resistive and capacitive. Presence of stray capacitances, and inductances in divider's elements (like resistors and capacitors in Resistive voltage divider and Capacitive voltage divider respectively), between the elements due to connecting points as well as between elements and the ground etc. can distort the true wave shape. Furthermore, division ratio also becomes frequency dependent. Though, special care in designing the elements of divider and use of different techniques can help in compensating or reducing the effect of these stray capacitances and inductances [89], [90], but still it is somehow difficult to completely eradicate their effects. However, in capacitive voltage divider unavoidable stray inductances result in a high sensitivity to noise and may result in unwanted ringing in the measured signals [91], [92]. Capacitive dividers are also made in shielded configurations for being immune to electromagnetic noise. Use of dielectric like oil, due to variation of its associated properties with temperature makes their use more complicated. These dividers are generally preferable in fixed configurations. However, in contrast the resistive voltage divider has the advantage of an easy structure, higher signal to noise ratio and simple electrical properties.

Therefore, resistive voltage dividers have been opted for present experiments. Details of voltage divider used in present work are mentioned below.

Basic principle of general resistive voltage divider can be understood by the schematic shown in Fig. 2.1.

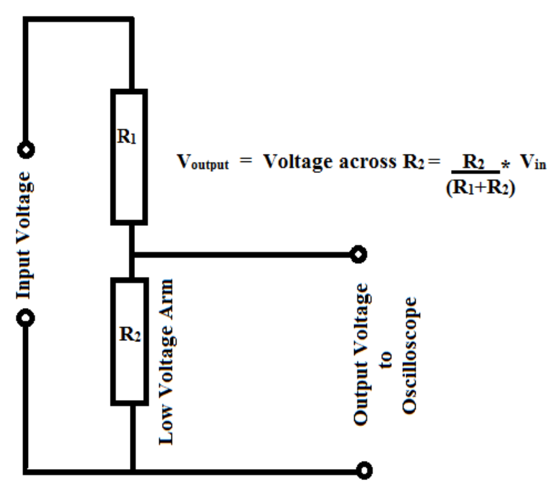

Fig. 2.1: Basic Schematic of Resistive voltage divider

The reduced (divided) voltages in low voltage arm are recorded in an oscilloscope. Impedance at two ends of connecting cable (at low voltage arm and at oscilloscope) is matched to avoid reflections. In our system, voltage divider is used to measure voltage across load in oscilloscope by reducing its voltage level in proportion of the incoming voltages. The details of the same are provided below:

2.1.1.3.1 Description of Resistive Voltage Divider Employed

In present work, voltage across load is measured using commercially available standard resistive voltage divider with sufficient frequency response to truthfully measure the voltage across exploding wire. Compensating circuits along with divider elements (Fig. 2.1) have been employed to reduce effects of stray inductances and capacitances. Typical specifications of voltage divider used in present experiments are as follow: Maximum pulsed Voltage which can be measured is 100 kV with maximum frequency of 80 MHz. Divider ratio for this divider is 1000: 1. Accuracy in voltage measurement is <3% for frequency > 5MHz.

2.1.2 Current Measurements

For current measurements, different techniques are employed in pulsed power systems like Rogowski coil, current viewing resistor, fast current transformer and devices based on magneto-optic effect (Faraday effect) etc. The brief description of these techniques is provided in following subsections.

2.1.2.1 Current Viewing Resistor (CVR)

This technique is based upon Ohm’s law. A small known resistance in the range of μΩ to mΩ is connected in series with the load, and the voltage developed across it is measured to calculate the current flowing through it.

Special designs or configurations are required to reduce the effect of stray inductances and capacitances which are prominent in pulsed current measurement. Electromagnetic interference even after taking precautions for high voltage (kVs) set-up and measuring large (>50 kAs) values of pulsed (ns-µs) currents can be a concern because of direct contact with apparatus.

2.1.2.2 Fast Current Transformer

Its principle is similar to that of step-down transformer. It has number of turns which behave like secondary coil and it surrounds the current carrying conductor acting as a single turn primary. Secondary coil is terminated with a low resistance load. This is special type of Rogowski which has iron or ferrite core instead of air core making it bulkier and heavy.

2.1.2.3 Magneto-optic Current Sensor

In this type of sensor, a material which exhibits significant magneto-optical properties is encircled over a current carrying conductor or arranged in other geometry by inserting current carrying conductor’s single loop around the material. The magnetic field generated by current carrying conductor changes the polarization direction of linearly polarised light, which in turn can be converted into intensity variations by using suitable arrangements of polarizers. These intensity variations can be recorded on an oscilloscope with the help of photo detectors. Angle of rotation is proportional to the applied magnetic field and hence the current flowing through the conductor. Since this technique is electrically isolated and immune to electromagnetic interference, hence this is one of the reliable methods for measuring current in pulsed power systems.

2.1.2.4 Rogowski Coil and Magnetic Pick up Coil

Rogowski Coil and magnetic pick up coil (or pick up loop), both work on the same principle which states that changing magnetic flux through these coils induces a voltage in proportion to rate of change of current. These diagnostics, simple in fabrication with least number of required components and non-contact type are highly sensitive to change in magnetic flux, hence, preferable over other options.

Magnetic pick up coil is generally kept in vicinity of current carrying conductor or can be located at a fixed distance from current carrying conductor where it can sense change in magnetic flux. On the other hand, Rogowski coil is toroidal in shape and encircles the current carrying conductor. Thus, magnetic pick up coil is position sensitive whereas Rogowski is position independent. Rogowski coil has been utilized in present experiments because of being position insensitive and flexible to be placed easily around the current carrying conductor. The details of the Rogowski coil used in present work are as follows:

2.1.2.4.1 Description of Rogowski Coil Employed

Rogowski coil is a high frequency current measurement device. It is a toroidal solenoid that encircles a conductor through which current is to be measured. It is developed in our laboratory using a coaxial cable and an insulated wire. A Teflon coated wire is closely wound on the inner dielectric of RG174 cable after removing its braid over certain length. One end of it is soldered with inner core conductor and other end is soldered to its braid after winding. It is then bent into a circular loop to form the toroid of Teflon coated wire (Fig. 2.2). Periphery of toroid or initial length of cable is decided as per experimental requirement as shown in its schematic Fig. 2.2. Insulation is maintained between HV conductor and Rogowski coil by winding Teflon tape over the complete toroid and it is also covered with an insulated sleeve. A BNC connector is connected to the other end of RG 174 to measure signal on oscilloscope.

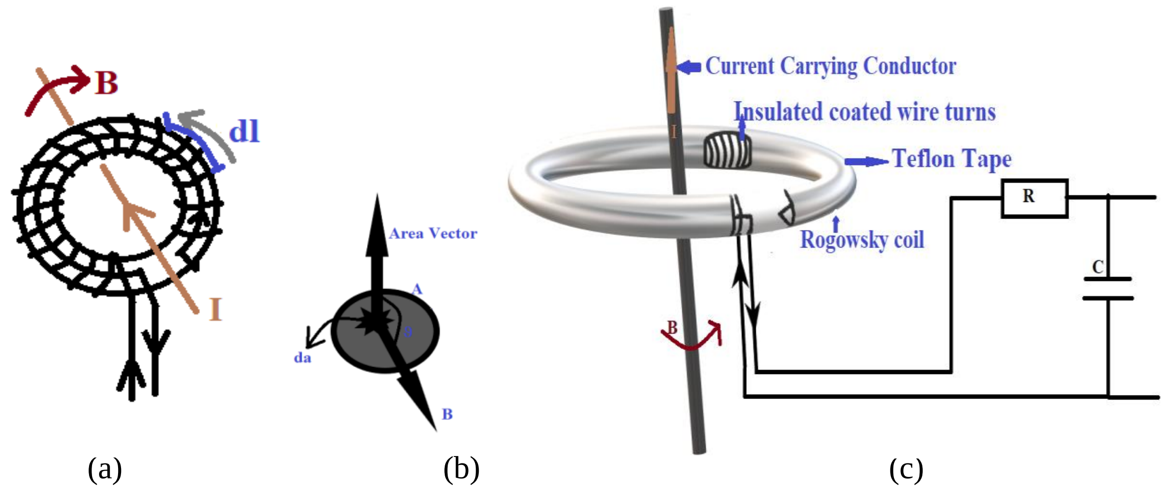

Fig. 2.2: Schematic of a) Rogowski Coil structure, b) Area of a single turn loop with direction of magnetic field, c) Rogowski coil along with integrator

(a) Principle of Working:

Rogowski coil is a current transformer. An alternating or pulsed current in a conductor develops a magnetic field that interacts with Rogowski coil. It is based on the principle of Faraday's law of electromagnetic induction and Ampere's law. When a high frequency current is flowing through a conductor, it produces a time varying magnetic field around it and hence the flux passing through loops of encircled Rogowski coil also changes. This change in flux (∅) with time induces voltage or emf (V) in coil as per Faraday's law and can be written as

$$V = -\frac{d\emptyset}{dt} \tag{2.2}$$

The negative sign indicates that the induced emf drives a current called induced current, in a direction that opposes the cause that induces it as per Lenz's law.

Suppose, for an infinitesimal length element 'dl' of perimeter of this coil, the magnetic flux linking the area '$\overrightarrow{ds}$' is 'dΦ' then voltage induced v_{dl} will be

$$V_{dl} = -\frac{d\Phi}{dt} = -\frac{d}{dt}\int \overrightarrow{B}.\overrightarrow{ds} = -\frac{d}{dt}\int \mu_o \; \Delta n \, \overrightarrow{H}.\overrightarrow{da} \tag{2.3}$$

Here, $\overrightarrow{da}$ is an area element of loop in direction of $\overrightarrow{dl}$ and Δn is number of turns in length dl; If 'l' is mean circumference of the torus and 'n' is number of turns per unit length then Δn = n dl. 'B' is magnetic flux density and 'H' is magnetic field strength due to current passing through the conductor. If '**θ**' is the angle between magnetic field lines and normal to infinitesimal small area of turn (da) as shown in Fig. 2.2 then V_{dl} will be

$$V_{dl} = -\frac{d}{dt}\int \mu_0 \; H \; \Delta n \; da \; \cos\theta = -\mu_0 \frac{dH}{dt} \; \Delta n \; \cos\theta \int da \tag{2.4}$$

So that

$$v_{dl} = -\mu_0 \frac{dH}{dt} n \; dl \cos\theta \; A \tag{2.5}$$

and A is area of each turn.

Total flux linking through the coil; $V_{Rog.coil}$ is given by integrating along a coil of length 'l'. So, the induced voltage is given by,

$$V_{Rog.coil} = \oint_0^l v_{dl} \tag{2.6}$$

$$= -\oint_0^l n \; \mu_0 \; A \; \cos\theta \; \frac{dH}{dt} \; dl \tag{2.7}$$

$$= -n \; \mu_0 A \frac{d}{dt} \oint H \cos\theta \; dl \tag{2.8}$$

If 'I' is the current in the conductor encircled by Rogowski coil, then as per Ampere's law, the line integral of magnetic field around the loop is equal to the net current enclosed by it. i.e.

$$\oint \vec{H} . \vec{dl} = I \tag{2.9}$$

So, Using (2.8) and (2.9), Voltage induced in Rogowski coil can be given as:

$$V_{Rog.coil} = -\frac{d}{dt}\int \mu_0 \overrightarrow{H}.\overrightarrow{da} = -n \; \mu_0 \; A \frac{dI}{dt} \tag{2.10}$$

Thus, it can be seen from (2.10) that induced voltage in the coil is proportional to the rate of change of current passing through conductor and here, product ($n\,\mu_0\,A$) decides the coil sensitivity, which is proportional to number of turns per unit length in coil and area of each turn.

Since, the induced voltage in the coil is directly proportional to the rate of change of current (dI/dt), so, to get the signal proportional to the current, integration of coil output is required. Here, a passive RC integrator (Fig. 2.2) has been implemented with a time constant of 82 µs which is appropriate for present experimental setup having time period of ~4 µs under short circuit conditions. Signals corresponding to dI/dt and current in an experiment are recorded in oscilloscope.

(b) Calibration of Rogowski Coil

Calibration factor (A/V) to predict the circuit current from the output signal of RC integrator, is obtained by comparing its first peak experimentally obtained under short-circuit conditions against theoretically estimated value of peak current for a capacitor discharge using the well-known relations for underdamped LCR circuit as mentioned in (1.2) of chapter1.

Calibration for dI/dt signal (A/s/V) is obtained by comparing its peak value at t=0 with the theoretical value obtained for (dI/dt) using following relation under short circuit condition:

$$V_{ch.} = L\cdot(dI/dt)_{t=0} \tag{2.11}$$

(c) Error Estimation

Calibrated values of current obtained from Rogowski coil along with RC integrator have been compared with the output of a standard current transformer (Maximum frequency response~0.7 MHz, sensitivity: 0.001 V/A, accuracy: ≤1%) to assess the precision of current measurement. Maximum deviation of RC integrated output from standard current monitor output at present frequency (0.23 MHz) of current signals does not found to exceed beyond ± 3%. Hence, maximum error in present current measurements can suitably be considered as ± 3%.

2.1.3 Estimation of Energy Deposition

Temporal profile of energy deposited in wire is determined by integration of resistive power drop over time from which specific energy is in turn inferred, by accounting for mass of the wire. Resistive voltage is obtained by subtracting inductive contribution from the measured voltage. The measured voltage (U) across wire for current (I) flowing through it, can be related as:

$$U = IR + L_W \frac{dI}{dt} + I \frac{d L_w}{dt} \tag{2.12}$$

Where R, L_w are resistance and inductance of wire respectively. Inductance of wire (L_w) is estimated from the recorded dI/dt and voltage signals using their initial values at t=0. Initial rise in voltage is assumed to be due to contribution by inductance of wire. Assuming negligible expansion till the time of burst, the last term can be neglected as mentioned by Tkachenko et al. [66] when L > L_w, which is also the case here (maximum L_w is ~30 nH for the thinnest wire used in this work, against ~ 250 nH; total inductance of system). This has also been elaborated in detail in our reported work [73]. Resistive voltage across the load is then considered for energy calculations by subtracting (L_w . dI/dt) from the measured voltage signal. Typical voltages profile before and after this correction is shown in Fig. 2.3 for coated wire of diameter 233 μm electrically exploded in air in one of our experiments [73].

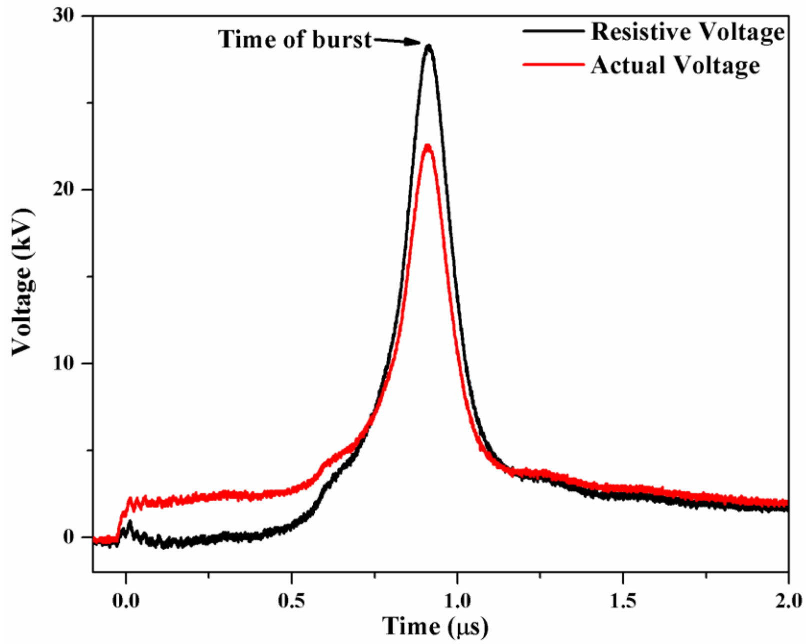

Fig. 2.3: Typical Voltage profiles before and after subtracting inductive contribution for wire of 233 μm diameter at charging voltage of 11 kV.

Error in experimental values of energy, arising from integration of product of current and resistive voltage, is assessed to be a maximum of ± 6% (based upon the errors in measurement of voltage and current separately). Specific energy deposited is taken as average of three shots.

For the same set of parameters, shots were found to be reproducible and shot to shot variation lies within experimental error. However, shot to shot variation in time of burst is within ± 5 ns.

For better illustration, temporal profiles of dI/dt, current and voltages are shown in Fig. 2.4 along with the estimated time profile of energy deposited (energy deposited up to that instant) for a specific shot from our experimental work [73].

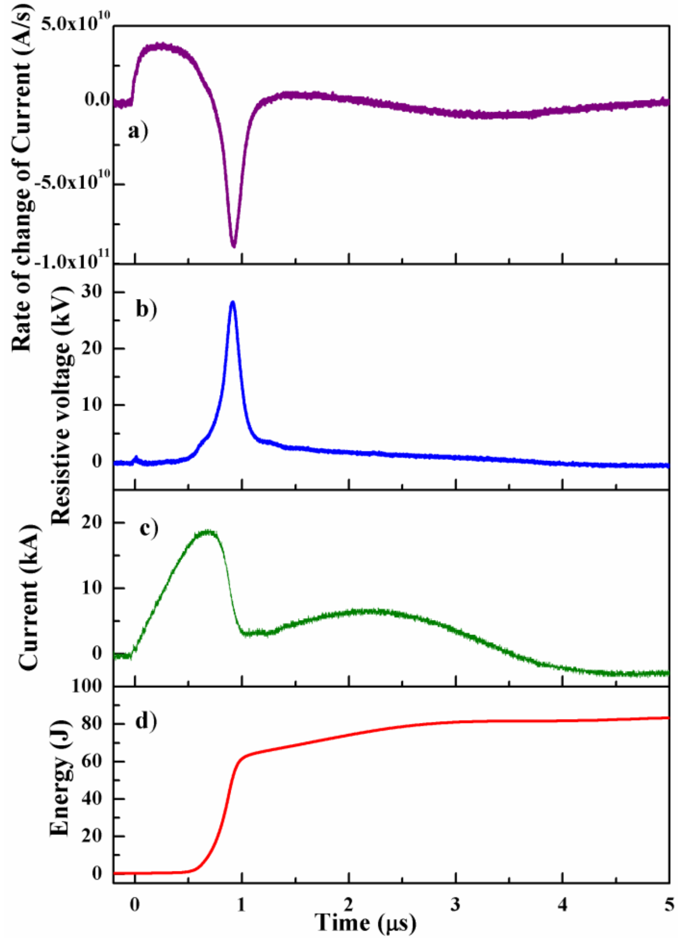

Fig. 2.4: Temporal profiles of (a) rate of change of current; (b) Resistive voltage (c) Current and d) total energy deposited for a specific shot of copper exploding wire in air at 11 kV. Wire is of diameter 185 μm with insulation coating on it making overall diameter of 233 μm and length is of 20 mm.

2.2 X-rays Diagnostics

Silicon photodiodes (Si-PIN diodes; AXUV5) with in-house designed filters have been used for measurement of x-rays yield for different energy range [93]. Filters made up of foils of different thicknesses viz. foils of Al, Be and Ti with thicknesses of 6.5 μm, 50 μm and 12.5 μm respectively have been used as X-ray filters to cover the X-rays energy range from about 1 keV to 5 keV. The transmission property of these filters for various energy ranges is reported in the

CXRO database [94]. Energy range of X-rays for transmission through these filters is given in Table 2.1 and also shown in transmission curves in Fig. 2.5

Table 2.1: Energy Range of X-rays for Transmission using foil filters

S.No.	Metal foil	Thickness of foil (μm)	Energy Range (keV)
1	Aluminium	6.5	1.7 >E>0.7 & E>2
2	Aluminium	9.0	1.55 >E>0.8 & E>2.2
3	Beryllium	50.0	E>1.3
4	Titanium	12.5	5 > E > 2.8

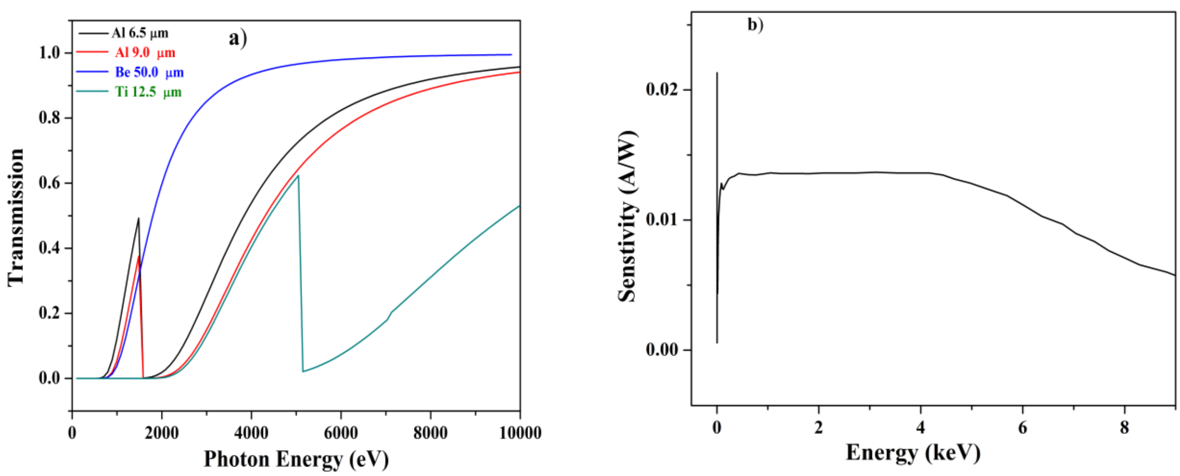

Fig. 2.5: (a) Transmission curves [120] for different filters in energy range of 100 eV-10 keV;(b) Spectral sensitivity of Si PIN diode used for present study.

Diode signals are registered in oscilloscope. Time delays of X-rays emission with respect to start of current are also observed using the signals of PIN diodes and Rogowski coil.

The radiation yield recorded by PIN diodes covered with a filter can be estimated from following relation

$$\gamma = \frac{1}{(\Sigma \cdot \rho)} \int_0^{\infty} V(t)dt \tag{2.13}$$

Where ‘V (t)’ is the output voltage pulse registered in the oscilloscope when X-rays radiation incident on Si-PIN diode. ‘ρ’ is the shaping resistance of biasing circuit and ‘Σ’ is the spectral sensitivity of Si-PIN diode.

In PIN diode, sensitive area is 5 mm^2. The spectral sensitivity of used detector (AXUV-5) is not available; its approximate value is obtained considering 5 mm^2 area and using the known value of sensitivity of the similar type of diodes like AXUV-100; in a similar way as considered by Pikuz et al. [95]. Sensitivity of AXUV-5 diodes is inferred to be about 0.0135 A/W from the sensitivity of AXUV-100 [95] which is 0.27 A/W for X-ray energy ranging from 100 eV to 4 keV with almost flat response.

Assuming X-ray emission to be isotropic, X-rays yield (w) of the source can be related to PIN diode Yield (γ) as:

$$w = \frac{16 \cdot r^2 \cdot \gamma}{s^2} \tag{2.14}$$

Where ‘r’ is the distance of diode from source and ‘s’ is the diameter of active region in Si-PIN detector. In experimental set-up, Si-PIN diodes (AXUV5) coupled with X-ray filters are kept at 22 cm from the center of the source. Actual photo of EEW system for X-rays diagnostics is also shown in Fig. 2.6.

(a) (b) (c)

Fig. 2.6: (a) Photograph of present system for X-pinch with PIN diode flange from inside chamber, (b) Top view of PIN diode flange with metal enclosure, (c) Side view for Pin diode Flange

2.3 Laser Interferometer for Electron Density Estimation

Another important parameter that characterizes the pulsed plasmas is its electron density profile. Diagnostic techniques which can be employed for the determination of electron density include plasma spectroscopy, Langmuir probe, laser interferometry and Thomson scattering technique. Out of these methods, if temporal as well as spatial profile of electron densities in plasmas is to be measured then interferometry is a versatile tool.

A Laser Interferometer is developed [96] as a part of this work for measuring electron density changes with a view to analyze the dynamics of pulsed plasmas. This interferometer is designed in Mach-Zehnder configuration (Fig.2.7) which is simple and easy to align. It has also advantage in the fact that there is sufficient possible space between optical components and plasma producing set-up. A CW (continuous wave) green laser of 532 nm wavelength and 5 MHz bandwidth is used as light source in Mach-Zehnder Interferometer (MZI). Two beams; out of which one passes through the plasma to be investigated are made to interfere, resulting in fringe pattern. Optical path difference between two beams due to introduction of pulsed plasma in one of the path causes the fringes to shift from their initial position which are monitored in the interferogram.

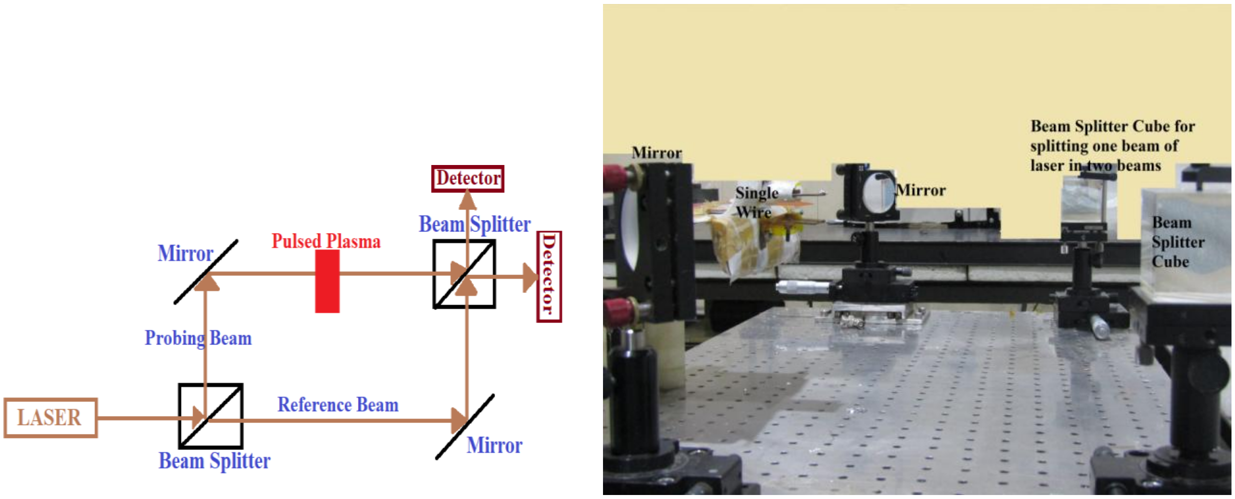

(a) (b)

Fig. 2.7: (a) Schematic of Mach Zehnder Laser Interferometer with two possible positions of detectors where interference can be observed, however only one detector is used; (b) Photograph of interferometer in our lab for EEW system for explosion in air.

If 'L_1' and 'L_2' is the optical path length up to detector travelled by two beams of wavelength 'λ' then phase difference (Φ_1-Φ_2) between these two is given by

$$(\Phi_1-\Phi_2) = \frac{2\pi}{\lambda} \cdot (L_1 - L_2) = \pi \times \text{no. of fringes shifted} \qquad (2.15)$$

Thus, as per well-known conditions of interference, one fringe shift corresponds to a phase shift of π; hence, total phase difference can be related with the total no. of fringes shifted due to plasma. This phase shift corresponds to line integrated electron density of plasma and can be written as

$$\Delta\Phi = \frac{2\pi}{\lambda} \int_0^L (N - 1)\, dL \qquad (2.16)$$

Here, plasma length is 'L'; 'N' and 1 are refractive indices of plasma and air, respectively.

Refractive index of plasma, 'N' is related with its electron density (n_e) as follows:

$$N^2 = 1 - \frac{\omega_p^2}{\omega^2} = 1 - \frac{n_e}{n_c} \tag{2.17}$$

Where 'ω_p' is plasma freuency ($\omega_p = \sqrt{\frac{n_e \cdot e^2}{m_e \cdot \varepsilon_0}}$) and '$\omega$' is angualr fequency of probing beam. 'n_e' is the electron density of plasma which decides ω_p and n_c is critical electron density; If $n_e >> n_c$, laser does not pass through plasma as refractive index will be a complex number (2.17). Therefore, it is essential to choose wavelength of laser such that $\omega_p << \omega$ or $n_c >> n_e$. Critical electron denisty can be estimated using angular frequency or wavelength of laser and is given as:

$$n_c = \frac{4 \cdot \pi^2 \cdot c^2 \cdot m \cdot \varepsilon_o}{\lambda^2 \cdot e^2} \tag{2.18}$$

Here, 'c' is the speed of light, 'm' the mass of electron, 'ε_o' permittivity, 'λ' the probe laser wavelength and 'e' is the electron charge.

Using (2.15), (2.16) and (2.17), number of fringe shifted after introducing plasma in one of the arms of interferometer can be given as:

$$\text{No. of fringe shifted} = \int_0^L \frac{n_e}{(\lambda \cdot n_c)} dL \tag{2.19}$$

Line integrated electron density along any path length can be written as:

$$\int_0^L n_e \cdot dL = (\lambda \cdot n_c \cdot \text{ no. of fringe shift}) \tag{2.20}$$

For laser wavelength of 532 nm used in present set-up, line integrated electron density, using equation (2.18) and (2.20), may be written as

$$\int_0^L n_e \cdot dL = (2.1 \cdot 10^{21} \cdot \text{ no. of fringe shift})\ m^{-2} \tag{2.21}$$

Hence electron density averaged over given path length 'dL' using laser of 532 nm will be:

$$n_e = \left(\frac{2.1 \times 10^{21} \times \text{no.of fringe shift}}{\int_0^L dL} \right) m^{-3} \tag{2.22}$$

Thus, line integrated electron density of plasma medium can be determined with the help of interferometer. The maximum density which can be probed; using this laser wavelength is 4×10^{27} m^{-3}.

It is necessary to synchronize triggering of camera with start of the event. Synchronization has been accomplished by placing an optical fiber in spark gap assembly. Optical pulse was generated by light produced in open air spark gap at the time of switching of the capacitor bank. This pulse triggers the camera using an optical to TTL pulse converter. Pick-up loop (based upon principal similar to that for Rogowski coil with relatively less number of turns on a straight conductor) is used to get dI/dt pulse, which, also starts with closing of the spark gap. Both pulses are simultaneous and camera can be synchronized using a delay circuit to capture the event after specific delay from start of current (Fig. 2.8).

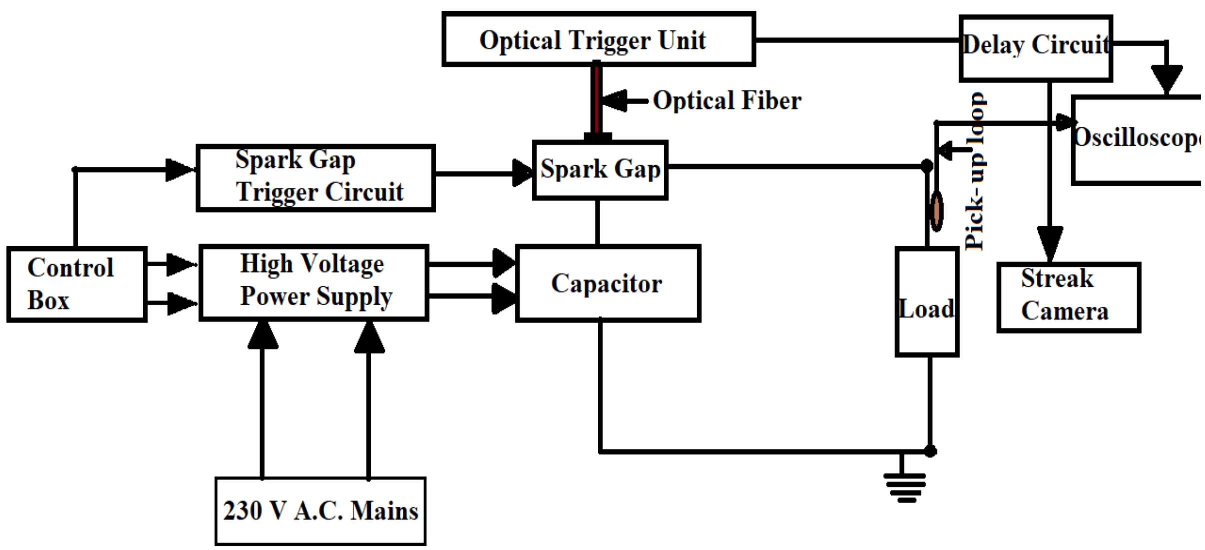

Fig. 2.8: Schematic of experimental arrangements for discharging capacitor through load and synchronizing this event with streak camera

Temporal and spatial variation of electron density is determined from experimentally measured fringe shift using a streak camera. The setup performance in streak mode has been initially assessed for the spark gap plasma and single exploding wires with lower discharge current rates, not exceeding 8 kA/μs. These experiments were carried out initially for performance evaluation of interferometer for implementing the same for estimation of electron density of exploding wires. It has been seen that the electron density measurement for exploding wire plasmas was not possible at very close to wire axis and also at near to the time of burst. This is because shift in fringes are unresolved in such situation in streak mode. In faster sweep speed of 3 ns/cm; there is no significant movement of fringes and in slower sweep speed of 3 μs/cm, change in fringe shift is too fast to be resolve. Probable reasons appears to be the rate of change of electron densities, its gradients and brightness of self-emitted light of plasma. Though initially some experiments have been carried out using this set-up for the performance evaluation of interferometer in streak mode as discussed in following subsection, the single frame mode of camera is used for probing exploding wires in later stage. The single frame mode has been used with higher current rates (>85 A/ns). A simple methodology; described later in this chapter; is used to infer spatial and temporal electron density.

2.3.1 Experimental Results using Streak Mode of Camera

Band of straight fringes were obtained with Mach-Zehnder Interferometer (MZI) and recorded in a streak camera. MZI set-up has been utilized initially to probe spark gap pulsed plasmas.

Spark gap, made up of two sharp edged electrodes, has been used as closing switch in a capacitor discharge circuit and was introduced in one of paths of interferometer. Capacitor was charged to 6.5 kV and delivered a peak current of around 0.8 kA upon discharging. Electron density of spark gap plasma estimated using fringe record (Fig. 2.9) from streak camera is around 10^{23} m^{-3}. Streak mode of camera registers the event for defined sweep durations as per the selected speed. Interferogram for spark gap plasma is recorded with sweep speed of 3 μs/cm for 2 cm giving total duration in streak record of 6 μs. Triggering of camera is synchronized with a delay circuit for recording the fringes in a time 0.56 μs earlier than sharp edged spark gap plasma starts forming.

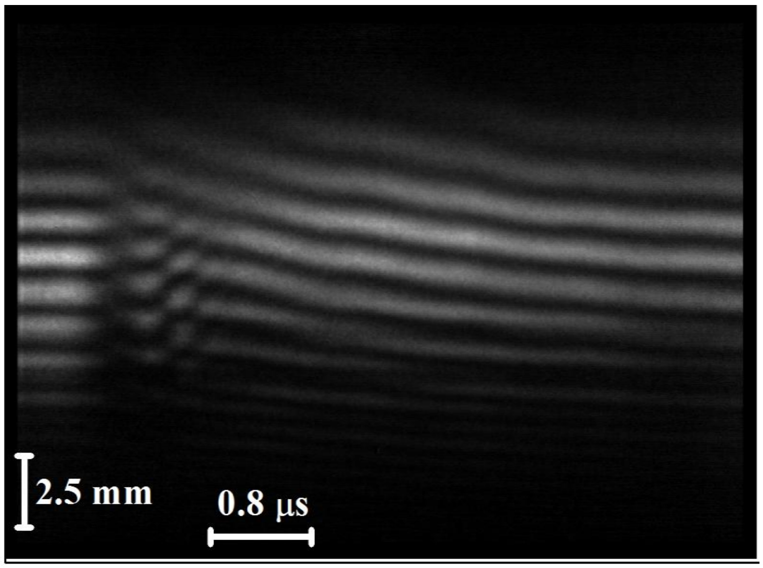

Fig. 2.9: Interferogram of spark gap plasma

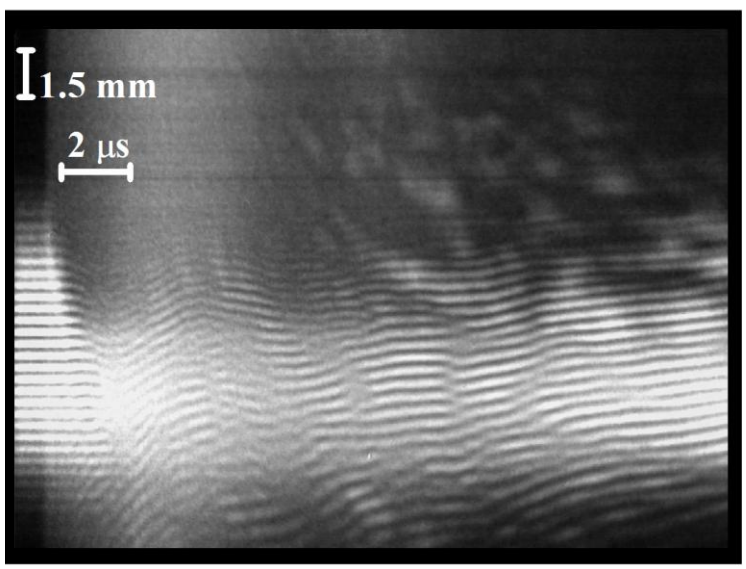

Fig. 2.10: Interferogram for exploding wire plasmas

Electron density profiles of single exploding wires; which have been exploded at slower current rate (< 8 kA/μs) are also probed. Fig. 2.9 displays the interferogram of plasma for copper wire of diameter of 70 μm exploded at 5 kV with current rate of 3 kA/μs recorded with streak speed is 10 μs/cm. This specific interferogram depicts the variation of electron density at 2.5 mm above the wire, which is obtained by keeping the laser beam at that distance. Electron density derived from this interferogram has been found to be order of 10^{24} m^{-3}.

2.3.2 Spatial and Temporal Profile of Electron Density in EEW using Frame Mode of Camera

To get spatial profiles near time of burst and along the wire length, Single frame mode of camera with short exposure times (~14 ns) has been used which has been found to be more useful whereas temporal profile can be approximately estimated by taking single frames of repeated shots at different instants. The camera is synchronized with dI/dt signal using an electronic delay circuit which provides a sharp pulse with rise time of 3 ns for precisely determining time of triggering of camera. The laser beam is expanded to 20 mm diameter to encompass full wire though portions of interferogram near anode and cathode ends are obscured due to load assembly components. Vertical axis of interferogram, which is along the length of wire (with anode towards top), is calibrated with respect to physically measured anode-cathode gap where wire is mounted. If wire is considered to be along Z-direction, then plasma shall expand in X-Y plane for which fringes in interferograms are generated in Z-X plane. Its schematic is shown in Fig. 2.11. If plasma is symmetric in nature then there are mathematical computation methods to get spatial profiles of electron density. Abel inversion [97] is generally used to get radial electron density profiles in symmetric plasmas like pinches and laser targeted plasmas. This computational method is tedious and requires rigorous mathematics. A more simplified technique is developed to get radial profiles of electron density in symmetric plasmas. This methodology is more advantageous for cases in which plasma has not expanded much at instant at which interferogram is captured and plasma needs to be divided into only a few numbers of shells of varying electron density.

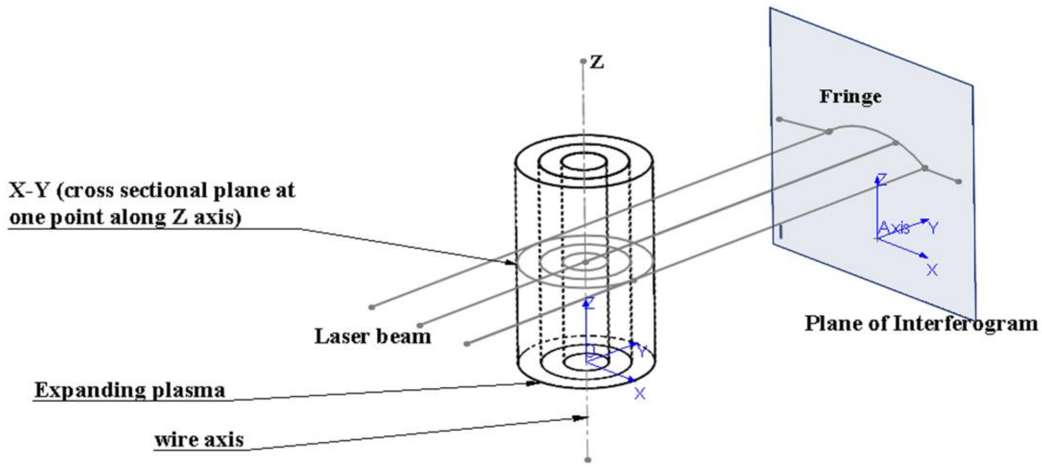

(a)

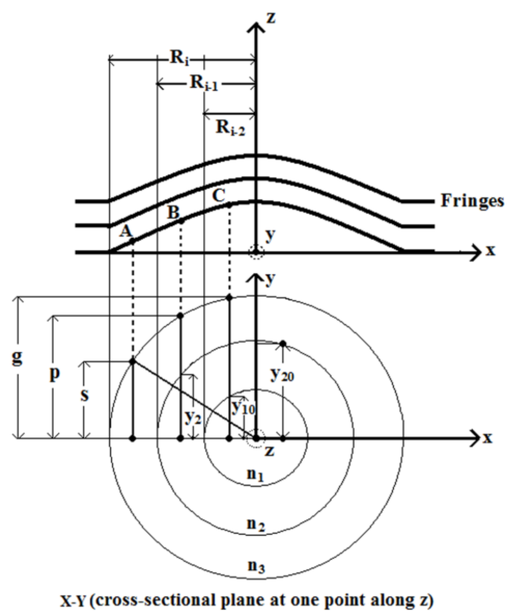

(b)

Fig. 2.11: (a) Three-dimensional view of expanding plasma indicating concentric cylinders of different electron densities, (b) Schematic of fringes in interferogram and corresponding top view of concentric circles of electron density of exploding wire plasma.

However, it may be noted here that present methodology gives flexibility in choosing variable (needs not to be equal) radii depending upon fringe profile and minimum resolvable fringe shift. Radial as well as axial profiles of electron densities can be estimated if each fringe is analyzed along length.

Since electron density is varying radially in exploding wire plasma. We have divided exploding wire plasma column into three equally spaced concentric cylindrical shells of radii R_i, R_{i-1} and R_{i-2} as shown in Fig. 2.11 (b), based upon the resolution of interferometer in discerning the relative fringe shift in adjacent shells. Outer most radius of plasma is decided by marking distance at which fringe shifts are negligible. Assuming constant electron density in each shell; fringe shift at central point of each shell thickness is considered to obtain averaged electron density in each of them.

Shift in each fringe corresponds to change in optical path length due to line integrated electron densities along cross sectional chord across cylindrical X-Y plane at each point along the length of wire (in Z-direction) as shown in Fig.2.11. Laser passes through cross sectional planes (X-Y) at different points along length of wire (Z-direction) as shown in Fig. 2.11 (a) then each fringe in Z–direction in Z-X plane of interferogram are used to estimate electron densities axially also. Different fringes along Z-direction correspond to different cross-sectional planes along length of wire. For analysis, two points are marked in fringe pattern, where negligible fringe movements are detected to draw the outermost cross-sectional circle of radius R_i, in X-Y plane as also shown in Fig. 2.11 (b). In present work, electron density is inferred at three points, one passing through center and other two are at radial off centers in expanding wire plasma on either side of axis. Fringe-shifts at these points marked as A, B and C are due to line integrated electron densities along chords passing through corresponding point of expanding plasma. Length of each chord is calculated using radius of X-Y cross-sectional circle and calibrated distance of each point from center as shown in Fig. 2.11 (b). This method gives spatial profile of line integrated electron density over chord lengths at mentioned specific points.

Line integrated cumulative electron density along different path lengths in X-Y plane is calculated (Using (2.22)) and further electron density in each shell are also computed mathematically by sequentially subtracting contribution from other adjacent shells, these calculations can be understood from following example.

Fringe shift at point A shown (Fig.2.11 (b)) in middle of radii R_i & R_{i-1} is result of refractive index change due to line integrated electron density of outer most shell only along path length 2s.

For outer most shell, averaged electron density n_3 will be;

$$n_3 = \left(\frac{21 \times 10^{20} \times \text{no.of fringe shift}}{\int_{-s}^{s} dy}\right)\ m^{-3} \tag{2.23}$$

The path lengths ‘s’, ‘p’ and ‘g’ are calculated using Pythagoras equation for right angle triangles formed (Fig. 2.11 (b)) by joining intersection points of circles with perpendiculars in y direction (‘s’, ‘p’ & ‘g’) to the centre of cylindrical shells & midpoint of thicknesses of respective shells. For ‘s’, it may be written as;

$$s = \sqrt{{R_i}^2 - a^2} \tag{2.24}$$

where R_i, R_{i-1} & R_{i-2} are radii of outer most shell, middle shell and inner most shell, respectively; and ‘a’ is average of two radii and is given as;

$$a = \frac{(R_i + R_{(i-1)})}{2} \tag{2.25}$$

Now in similar way as one move from outer shell to central region, electron density for specific shell is estimated by subtracting contributions from outer shells already computed. The electron density n_{2T} along path length 2p can be given by using (2.22):

$$\int_{-p}^{p} n_{2T} \cdot dy = (2.1 \times 10^{21} \times \text{ no. of fringe shift}) \quad m^{-3} \qquad (2.26)$$

Here, n_{2T} consists of electron density contribution n_3 from outer most shell and that from middle shell. The averaged electron density n_2 in the middle shell can be obtained as follows:

$$\int_{-y2}^{y2}(n_2 \cdot dy) = \int_{-p}^{p}(n_{2T} \cdot dy) - 2 \cdot (\int_{y_2}^{p} n_3 \cdot dy) \qquad (2.27)$$

Similarly, electron density in inner most shell (n_1) is also estimated. Each fringe is used to estimate electron density at different shells to get radial profile. All fringes in an interferogram are analyzed to estimate axial as well as radial electron density profiles.

Error in electron density estimation depends upon the ability of camera to spatially resolve fringe pattern. Averaged electron density is function of fringe shift which is ratio of spatial movement of particular fringe in vertical direction to its width in interferogram. Estimated error in measurements of averaged electron density considering resolvable spatial limit of camera (10 lines pair/mm) comes around 14%. It may also be noted here that measured densities are averaged over the exposure time (14 ns) of the camera.

2.4 Faraday Cup

To characterise the ion beam emission from the pulsed plasmas, a Faraday Cup (FC) is developed [98]. It consists of a metallic collector biased at a predefined voltage. As the ion flux strike its surface through a small aperture, the flow of charge in circuit induces a current proportional to it. The applied biasing voltage supplies the required charge in proportion to incident ions flux which neutralise on its surface. Inner core of this designed FC is made up of graphite due to its relatively low secondary electron emission coefficient. Inner electrode of inverted conical shape with apex having a narrow diameter opening for beam entrance (Fig.

2.12) has been designed for further reduction in secondary electron emission by increasing geometry-based possibility of recapturing the scattered secondary electrons.

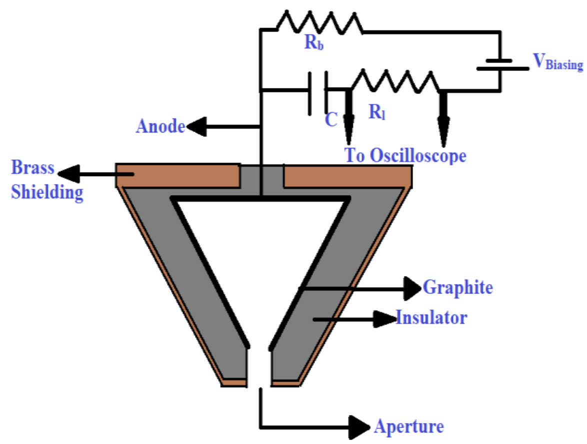

(a) (b)

Fig.2.12: (a) Designed Faraday Cup (b) Schematic of biasing circuit

Outer electrode is made up of brass. The two electrodes are separated by an insulator which is Teflon with dielectric constant (k) of 2.15. FC has length of 60 mm with an opening diameter of 1.9 mm at its apex. Designing parameters of FC have been decided so that the characteristic impedance (Z) obtained employing following relation is around 50 Ω to match with that of the connected coaxial cable (RG58).

$$Z = \frac{138}{\sqrt{k}} \times \log\left(\frac{d2}{d1}\right) \tag{2.28}$$

Here, k is dielectric constant. Brass shield has inner diameter (d_2) of 40 mm and outer diameter (d_1) of inner electrode is 12 mm at broader side of cup. The schematic of FC with biasing circuit is shown in Fig. 2.12.

This Faraday cup has been characterized by measuring the ion flux generated in a Plasma focus based z-pinch device [98]. Energy of ions flux is also estimated using time of flight method. Faraday cup was capable of registering ions in wider energy range varying from eVs to hundreds of keVs. Effect of filling gas pressure (1-5 mbar) on deuterium ions flux for higher (tens of keV to hundreds of keV) and lower (1-5 eVs) energy range have been studied. Temporal profiles of ion flux emission are experimentally determined by recording the voltage signals in oscilloscope using faraday cup (Fig. 2.13). Time of dip in dI/dt of plasma focus discharge current has been taken as t=0.

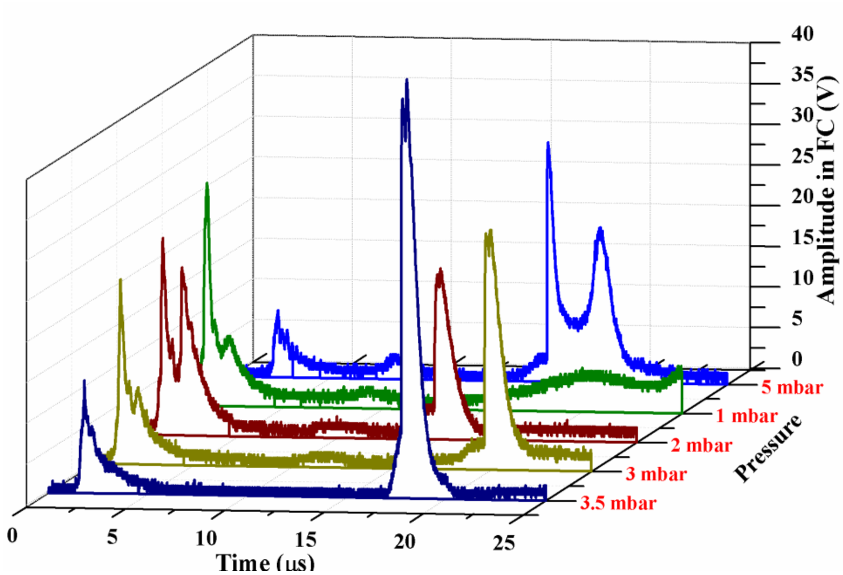

Fig. 2.13: Temporal Ions flux measurement with pressure

It has been found that the ratio of this higher energy ions flux to lower energy ions flux decreases with decrease with in filling gas pressure. This study may be useful in optimisation of filling gas pressures in chamber of Plasma Focus device to get ions of desired range of energy for practical applications. Detailed results of this work and analysis of mechanisms involved are described in our reported work [98].

At present, Faraday Cup has been used for measurement of ions flux from pulsed source of plasma focus device. However, in future this may be used in electrically exploding wire studies.

Chapter 3

Description of Experimental Set-up and Numerical Scheme

This chapter provides the description of experimental set-up; used for carrying out different investigations discussed in subsequent chapters. The details of pulse current source viz. capacitor and its operating parameters, discharge circuit components, load configuration (including its dimensions, geometry, surrounding medium, material) and experimental chamber are covered in different subsections. A brief overview of one dimensional magnetohydrodynamic numerical scheme, used for understanding some experimental results, is also included in this chapter.

3.1 Experimental Set-up

The experimental set-up consists of a capacitor of 2 μF, pressurized spark gap, transmission lines, and load assembly. Its schematic is shown in Fig. 3.1. The load assembly is kept inside vacuum chamber for carrying out experiments in vacuum. Photograph of present experimental set-up is shown in Fig. 3.2. Capacitor is charged to a specific charging voltage $V_{ch.}$ using a power supply. The charged capacitor is discharged through load with the help of spark gap switch and transmission lines. Spark gap is operated with a trigger pulse applied to a trigger pin which is inserted; into spark gap enclosure; between the two electrodes at off-center and closer to cathode; by about 30 % of total gap between electrodes. An electronic circuit capable of generating high voltage pulse of about -35 kV is used to trigger the spark gap at a desired charging voltage. Spark gap is operated in air at atmospheric pressure for lower charging voltages (till 25 kV) but for still higher voltages up to 40 kV, spark gap is pressurized at a pressure ranging from 4-8 psi above atmosphere. Use of pressurized spark gap with trigger makes this system operable in a wide range of charging voltages to achieve required current rates. Current rate is controlled by the inductance of complete system and charging voltage. The complete set-up including capacitor, transmission lines, load and current return path has a total system inductance of around 250 nH. Schematic of equivalent electrical circuit is shown in Fig. 3.1 (b). This simple and compact system can generate current pulses of peak magnitude of about 28 kA to 104 kA with quarter time period of 1.1 μs under short circuit at load end for charging voltage varying from 11 kV to 40 kV respectively. For this range of charging voltages, the energy stored in the capacitor corresponds to 121–1600 J.

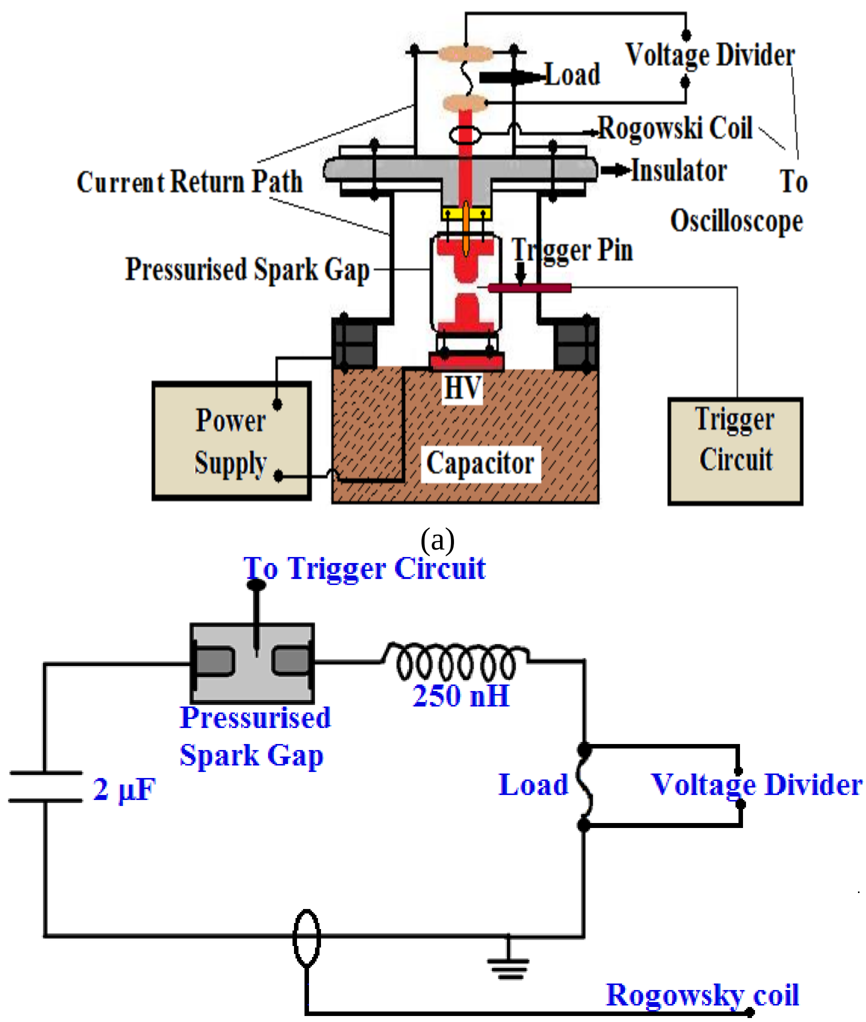

(b)

Fig. 3.1: (a) Schematic of Experimental set-up and (b) equivalent electrical circuit

Fig. 3.2: Photograph of Experimental Set-up

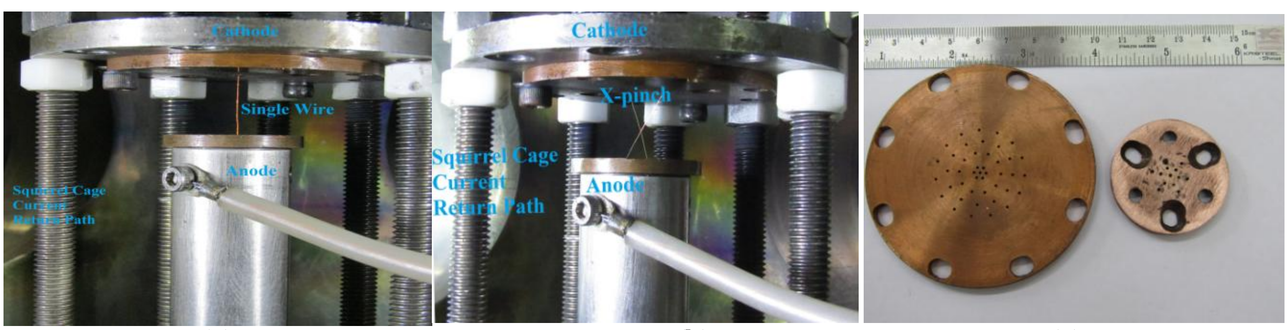

(a) (b) (c)

Fig. 3.3: (a) Single Wire and (b) X-pinch Load between anode and cathode within squirrel cage geometry (c) Sub assemblies of EW load (Copper plates serving as cathode and anode with several holes to mount exploding wires in different configurations)

3.1.1 Details of Load

A single wire has been used as load (Fig.3.3) for characterizing its behavior with respect to current rate, surrounding medium, material in present experiments. After optimizing the length of wire [78], it is kept fixed at 20 mm for this set-up. Diameter of wire varies in range from 20 μm to 233 μm. So, this system is capable of producing current densities of 10^7 to 10^8 A/cm^2 in single wire. Material of wire considered for investigation covers three different groups; categorized as per the mechanisms involved in EEW [67]. Behavior of six metals; Cu, Au, Al, Ti, Pd and W (representing wide range from low to high atomic numbers and belonging to the three different groups) are examined. For comparative study, the diameter of each wire of these materials is kept fixed (125 μm) with each having purity of at least 99.9%.

To study the effect of coating, insulating coating of polyimide and silicone-based lubricant have been used on electrically exploding single wire and X-pinches, respectively. A comparative study on exploding behavior of wires of different materials (Cu, Au, Al, Ti, Pd and W) under air and vacuum has also been carried out. Experiments in vacuum have been carried out with chamber evacuated to better than $1\text{x}10^{-4}$ mbar. Details of experimental chamber are discussed in next subsection.

Apart from single wire study, various configurations of EEW including X-pinches have also been examined to study effect of configurations on X-rays emission. These configurations will be discussed in chapter 6. After conclusive results on effect of configuration on radiation emission, X-pinches as load have also been studied (Fig. 3.3) to observe the effect of coating on X-rays emission.

3.1.2 Experimental Chamber

The experimental chamber (Fig.3.2) consists of six radially aligned ports for diagnostics and one port on top for creating vacuum. Two diagonally opposite ports have optical windows which are aligned in path of probing beam of Laser Interferometer so that laser passes through load. In one single port, three feed through electrically isolated connectors; are used to connect two cables of voltage divider placed across the load and one cable of Rogowski coil mounted around the load to oscilloscope. Other three ports are used to fix three PIN diodes; at center of these ports with same distance of around 220 mm from center of the load to receive same radiation flux assuming isotropic radiation emission. Experimental chamber is electrically isolated from capacitor discharge circuit and all the diagnostics used. Rotary and diffusion pumps are used to create vacuum slightly better than 1×10^{-4} mbar with the help of vacuum port at top of chamber in some of the experiments.

3.2 1-D Magnetohydrodynamic Numerical Scheme

A 1-D numerical scheme based upon Lagrangian finite difference formulation, earlier implemented to assess the performance of electrically exploding foil-based accelerators [99], has been used to investigate the dynamics of exploding wires after necessary modifications required for incorporation of cylindrical geometries of wire. Numerical simulations are carried out to understand dynamics and a post burst feature observed for copper exploding wire in air in some of the experiments discussed in Chapter 4.

The code uses three terms empirical EOS reported by McCloskey [100] along with two resistivity models for different ranges proposed by Burgess [32] and Stephens [101]. Stephens semi-empirical model is used to obtain resistivity depending upon temperature up to 30 kK and densities of more than 0.01 g/cm^3. Beyond this range of temperature and densities or volumes, wide range empirical model reported by Burgess [32] is used. As the latter model predicts lower conductivities than those predicted by Stephens model [101], therefore it has been linearly scaled up, to maintain continuity at 30 kK temperature. In all the cases reported here, the wire remains within the limits of Stephens's model near to voltage peak in pre burst region. The model by Burgess considers different phases including solid, liquid, and partially ionized vapor as well as a mixed phase (combination of cold vapor and condensed phase) decided by a mixing parameter defined therein for exploding conductor. Thus, it appears to be better suited for post-burst dynamics with temperature exceeding 30kK.

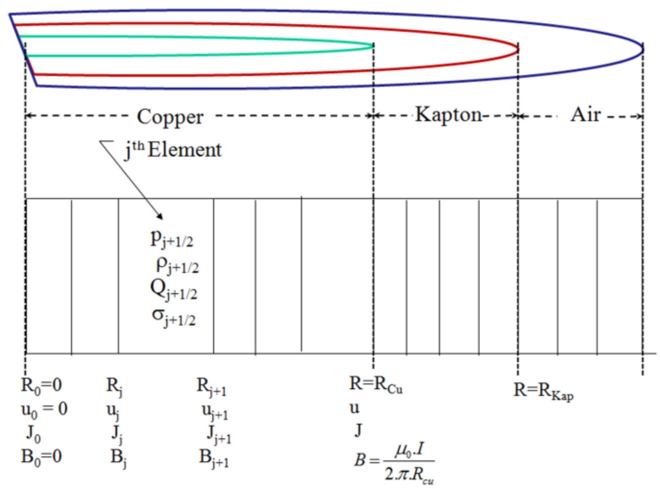

Fig. 3.4: Axi-symmetric 1-D mesh scheme used for exploding wire simulations.

The wire is considered as made up of discrete concentric cylindrical shells (meshes) as shown in Fig. 3.4 [80]. Three regions respectively of copper, Polyimide (Kapton) and air are considered for creating 1D axi-symmetric mesh scheme for simulations of exploding wire. The complete region is divided into finite number of meshes with each mesh having different electrical and thermodynamic properties. In Fig. 3.4 the subscript indicates mesh number, while the quantities p, ρ, Q, u, J, σ, B, R represent respectively the pressure, mass density, electrically deposited energy, velocity, current density, electrical conductivity, magnetic field and spatial coordinates of different meshes. The R_0, R_{Cu}, and R_{Kap} indicate the centre, dynamic radius of copper and polyimide (Kapton) boundaries respectively. The quantities like p, ρ, Q, σ are calculated at centre of the meshes and are represented by half subscript, while other quantities like u, J, B, R are calculated at the mesh boundaries. Air is considered in a shell of thickness 20 mm for all the cases of simulations presented in this work. The current (I) flowing through the wire is calculated using capacitor bank parameters along with time dependent dynamic resistance and inductance of the wire. The value of magnetic field (B) at different mesh boundaries of exploding conductor are obtained by solving the diffusion equation along with its boundary values at center and R_{Cu}.

The current density at the center of each metallic mesh is computed by using the value of magnetic field at adjacent mesh boundaries by using following relation:

$$\boldsymbol{\nabla} \times \vec{B} = \mu_0 \vec{J} \tag{3.1}$$

The obtained current densities and magnetic field are then used to calculate the deposited specific electrical energy and magnetic force at each mesh center and its boundary by following relations (3.2) and (3.3) respectively.

$$Q = \frac{J^2 \cdot \sigma \cdot \Delta t}{\rho} \ \mathrm{j/g} \tag{3.2}$$

$$\vec{F} = \vec{J} \times \vec{B} \tag{3.3}$$

Equations of fluid dynamics for conservation of mass, momentum and energy along with a three-term equation of state reported by McCloskey [100] are implemented for calculating pressure and temperature in each mesh in finite difference form as reported in detail elsewhere [99]. However, for air; ideal gas behavior is assumed. Using gradient of pressure and magnetic forces at mesh boundaries, following momentum conservation equation is used in finite difference form to calculate the velocity at different time steps:

$$\rho \frac{\mathrm{du}}{\mathrm{dt}} = -\nabla \mathrm{P} + \vec{\mathrm{J}} \times \vec{\mathrm{B}} \tag{3.4}$$

The voltage (V) developed across the wire of length *'l'* is determined by the product of circuit current (I) and total resistance of the wire. Resistance of wire is calculated as a parallel combination of all 'n' numbers of metallic cylindrical meshes, i.e:

$$\mathrm{V} = \frac{\mathrm{I}}{\sum_{\mathrm{j}=1}^{\mathrm{n}} \sigma_{\mathrm{j}} \cdot \frac{\pi \cdot (\mathrm{R}_{\mathrm{j}+1}^2 - \mathrm{R}_{\mathrm{j}}^2)}{l}} \tag{3.5}$$

To maintain the numerical stability in presence of shock, a dissipative term, usually known as artificial viscosity is added in pressure term as suggested by VonNeumann [103] but at present the code does not include radiation losses. The time step in the code is dynamic and during execution it is increased or decreased as per the relative change in different variables but its value is restricted by Courant-Friedrichs-Lewy [102] condition. Here, basic details of numerical simulations required for present work and its brief overview have been discussed. However, more details about this code may also be found elsewhere [99], [104].

Chapter 4

Burst Characteristics and Post Burst Dynamics of Copper Wire Explosion in Air

In electrical explosion of wire, optimisation of circuit parameters for efficient energy deposition is crucial to utilize it for specific applications. Specific energy (energy deposited per unit mass) is one of the dominant parameters which is critical in determining the exploding wire behavior. The maximum voltage generation at the time of burst, total radiated power, and shock wave generation are governed by specific energy deposition up to burst as well as it is a considerable parameter to characterize the behavior of exploding wire plasmas. Time of burst as already defined in Chapter-1 is the instant at which voltage reaches to the peak and afterwards breakdown initiates. Energy to be deposited can be enhanced if time taken for burst is elongated before breakdown is initiated. Intrusion of disrupting instabilities (like mechanical and magnetohydrodynamic instabilities) depending upon the time scale of energy deposition and time scale of their development and inhomogeneities (microscopic and macroscopic) in heating along the wire length are responsible mechanisms for hindering the energy deposition process. Major experimental circuit parameter which can enhance the energy deposition and helps in uniform heating of wire is the current rate. It has been reported by many researchers [69], [70] that enhancing current rate of the pulsed power source can increase the specific energy deposition in exploding wires up to burst. However, the prerequisite value of current rate required for suitable range of energy deposition itself is specific to the diameter of wire [24], [30], [50], [54]. Therefore, these two circuit parameters are intertwined with each other. Experiments have been carried out to examine the effect of current rate and diameter on explosion of copper wire explosion in air as investigations on copper metal for EEW in air are only few [74], [75], [77]. In the work reported in present chapter, the behavior of EEW is studied in atmospheric air (1 bar) at relatively fast time scales (with time of burst in the range of 50 ns-1 μs and current densities of 10^8–10^9 A/cm^2) as compared to that reported earlier in similar investigations [77] (with time of burst in the range 2-8 μs and current density of around 10^7 A/cm^2).

The diameter of wire which shall burst at the peak of the current is calculated *a priori* using the action integral. Further, the action integral (defined in chapter 1), a material dependent parameter which is generally taken as constant, has been demonstrated experimentally in present study to vary with thickness of wire and rate of rise of currents, in line with already reported theoretical work [50], [79].

Apart from the above mentioned two circuit parameters, i.e., current rate and diameter, surrounding medium properties also significantly influence the energy deposition [28], [67], [82]. For example, the restricted expansion of wire by dense surrounding medium supports in enhancing the energy deposition [24], [51], [72]. This effect has been observed in our experimental study also on polyimide coated copper wire explosion in air, which to best of our knowledge has not been reported in literature [73]. Apart from this, it has also been observed that a distinct post burst feature appears in voltage profiles of insulated copper wires under certain experimental conditions which have been investigated in detail. Though this kind of feature can also be noticed in voltage profiles of earlier experimental works [31], [59], [67], [81], [105], [106] for EEW in vacuum [31], in air [67] as well as in water [105], [106], but it is either overlooked or has been not investigated in detail.

All of our above mentioned experimental investigations including the effect of diameter (58-233 μm), current rate (25-90 A/ns) and insulation coating on specific energy deposition for copper wire explosion in air are presented in this chapter of the thesis. This systematic study to observe the effect of variable circuit parameters (diameter, rate of rise of current, and insulation coating) on the behavior of copper wire explosions provides guidelines in optimizing experimental parameters for efficient energy coupling. Experimental results showing dependence of action integral on diameter and rate of rise of current are also discussed.

This chapter also elaborates and discusses the analysis of post burst dynamics in single copper wire explosion. One dimensional magnetohydrodynamic numerical simulation has been carried out to explore the possible causes for the appearance of kink type feature in post burst voltage profiles. Numerical results and its analysis have been discussed in present chapter.

This chapter also elaborates and discusses the analysis of post burst dynamics in single copper wire explosion. One dimensional magnetohydrodynamic numerical simulations carried out to explore the possible causes for the appearance of kink type feature in post burst voltage profile have also been discussed in present chapter. Additionally, the experimental results on estimation of electron density in various shots, in which kink type of feature appears in post burst voltage profiles, have also been presented.

4.1 Effect of Coating, Diameter and Rate of rise of current

Initial experiments have been conducted on coated and bare copper wires of fixed diameter to observe the effect of coating on explosion. Further, Experiments have been carried out on coated copper wires to examine the effect of diameter (58-233 μm) on specific energy deposition up to burst at a specific rate of rise of current. Rate of rise of current is governed by the charging voltage for a specific capacitor based pulse power system. Rate of rise of current or current rate is estimated at particular charging voltage by dividing the peak value of current under short circuit condition to quarter time period viz. time taken to reach that value. Effect of diameter is studied for varying rate of rise of currents (25-90 A/ns) achieved by charging the capacitor at different voltages.

To explore the effect of coating on the energy deposited per unit mass up to burst, experiments have been conducted on two copper wires of nearly same core diameter (because coated wire with exactly same core diameter was not available) viz. one just bare wire (diameter ~ 100 μm) while other with polyimide coating (coated diameter of 122 μm with the core diameter of 90 μm, i.e. coating thickness ~36% of the core radius). In a set of experiments on these two kinds' wires, the energy deposited per unit mass has been determined as a function of charging voltage ranging from 16 kV to 40 kV and compared (Fig. 4.1 (a)). It can be seen from Fig. 4.1(a) that dielectric coating of 36 % enhances the deposited specific energy by 45-60 % for entire range of considered charging voltages. Possible cause seems to be the confinement of wire for longer time to limit its expansion; and causing delay in voltage breakdown as also seen by other researchers [71], [72], [107], [108]. Fig. 4.1(a) indicate that beyond a threshold charging voltage, rate of increase in specific energy deposition in coated wire is relatively smaller than at lower charging voltages; resulting in bilinear curves. Reason of such behavior appears to be higher energy deposition rate (for a specific diameter) with increase in charging voltage (or rate of rise of current) as expected initially but beyond a certain charging voltage, the counteracting inertial expansion starts reducing this effect and hence cause a change in slope.

In second set of experimental study, the aim was to study the effect of varying diameters in coated wires with same percentage (36%) of coating on the energy deposited per unit mass as a function of various charging voltages (16-40 kV). For this study polyimide coated copper wires of diameter 58 μm, 81 μm, 122 μm, and 233 μm with core diameters of 43 μm, 60 μm, 90 μm, and 171 μm, respectively have been chosen. Fig. 4.1 (b) shows energy deposited per unit mass as a function of wire diameter for various charging voltages. It is noted from the Fig. 4.1(b) that the specific energy deposited up to the burst increases with increasing wire diameter for all charging voltages. Experimental results seem to support evaporation wave theory. Initially, Evaporation theory was introduced by Bennett [52] and later used by Rakhel [53] and Tkachenko *et al.* [30] to explain wire explosion by the evaporation wave which initiates from the surface. If an evaporation wave is considered to travel from outer surface to its core axis then it is expected that larger travel time can contribute in larger energy deposition because of the sustained current density in its conducting part. Thus, more energy is seen to be deposited in thicker wires at a specific charging voltage. Fig. 4.1 (b) indicates that the rate of increase in the deposited specific energy decreases with increase in diameters. This might be because of non linear behavior of evaporation wave with diameter for time taken for energy deposition till evaporation wave reaches from surface to its axis. Increase in diameter beyond certain thickness is not making any significant difference in energy deposition.

Further, as mentioned, for first set of experiments, due to non availability of coated wire of 136 μm diameter with core diameter 100 μm, we have chosen the most nearest available coated wire (coated diameter 122 μm with core diameter 90 μm) and compared it (in terms of energy deposition per unit mass) with bare wire of diameter 100 μm. In order to see the deviation due to this ~10% difference in core diameter, we have interpolated the specific energy deposition from the plots of Fig. 4.1 (b) for coated wire of diameter 136 μm. It is evident that interpolated specific energy deposited for 136 μm diameter coated copper wire is slightly higher as compared to that for experimentally measured value for 122 μm coated wire as expected.

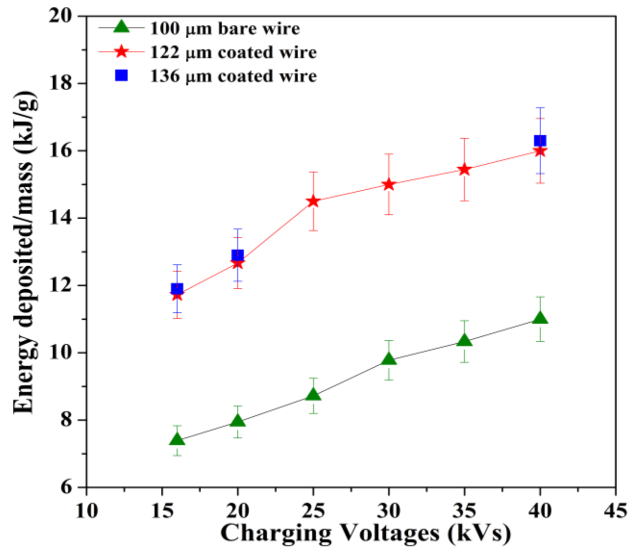

(a)

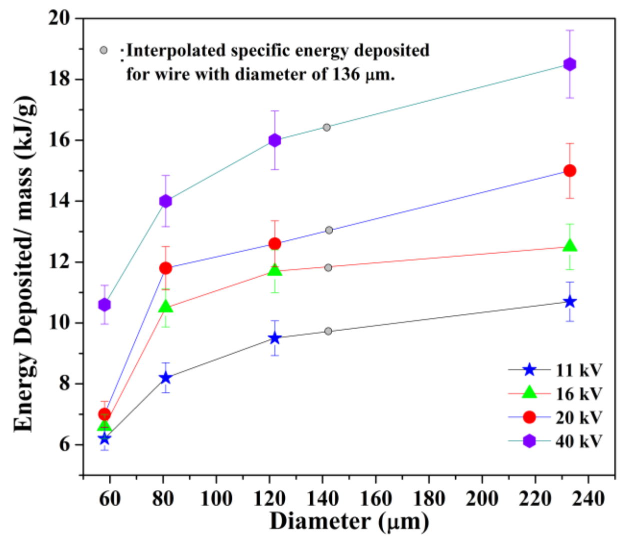

(b)

Fig. 4.1: (a) Specific energy deposited up to burst versus charging voltage in the case of 100 μm bare wire, 122 μm coated wire, and 136 μm (see text) coated wire, (b) Specific energy deposition up to burst versus diameter of wire at different charging voltages.

It is to be noted from the experimental data (Fig. 4.1(b)) that specific energy up to burst increases with increase in diameter as well as with the increase in charging voltage.

In several earlier reported works [33], [109]-[111], efforts have been made to derive a relationship between circuit parameters and energy deposition in exploding wires. Empirical relation given by Kotov et al. [33] is expected to be valid for a wide range of initial conditions with an error of not more than 20%. As per Kotov et al. [33] the energy ‘W’ injected into the wire during the first current pulse is as follows;

$$W = (h_b \times W_o \times S^2 \times Z)^{0.5} \tag{4.1}$$

and $W_o = (\frac{1}{2} \cdot C \cdot V_o^2)$ is the stored capacitor bank energy in joules, V_o is the capacitor charging voltage in kilovolt, $Z = \sqrt{(\frac{L}{C})}$ is the circuit characteristic impedance in ohms, S is the wire cross-sectional area ($= \pi \times \frac{D^2}{4}$) in mm^2, and h_b is an action integral in $A^2 \cdot s/mm^4$.

If the energy deposited per unit mass using (4.1) can be calculated as;

$$\text{Energy deposited per unit mass} = \frac{W}{(\rho \cdot V)} = \frac{(h_b \cdot W_o \cdot S^2 \cdot Z)^{0.5}}{(\rho \cdot S \cdot l)} \tag{4.2}$$

Where ρ is density of metal wire; V and l are volume and length of wire respectively.

This relation given in (4.2) suggests that energy deposited per unit mass is independent of diameter; but it does not appear to be so from our experimental results. The disagreement between the two could be due to the consideration of constant value of action integral in previous reports. In order to demonstrate that the action integral for a given metal wire varies with its dimension as well as with charging voltage, we have noted the experimentally observed time of burst for copper wires of different diameters and also performed the theoretical calculation of the same assuming the constant action integral value of 2.1×10^{17} A^2 s/mm^4. The difference between experimentally measured value and theoretically calculated value of burst time has been determined as a function of wire diameter for various charging voltages and is considered as the marker indicating the variation of action integral. The theoretical calculation of time of burst for a specific current density corresponding to the charging voltage is carried out by solving the following transcendental equation graphically. This transcendental equation is obtained by considering the current as a sinusoidal function of time and solving the action integral equation (1.4) within limits from 0 to t_b. .

$$\frac{\pi^3 \cdot d^4 \cdot h_b}{I_0^{\,2} \cdot T} = 4 \cdot \omega \cdot t_b - 2 \cdot \sin(2 \cdot \omega \cdot t_b) \tag{4.3}$$

Here, 'ω' is angular frequency of LCR circuit and is given by $\frac{2\cdot\pi}{T}$; 'T' is time period of complete cycle in seconds and 'd' is diameter of wire in mm. 'I_o' is peak current in A (Amperes).

The differences of the experimentally measured values of time of burst with those derived theoretically are plotted in Fig. 4.2 as a function of diameter of wire for different charging voltages.

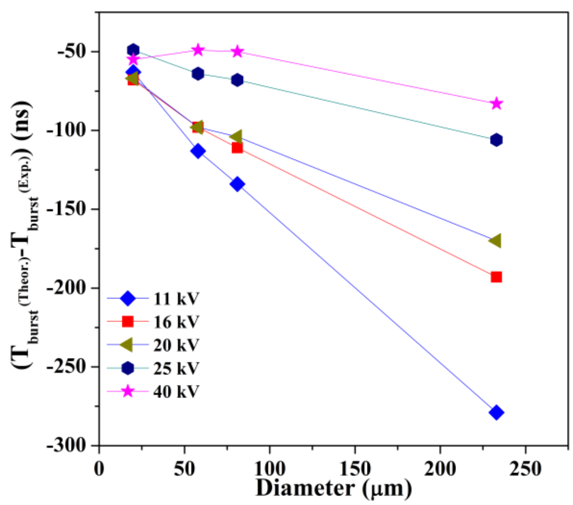

Fig. 4.2: Difference between 'time of burst' expected theoretically using action integral of copper [33] and experimentally measured values versus diameter at different charging voltages ranging from 11–40 kV.

As it can be seen from Fig. 4.2, for a given charging voltage; this difference widens with increasing wire diameter. It may also be noted that the widening of difference with increasing wire diameter is more pronounced for lower charging voltage i.e. relatively slower current rate. Therefore, it is concluded that action integral varies with thickness of wire and also with rate of rise of current, in line with already reported theoretical predictions [50], [79]. This can be attributed to difference in wire explosion mechanisms associated with varying energy density in wire and its rate because of varying current density and diameters.

Trend of energy deposition as displayed in Fig. 4.1 and time of burst shown in Fig. 4.2 with thickness of wire can be utilized to look into the exploding wire process. Influence on energy deposition can be understood by considering the propagation of evaporation wave from the surface of the wire to its core.

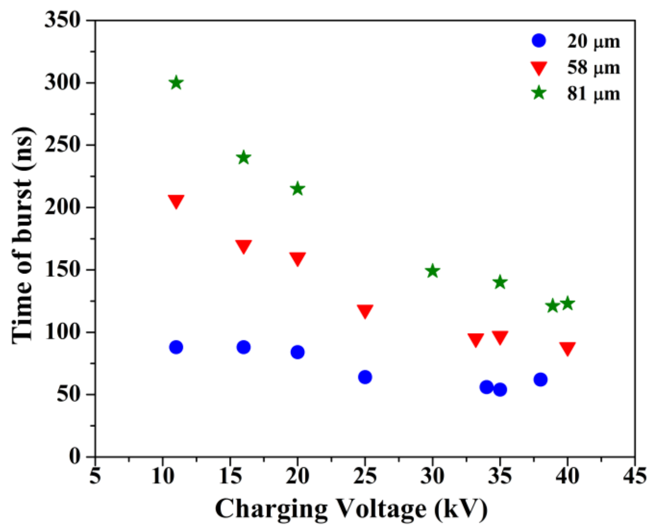

Fig. 4.3: Time of burst versus charging voltage for relatively thin wires (20, 58, and 81 μm).

Since time of burst in an important parameter to be considered in this regard, therefore, experimentally measured time of burst is plotted with varying diameter and charging voltage (Fig. 4.3).

Time of burst is seen to increase with diameter at a particular charging voltage. However, for a specific diameter, this decreases with charging voltage and the rate of decrease also decreases with increasing charging voltage. It seems that for a specific diameter, the increased rate of rise of current is reducing the evaporation wave time and also reducing the time taken for expansion before voltage breakdown. Thus, it is anticipated that faster rate of change of current can help in hindering the expansion before the voltage breakdown as compared to the slower rate of change of current. Results of these experiments indicate that if charging voltage and surrounding medium; as insulating coating in present case; are suitably chosen for wire of a specific diameter then specific energy deposition can be enhanced due to the limited expansion before voltage breakdown which appears to be due to the confinement by their own inertia [73]. If wire is surrounded by coating then initial expansion of gaseous state of wire is restricted and wire is confined for longer duration in its volume till coating gets burst. Thus, current rate and surrounding medium has effect on limiting the plasma expansions and enhancing energy deposition.

4.2 Experimental Observation and Analysis of a Post Burst Feature

Experimental results for copper wire explosion in air, discussed in last section, suggest that specific energy deposition can be enhanced in coated thinner wires with increase in rate of rise of current; governed by charging voltage [73]. An interesting post burst feature is observed in voltage profiles of those wire explosions for which time of burst starts saturating after a specific charging voltage. Though this kind of feature or appearance of a short duration kink in voltage profiles can be noticed in earlier reported works [31], [59], [67], [81], [105], [106] but it is not investigated in detail. However, present study analyses dynamics of this feature experimentally as well as numerically.

4.2.1 Experimental Observations and Analysis

Voltage profiles of coated exploding wires with diameters of 20-233 µm for charging voltages in range of 11-40 kV are considered [73] to investigate the appearance of kink or pause in voltage profile.

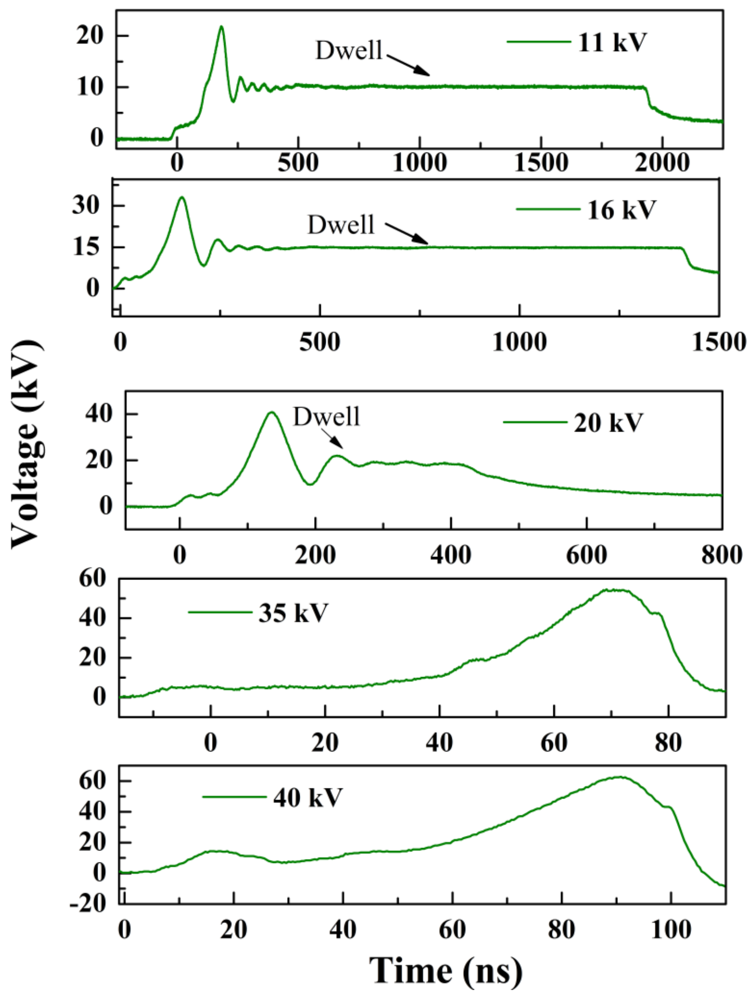

Fig. 4.4: Typical profiles of voltage across the wire for specific diameter of 58 µm at variable charging voltages.

It has been noticed from the voltage profiles that a dwell period occurs after the burst for wire of each diameter in general at relatively lower charging voltages and for illustration it is shown in Fig. 4.4 [80] for a particular wire of diameter 58 µm (~ 42 µm basic copper wire diameter with polyimide coating of about 16 µm). It may be noticed from Fig. 4.4, for wire of diameter 58 µm, the dwell period reduces with increasing charging voltage and this feature has been observed for wires of other diameters also (not shown in figure). Further, a kink kind of signature appears in voltage profiles beyond certain threshold voltage specific to the diameter (e.g. for 35 kV and 40 kV as shown in Fig. 4.4) which is found to be reproducible under same conditions of experimental parameters.

Additionally, in Fig. 4.5, the exploding wire voltage profiles for wires of different diameters are displayed at charging voltage of 40 kV. It may be noticed that the kink in the profile is missing for thicker wire of diameter 233μm.

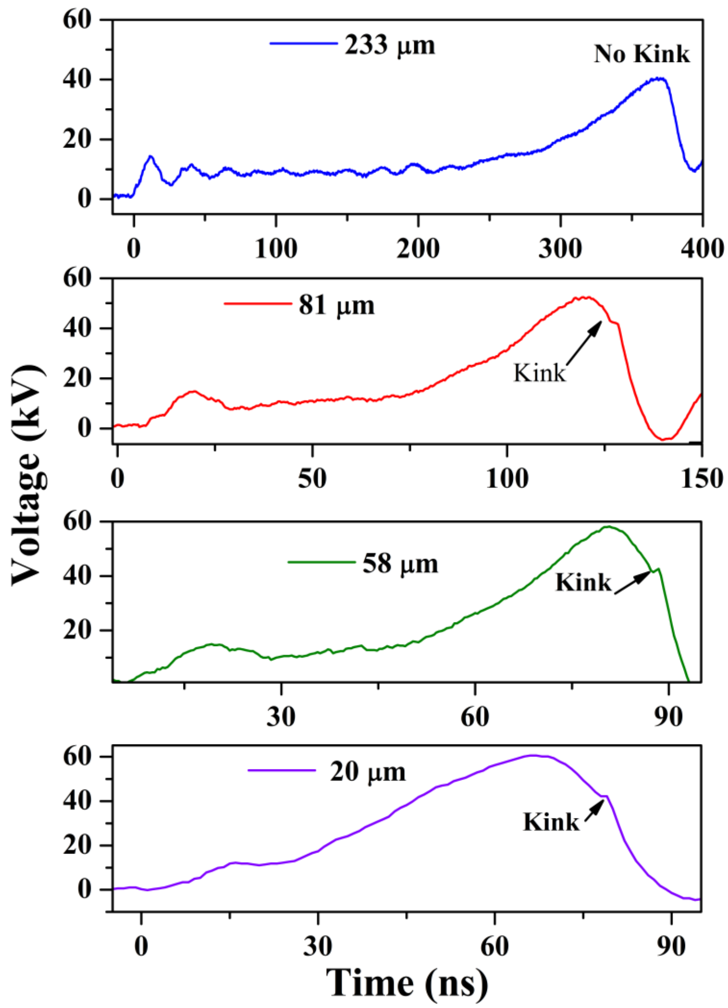

Fig. 4.5: Typical profiles of voltage across the wire for varying wire diameters at charging voltage of 40 kV.

Table-4.1: Effect of diameter and charging voltages on experimental characteristics (Time of burst, Specific Energy deposited and its rate along with observance of kink).

Diameter (μm)	Charging Voltage (kV)	Current rate ($\times 10^9$ A/s)	Time of burst (ns)	Specific Energy deposited (kJ/g)	Average Rate of Specific energy deposited up to burst (J/g/ns)	Kink Observed
58	16	39	170	6.5	38.2	No
58	20	48	150	7	46.7	No
58	30	72	97	8.1	85.2	Yes
58	35	84	95	9.8	97	Yes
58	40	96	88	10.6	120.4	Yes
81	16	39	240	10.5	43.7	No
81	20	48	208	11.7	56.3	No
81	30	72	151	12.2	80.8	Yes
81	35	84	143	13.1	91.6	Yes
81	40	96	120	13.6	113.3	Yes
233	16	39	735	12.5	17.0	No
233	20	48	630	14.5	23.0	No
233	30	72	464	15.6	33.6	No
233	35	84	411	17.2	41.8	No
233	40	96	395	18.8	47.6	No

It is interesting to note here that presence of kink is marked beyond those charging voltages where value of time taken for burst becomes almost constant (Fig. 4.3). This implies that more energy can be pumped into the exploding wire together with a higher value of current at nearly same time of burst using higher rate of rise of currents. Thus, experimental parameters which seem to be of significant importance for analysis of this study and considered are time of burst, specific energy, specific power (specific energy deposited averaged over time of burst), current density and rate of rise of current. Though the “Specific power estimate till burst” is generally not considered for EEW studies but it is considered in present study as this parameter takes into account the time of energy deposition, seems to be of more importance.

Dependence of specific energy deposited, burst time, average Rate of Specific energy deposited up to burst and appearance of kink on circuit parameters (diameter, charging voltage, rate of rise of current) are tabulated in Table 4.1. It is concluded from Table 4.1 that following two factors are essential for appearance of this kink in voltage profiles.

1. The threshold value of specific power (~ 80 J/g/ns) irrespective of diameter of wire.
2. The specific value of rate of rise of current, hence charging voltage, beyond which rate of decrease in time of burst goes minimal.

A pause or kink observed during the downfall of voltage profile after its peak appears to mark stagnation or transient rise in voltage for a short duration (~2 ns) indicating a rise in resistance contrary to continuous fall in voltage or resistance after burst. To understand the physical process of this voltage pause, a 1-D magnetohydrodynamic (MHD) numerical scheme, earlier utilized for electrically exploding foils [99], has been used.

4.2.2 Numerical Observations and Analysis

Brief description of this one-dimensional magnetohydrodynamic (1D MHD) code has already been given in chapter 2. This 1 D code has been first used to generate voltage and current profiles for a specific wire explosion in which kink is observed, using the present system parameters. These simulated current and voltage profiles are compared with experimental ones for a wire of diameter 58 μm exploded at a capacitor charging voltage of 35 kV. The two voltage profiles have been found in close match with each other as shown in Fig. 4.6 and a post burst pause is also distinctly visible in simulated profile [80]. Different parameters (Electrical resistivity, mass density, magnetic force, and current density have been considered for analysis and their radial distributions at five-time instants have been studied to explore the physical cause.

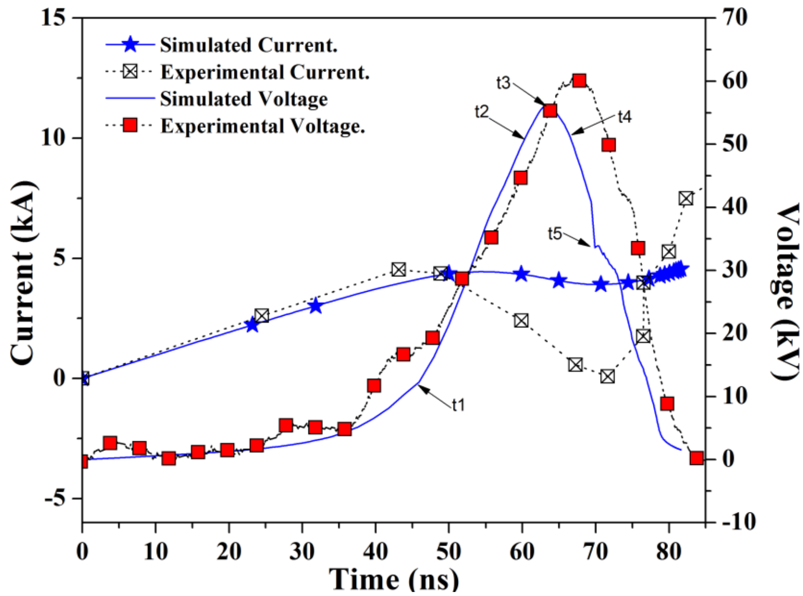

Fig. 4.6: Experimental and simulated profiles of voltage and current for wire of diameter 58µm exploded at a charging voltage of 35 kV. Five-time steps t_1 to t_5 are marked for detailed analysis

These five-time instants are chosen corresponding to different stages of wire manifested in voltage profile viz. start of vaporization (t_1), before peak (t_2), at peak (t_3), after peak (t_4), and near the pause (t_5) as shown in Fig. 4.6.

There are mainly two regimes; one before burst and other is after burst. Detailed analysis at these time instants hint towards the formation of a density front inside the wire which seems to be induced by non-uniform radial expansions in pre-burst regime. These two regimes are discussed separately; as given in following subsections; for better understanding.

4.2.2.1 Pre-burst Regime

Radial distribution of mass density, electrical resistivity, current density and Lorentz force ($\vec{J} \times \vec{B}$ multiplied by mesh volume) are determined in different meshes in pre-burst regimes at three different time instants (t_1, t_2 and t_3) as shown in Fig. 4.7. Mass density profiles in Fig. 4.7

shows that it is uniform over the wire radius till time t_1 and it decreases rapidly with time near the outer surface of wire as can be seen at time t_2 and t_3.

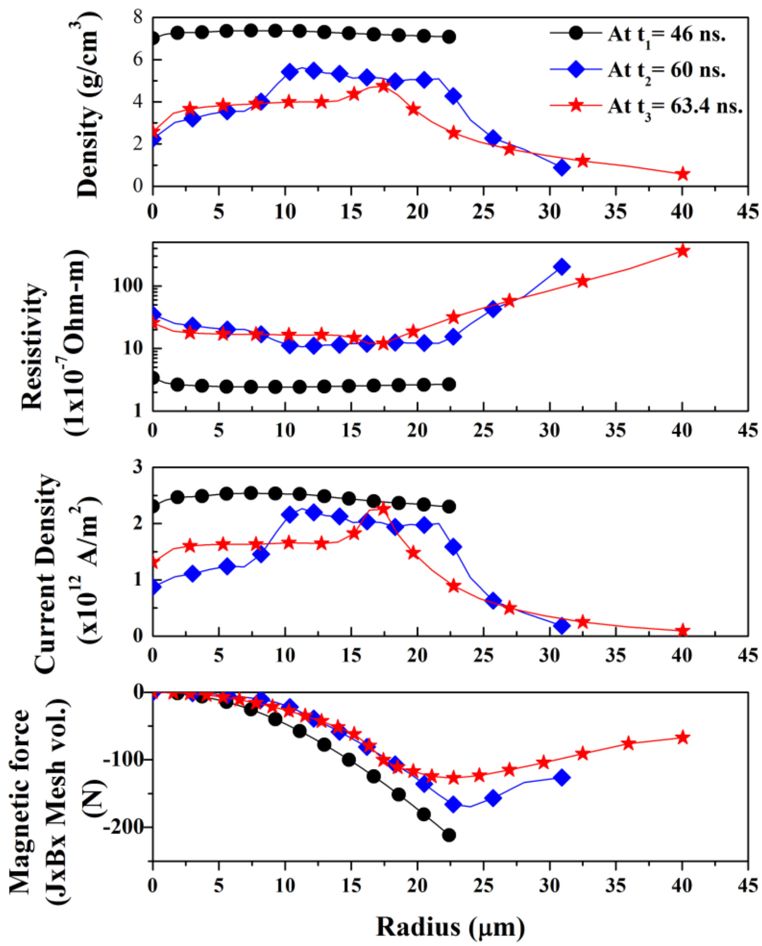

Fig. 4.7: Pre-burst behavior: Radial profiles mass density, resistivity, current density and Lorentz force acting on different meshes at three different time instances i.e. near to start of vaporization (t_1 = 46 ns), before voltage peak (t_2= 60 ns), and at voltage peak (63.4 ns).

It is also observed that this decrease in mass density is relatively slower in the inner regions. This difference in rate of fall in mass density at outer surface and in inner region seems to be due to the inertial effect of adjacent outer surroundings which comprises lower density polyimide at outer surface and higher density copper layers in inner regions. This radial non-uniform expansion across the wire evolves to appear like a density front near the time of voltage peak (t_2=60 ns). Since higher density region is expected to be more conductive as is the case for most of the metals [32], therefore current starts shifting with time from outer regions to inner regions of higher mass density as can be seen clearly in Fig. 4.7. Thus, difference in current densities across the wire radius causes difference in energy to be deposited in these regions leading to the spread of high-density front to nearby regions. However, Lorentz Force also peaks in the regions with higher mass density and current density, supporting the inertial forces responsible for slow expansion of inner regions of wire.

It is to be noted in simulation results that certain variations are visible near the axis (r=0), which looks to be caused by rigid boundary conditions (u=0, B=0) used in simulations. These variations can be attributed to numerical artefact and remain localized in a small region near the axis.

4.2.2.2 Post-burst Regime

Radial distribution of mass density and electrical resistivity, estimated from numerical simulations for instants t_4 and t_5, corresponding to the post burst region, is plotted in Fig. 4.8.

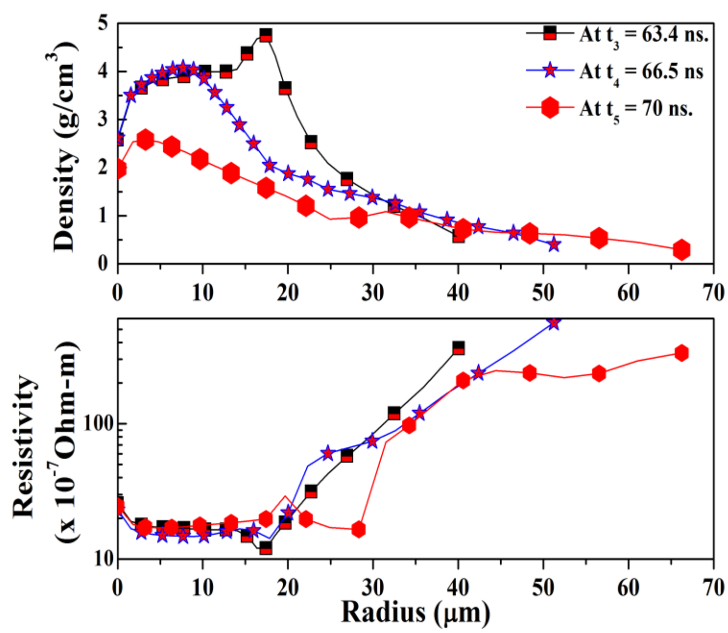

Fig. 4.8: Post-burst behavior: Radial profiles mass density, electrical resistivity of different meshes at three different time instances i.e. at voltage peak (63.4 ns), just after the peak (t_4 =66.5 ns) and at pause (t_5= 70 ns).

It is to be noted here that the voltage is an indicative marker of resistance of overall wire at any time instant, as the simulated current doesn't change much during the explosion process (Fig.4.6). Resistance of overall wire can be considered as parallel combination of resistances offered by its different radial sections. Thus, the region of least resistance in the parallel configuration of resistances; may have dominating effect on the voltage developed across the wire. The region of least resistance is expected to be of relatively higher mass density and current density. If these dominating regions of least resistance get transitionally disappeared then it can cause a pause or even slope change in voltage profile. In addition to this, spread of high-density regions in its vicinity also influences the radial distribution of mass density and its rate of fall with time hence change in slope of fall in resistivity profiles as can be noticed in Fig. 4.8. Therefore, it is inferred from simulation results that formation of a density front and its survival till burst, is responsible for observing a pause in post-burst voltage profile. It is confirmed by numerically simulating the radial profiles of mass density for wires corresponding to different diameters which differ in terms of experimental observation of appearance of strong kink or no kink as shown in Fig. 4.9. Simulation results (Fig. 4.9) show that a clear distinctive density front is noticed for wires of diameter 20 µm, 58 µm, and 81 µm where a kink is observed in voltage profiles. However, no structured density front is formed for wire of diameter 233 µm but has small radial perturbations till burst. Resistivity profiles shown in Fig. 4.9 indicates a transitional decrease in the resistivity values (difference between maximum to minimum value near front) for wires of diameters 20 µm, 58 µm and 81 µm because of associated density fronts in these wires. The non-uniform radial expansion of density and hence magnetic forces causes radial variation in resistivity whereas energy deposition in high density regimes tries to mitigate this non-uniformity.

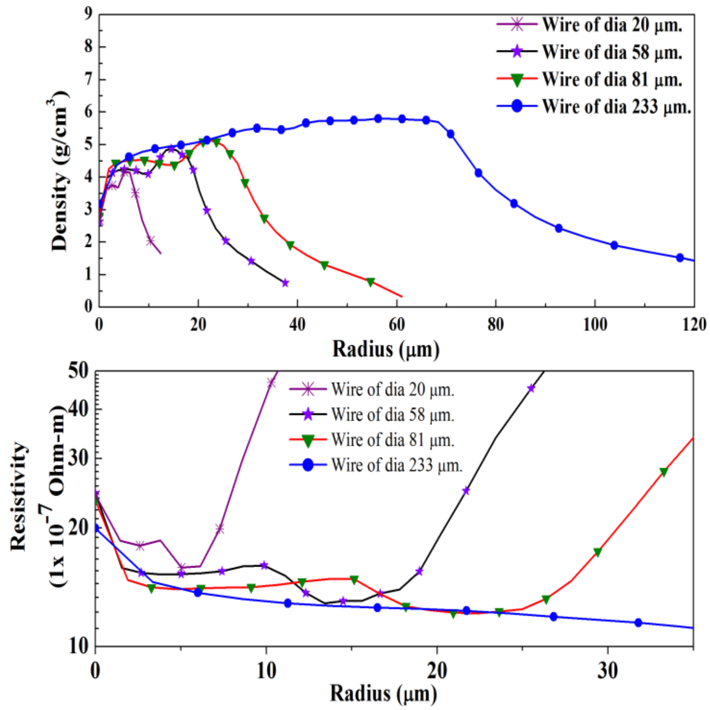

Fig. 4.9: Radial profiles of mass density for wires of diameters 20 μm, 58 μm, 81 μm and 233 μm at 40 kV in upper graph. An expanded view of corresponding resistivity profiles is shown in lower graph.

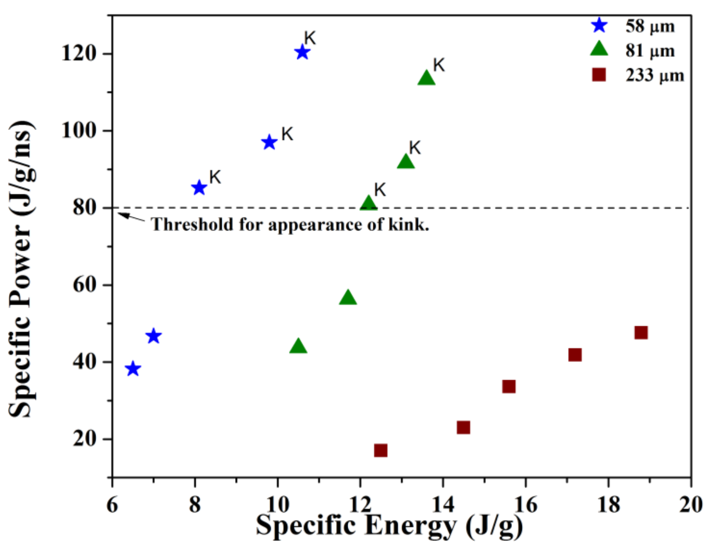

Fig. 4.10: Specific power vs. specific energy

The data listed in Table 4.1 confirms that this post burst feature appears in voltage profiles of those cases only where specific power exceeds 80-85 J/g/ns and this can be further seen in Fig. 4.10, where specific power has been plotted as a function of specific energy. This seems to be more important parameter than specific energy itself for bringing transitional changes after burst.

Further, it appears, from presently determined experimental conditions under which kink is observed and from results of numerical simulations, that if rate of specific energy deposition over the complete wire is higher than the energy corresponding to thermal expansions of wire then non-uniformities are expected to develop in radial mass density profiles, which in present case seems to be happening for wire of diameter 58 μm. In relatively thicker wires, for example wire of diameter 233 μm, the time of burst is relatively large and rate of energy deposition is slower where there is more probability of uniform expansion till burst against the probable transient appearance of density fronts. Thus, rate of specific energy deposition is an important criterion to clarify the appearance of kink.

4.3 Results of Electron Density Measurement using Laser Interferometer

Laser Interferometer is employed to measure electron density distribution of exploding wire radially as well as axially. Interferograms are recorded at two different time instants; one prior to kink and other after the kink; to probe electron densities in shots where kink is observed.

Basic details of interferometer and methodology used for radial and axial electron density measurement using single frame of camera are already elaborated in chapter 2. Exploding wire plasma is assumed as cylindrically symmetric around the wire axis. The size of laser beam is optically expanded to a diameter of 20 mm to probe the complete-wire length, but some portions of interferogram on both the ends (near anode and cathode) are obscured due to load assembly components. Vertical axis of the interferogram (bottom to top) which is along length of the wire is calibrated with respect to already known distance between anode and cathode.

Before Kink

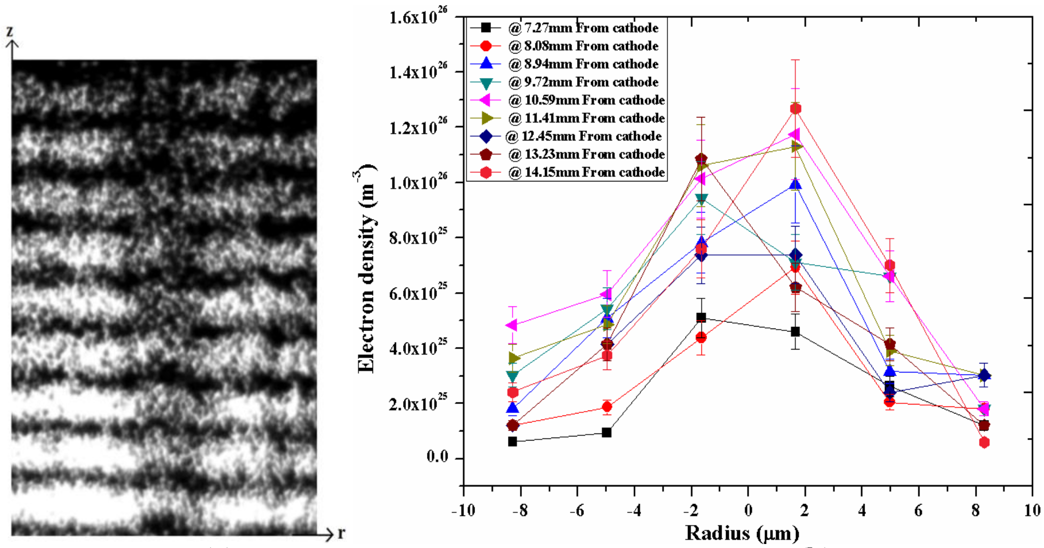

(a) (b)

Fig.4.11: (a) Interferogram captured for exposure time of 14 ns till time of kink and (b) Electron density profile inferred corresponding to interferogram in (a).

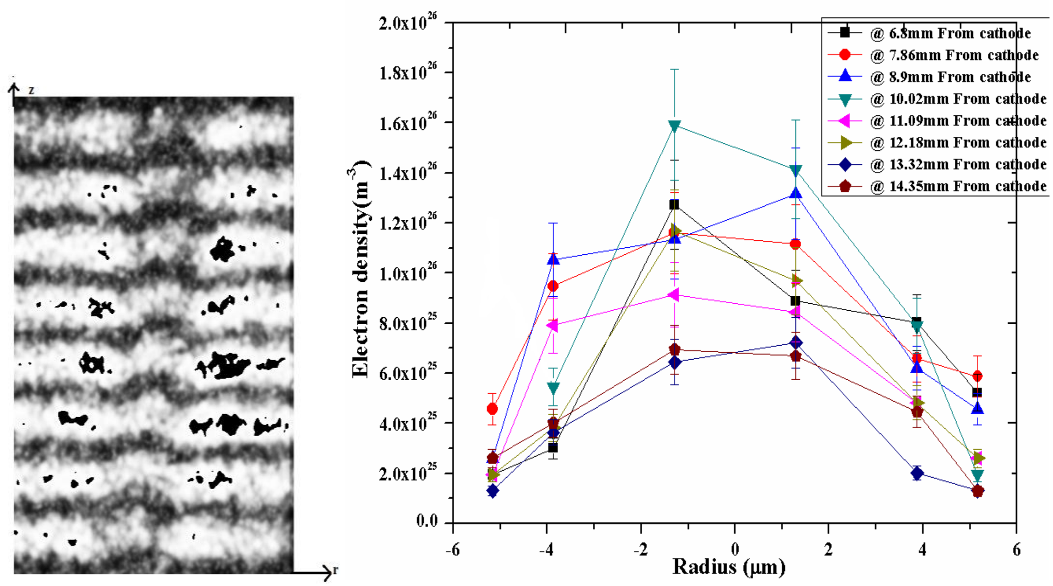

(a) (b)

Fig. 4.12: (a) Interferogram captured for exposure time of 14 ns till time of kink for second shot repeated under same conditions, (b) Electron density profile inferred corresponding to interferogram in (a).

After Kink

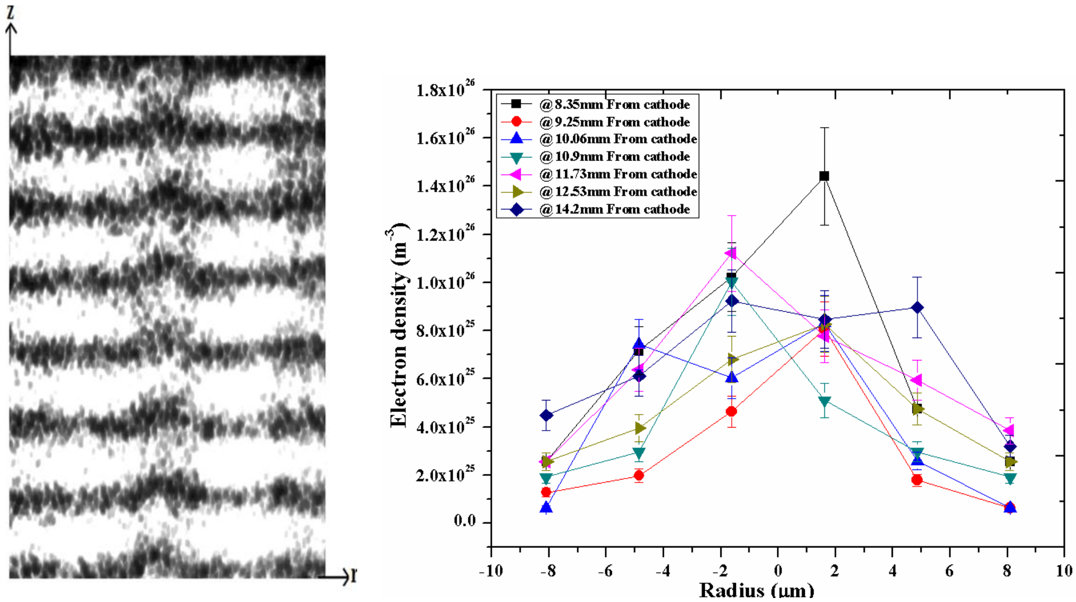

(a) (b)

Fig. 4.13: (a) Interferogram captured for exposure time of 14 ns just after time of kink, (b) Electron density profile inferred corresponding to interferogram in (a).

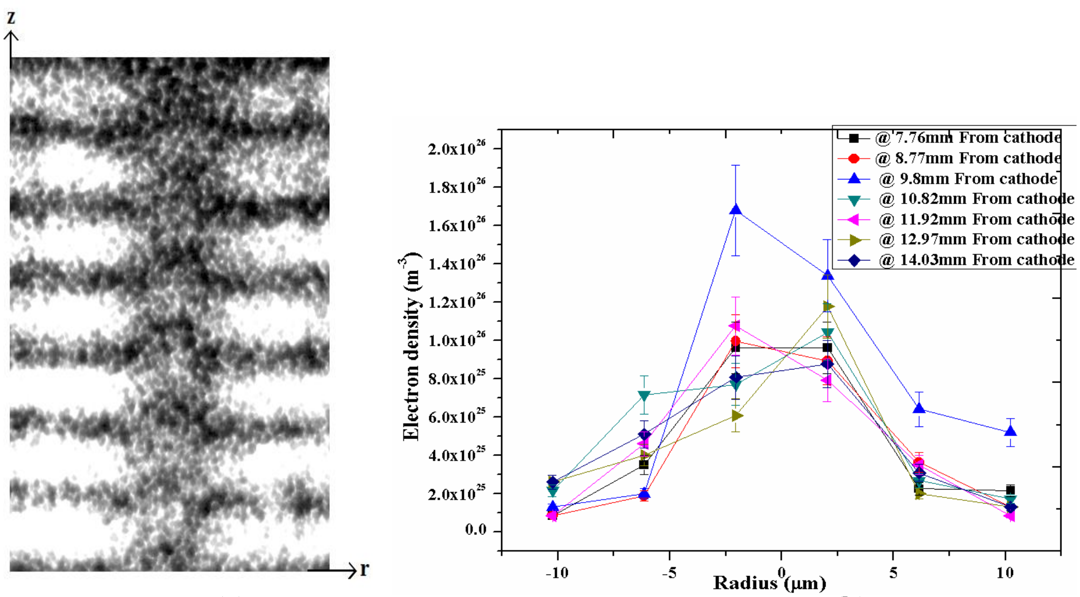

(a) (b)

Fig. 4.14: (a) Interferogram captured for exposure time of 14 ns just after kink for second shot repeated under same conditions, (b) Electron density profile inferred corresponding to interferogram in (a).

Interferograms are shown in Fig. 4.11 to Fig. 4.14 for explosion of coated copper wire of 58 μm diameter at charging voltage of 35 kV. Corresponding radial and axial profiles of electron densities estimated by using the methodology discussed in Chapter 2, at centers of different cylindrical shells, are also shown along with interferograms in each figure. Experiments were repeated with same circuit parameters. Among the four interferograms shown in Fig.4.11- Fig. 4.14; Fig. 4.12 and Fig. 4.14 are repeated shots for same circuit parameters corresponding to Fig. 4.11 and Fig. 4.13 respectively.

The triggering of camera corresponding to start of frame exposure (14 ns) is synchronized with time instants just before the kink (Fig. 4.11 and Fig. 4.12) and just after the kink (Fig. 4.13 and Fig. 4.14). Since minimum frame exposure time of camera is 14 ns (due to limitations of present camera), so these profiles of electron densities are time integrated over that duration of exposure of camera before kink and after kink.

Electron density profiles differ in these cylindrical shells along length of wire; but not by orders of magnitude; even in repeated shots (keeping all other parameters same). It was expected in these experiments that electron density in both shots (before and after kink) repeated independently can show some variation in electron density profile radially and axially because plasma column formed in EEW could be prone to instabilities [54].

Table 4.2- Range of electron densities measured over the length of wire near wire axis at fixed radii (2 µm and 5 µm) before and after instant of kink.

S.No.	Till time of kink		S.No.	After time of kink	
	2 µm	**5 µm**		**2 µm**	**5 µm**
Shot 1 (Fig. 4.11)	4×10^{25} m^{-3}- 1.2×10^{26} m^{-3}	1×10^{25}-7×10^{25} m^{-3}	Shot 3 (Fig. 4.13)	4×10^{25} m^{-3}- 1.4×10^{26} m^{-3}	2×10^{25}-9×10^{25} m^{-3}
Shot 2 (Fig. 4.12)	5×10^{25} m^{-3}- 1.25×10^{26} m^{-3}	1×10^{25}-6×10^{25} m^{-3}	Shot 4 (Fig. 4.14)	6×10^{25} m^{-3}- 1.7×10^{26} m^{-3}	5×10^{25}-8×10^{25} m^{-3}

Electron density is found in range of around $1x10^{25}/m^3 – 1.7x10^{26} /m^3$ with lowest at outer most radius to highest at inner most core along the length.

From the results of experimental measurements of electron densities listed in Table-2, it may be inferred that at closer distance to center viz. 2 μm, electron densities do not differ much but range of electron density is slightly higher at same radial distance (5 μm) after kink than before kink hinting more electron density after pinch at this distance.

Chapter-5

Experimental Investigations on Effect of Material Properties on EEW Characteristics in Air and Vacuum

Energy deposition and its rate influence the temperatures and pressures generated in the process of electrical explosion. These parameters also affect the development of instabilities and hence non-uniformity in expansion of exploding wires plasma. Energy deposition and its rate are crucial parameters in electrical explosion dynamics and in determining the utilization of electrically exploding wires (EEW) for various applications like opening switches, radiation emission, shock wave formation, and nano particles generation. In inertial confinement fusion studies also, the specific energy deposited till time of implosion has a bearing on the residual mass left in wire array and hence in contribution of radiation emission.

Various parameters which can influence energy deposition are temporal current profile, polarity, geometry of load, surrounding medium, dimensions and material of wire etc. Among these circuit parameters, the current rate and material of wire in a specific medium (with all other factors kept fixed) can significantly drive mode of explosion [27], [30], [67], [69], [70], [84]. Slow and fast regimes with current rise rates of < 20A/ns and > 100A/ns, respectively [27], [30], [84] have different explosion mechanisms. If energy deposited up to the burst is a significant fraction of energy required for complete vaporization of wire then uniform and rapid expansions are expected as reported in [65], [112]. However, at a specific current rate, mode of explosion for wire in particular surrounding medium depends upon properties of the metal used [28], [65], [67], [82], [112]. If parallel energy diverting channels are formed in the process of explosion till burst then energy is not deposited uniformly across mass of wire [28], [76], [112]. It depends upon properties of metal and surrounding medium which can support formation of these parallel energy diverting channels.

On the basis of similarity in electrical characteristics exhibited in explosion process, metals are generally categorised into [83] two groups viz. refractory metals and non-refractory metals or also referred to as “tungsten” group and “copper” group, respectively. However, based on the characteristics mixed to both the groups shown by some metals (e.g. Fe, Ni, Pt and Pd), Romanova et al. [67] have introduced a third category known as Nickel group. Tungsten group comprises metals like W, Mo, and Ti whereas copper group includes Au, Ag, Al, Cu, Zn, Sn and Cd etc. The former group metals have relatively higher boiling point and melting point along with higher resistivity, and hence exhibit characteristic of earlier breakdown in desorbed gases along the wire surface. Therefore, relatively lesser energy is deposited up to time of burst in these metals especially in a surrounding medium where lower ionised parallel discharge channel or corona is more supported and facilitated.

This chapter presents the experimental investigation carried out to understand the effect of wire material on fast electrical explosion characteristics for high current rate of 90 A/ns in two different surrounding media (air and vacuum). For this purpose, six metals Cu, Au, Al, Ti, Pd and W covering a wide range of atomic numbers (low to high) and representing the three different groups have been chosen. Dependence of electrical and thermophysical properties of various materials on parameters linked with energy deposition is discussed. The parameters which are considered for this study and related to deposition of energy are “specific energy deposition, and overheating factor ‘K’; Here, ‘K’ is defined as the ratio of specific energy deposited till burst to the enthalpy of atomization”. Other parameters which have been considered are voltage profiles, burst current, time durations for various stages of wire explosion. These time instants corresponds to the stages viz. time up to melting t_m, and time of burst t_b as per reported work in [23], [24]. Timings for different stages are referenced with respect to the start of the current (or dI/dt) labelled as t_o. Accuracy in measurement of time of different events is decided by the sampling rate of oscilloscope and for all the results reported in present work, it is 0.4 ns. Thus, error in t_b-t_m, t_m-t_o is ± 0.8ns.

To have in-sight into the possible mechanisms involved in the explosion process, the temporal profiles of optical emission have also been measured experimentally using streak camera.

Dependence of energy deposition parameters on electrical and thermophysical properties can be useful as a qualitative criterion for selection of metals in two different media for specific application. Some novel and unconventional behavior observed in these experimental studies in contrast to previously reported similar works [84], [85] are mentioned and discussed in this chapter.

5.1 Effect of Electrical and Thermophysical Properties of Metal on Electrical Explosion Characteristics

To understand the effect of thermophysical and electrical properties of metals on electrical explosion characteristics and temporal profiles of optical emission in air and vacuum; experiments have been conducted on wires of various metals including both refractory and non-refractory type. The experimentally measured parameters used in predicting the behaviour of EEWs and correlating these with electrical and thermophysical properties of metals are presented in this section. The values of some general properties of metals utilized for this purpose are taken from literature as given in Table 5.1. The metal Pd has been found to exhibit mixed electrical characteristics of both groups in present experiments as also reported by Romanova et al. [67] and hence categorized in third group. However in present work, trend of dependence of electrical and thermophysical properties of Pd on overheating (specific energy deposition) is found to be closer to that of refractory group metals. So, for better explanation and understanding, it is discussed along with refractory group metals.

Table 5.1: Material properties of wires under investigation

Metal	Resistivity at Room Temperature and atmospheric pressure ($x10^{-8}$ Ω-m) [23],[112],[113]	Melting Temperature [112],[113] (K)	Boiling Temperature [112],[113] (K)	Speed of sound at Room Temperature [114] (m/s)	Enthalpy of atomization [115] (kJ/mol)
Non-Refractory metals					
Cu	1.7	1358	3200	4760	339
Au	2.4	1337	3129	3250	368
Al	2.7	933	2792	6400	326
Refractory metals and Pd					
W	5.6	3695	5828	5220	860
Pd	11.0	1828	3236	4680	377
Ti	41	1941	3560	6160	471

5.1.1 Electrical Explosion in Air

Experimentally measured parameters for six wires exploded in air medium at atmospheric pressure are listed in Table 5.2. Further, the typical experimentally measured resistive voltage profiles are shown in Fig. 5.1 (a). To mark the clear indications of time instants up to melting and burst, the expanded view of voltage profile along with current profile for copper is shown in Fig. 5.1 (b).

Table 5.2: Observed experimental parameters for electrical explosion of wires in air.

Metal	t_b[1] (ns) [±5 ns]	V_p[2] (kV) [± 3%]	I_b[3] (kA) [± 3%]	E_b[4] (J) [± 6%]	E_{sb}[5] (kJ/mol) [± 6%]	E_p[6] (1x 10^{-3} eV/ atom/ns)	K factor [± 6%]	t_m-t_o (ns) [± 0.8ns]	t_b-t_m (ns) [± 0.8 ns]	t_{so}[7] (ns) [± 2 ns]
Non-Refractory metals										
Cu	255	41	21	41.61	1207.5	49	3.6	180	75	170
Au	190	41.4	19	25.54	1063.8	58	2.9	140	50	127
Al	185	46	18	21.18	863.4	49	2.65	140	45	>103
Refractory metals and Palladium										
W	200	24	13	23.7	919.2	48	1.06	130	70	109
Pd	250	37	17	32.34	1170.4	49	3.1	120	130	109
Ti	210	28	12	27.75	1196.8	59	2.54	71	139	111

1. t_b : Time of burst;
2. V_p : Peak Resistive Voltage
3. I_b: Burst Current
4. E_b: Energy Deposited up to burst
5. E_{sb} : Specific Energy Deposited up to burst
6. E_p : Time averaged energy deposited per atom up to burst
7. t_{so} : Time of start of optical Emission

5.1.1.1 Non-refractory Metals

As listed in Table 5.2, the experimentally determined overheating factor (K) for non-refractory group of metals Cu, Au and Al, display a monotonous reduction upon moving from Cu to Al. This monotonically decreasing overheating factor follows the decreasing trend in initial electrical resistivity from Cu to Al (Table 5.1 and Fig. 5.2). Similar kind of trend is also followed with energy deposited up to burst and time of burst in these metals. Unlike a correlation of overheating factor, energy deposited up to burst and specific energy deposited with the initial resistivity, no correlation of these quantities with enthalpy of atomisation has been observed. To the best of author’s knowledge, the examination of dependence of overheating factor on initial

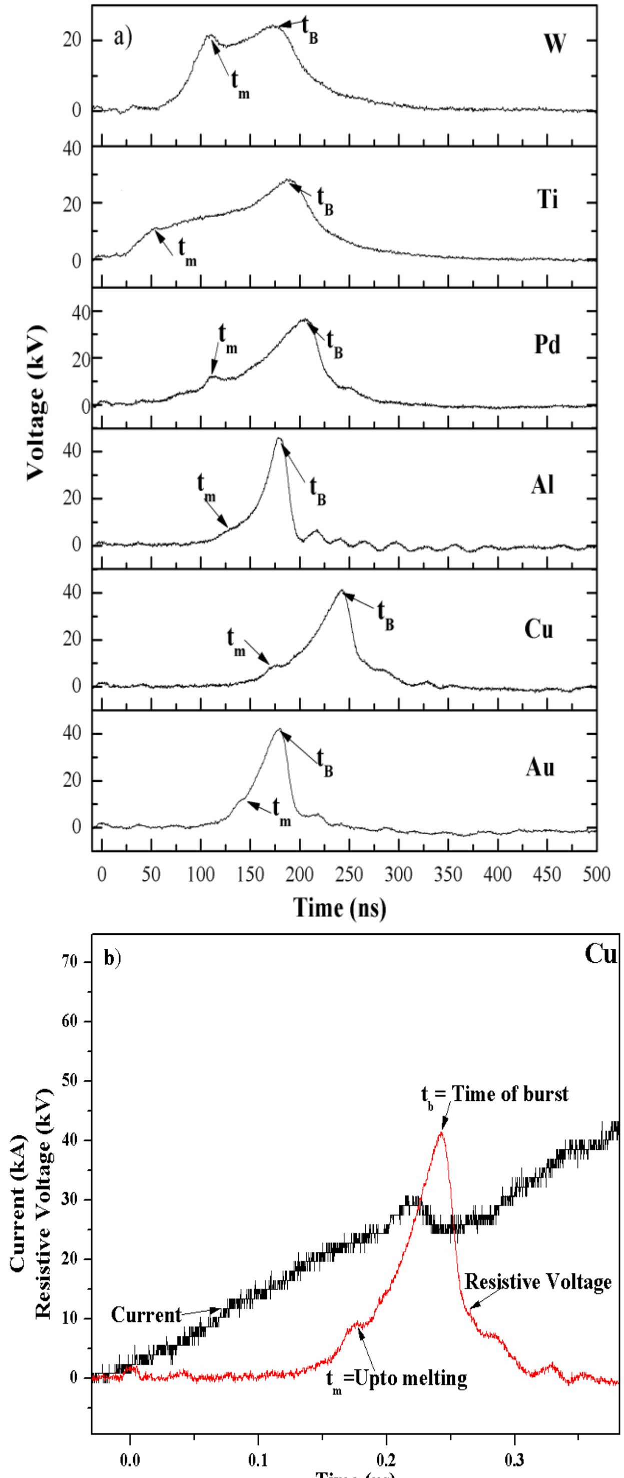

Fig. 5.1: (a) Typical voltage profiles of all six metals in air, (b) Expanded Illustration of Current and Voltage profiles with indication of time instants of melting & burst for copper wire.

resistivity and enthalpy of atomisation particularly for explosion in air at atmospheric pressure for the presently investigated metals has not been reported so far in literature.

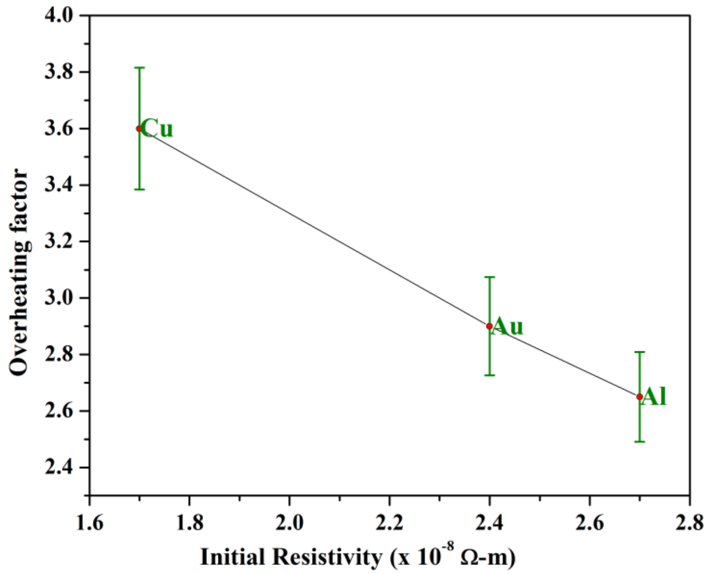

Fig. 5.2: Dependence of overheating on initial resistivity of non-refractory metals considered

Present observed behaviour of non-refractory metals can be understood by considering the two processes involved, one is the formation of parallel weakly ionised channels around the wire and other is the energy deposition within the wire. Since these metals are highly conducting, so the process of energy deposition is expected to dominate as major current is likely to flow within the wire instead of parallel weakly ionised channels formed during the process of explosion.

Temporal optical emission profiles have also been looked into for observing signatures of such parallel channel formation. These optical emission profiles have been recorded in streak mode of camera with total sweep duration of ~200 ns. Sweep rate of streak is set to be 100 ns/cm with total sweep length of 2 cm and temporal resolution of 2 ns. The minimum spectral sensitivity of photocathode in camera used is 20mA/W and sensitivity of camera is kept same for all metal wires by using same neutral density filter of optical density 2.0 in front of focussing lens. The recorded optical emission profiles along with radial expansion profile of outermost boundary of self-emitted light observed in these streak records is displayed in Fig. 5.3. The obtained streak images (8 bit gray scale) are digitally analyzed to get the line intensity profiles perpendicular to wire axis at different time instants. In these plots (Fig. 5.3), first point corresponds to the instant at which light becomes discernible in streak image and intensity on axis crosses the background level (dark) by a significant amount (minimum 2.5 times). The time of start of optical emission with respect to start of current inferred from these plots are listed in Table 5.2. It can be noticed from Table 5.2 that light emission starts much before the burst as indicated in the streak images and corresponding graphs. Recently, Liu et al. [117] have also reported temporal profiles of light emission in EEW of Al in argon gas at ambient pressures using streak camera. In their reported work also, light also started appearing much before the burst. This light appears to be arising due to weak ionisation of desorbed gases around the heated wire. Diameter of this luminous pattern is obtained by marking the points at which intensity falls at nearly 50% of its peak values.

Now as reported in earlier works [28], [68], [116] also, some portion of current can be diverted in outer corona developed around wire apart from current flowing through the central conducting part of wire. If major current flows for longer duration before current is diverted or shunted in outer ionised channels till burst then more energy can be deposited in the wire. Since non-refractory metals are highly conducting metals, it is expected for current to flow through central conducting part instead of outer ionised channels for longer durations and contribute in relatively more energy deposition. The occurrence of breakdown as inferred from the light emission (Fig. 5.3 and table 5.2) is much before the burst for all the three metals. The occurrence of breakdown much before the burst can be associated with the formation of weakly ionised channels. Further, the breakdown appears earliest for Al followed by Au and then for Cu (Fig. 5.3 and Table 5.2) with similar trend seen for the time taken from melting to burst. These facts

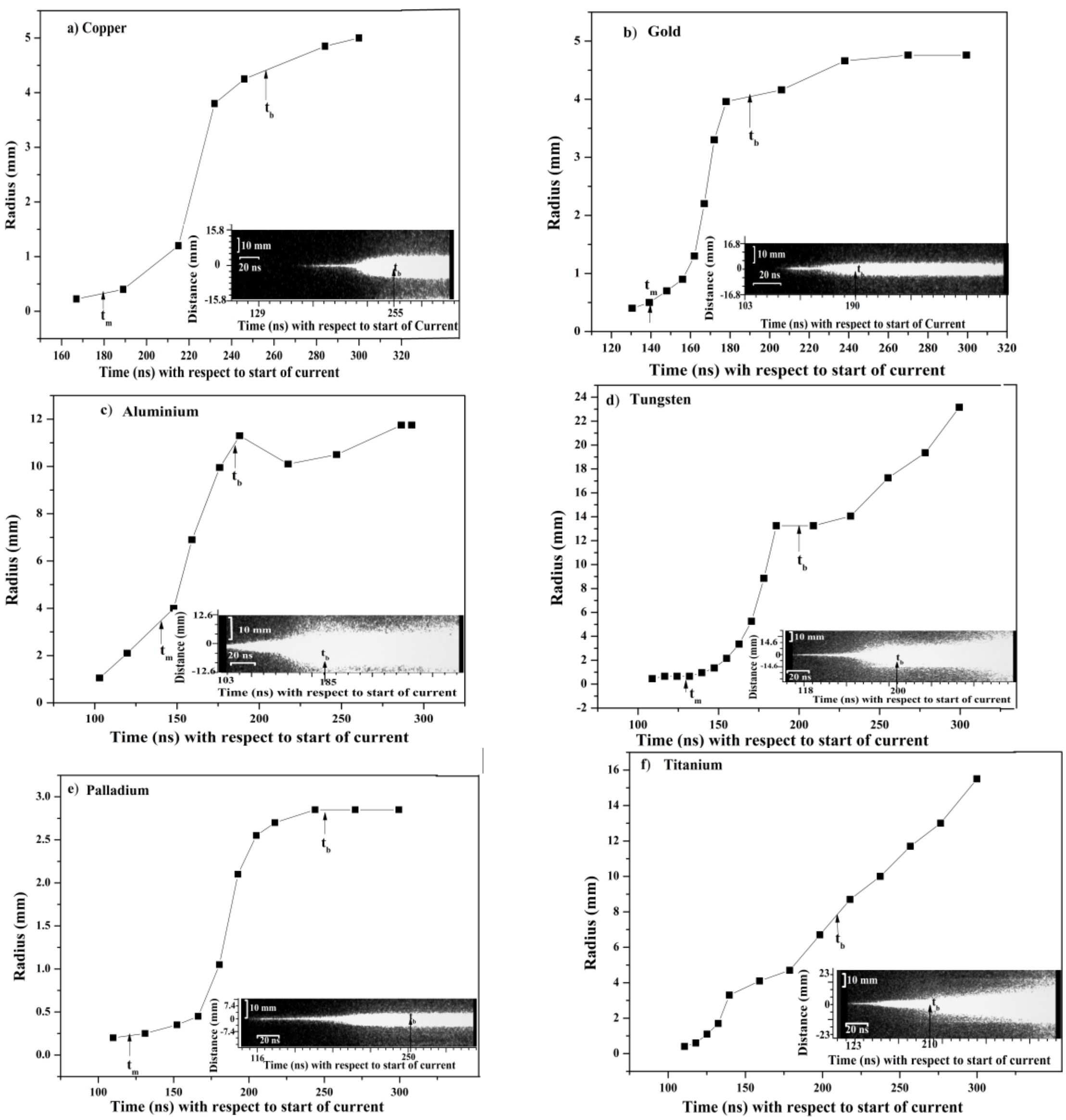

Fig. 5.3: Radial expansion of light emitted and Streak photographs of optical emission from EEW in air a) Copper, b) Gold, c) Aluminium, d) Tungsten, e) Palladium and (f) Titanium with sweep speed of 100 ns/cm

can be related to their initial electrical resistivity, i.e. the higher initial electrical resistivity implies earlier breakdown and the burst. Thus, it can be concluded that the duration for which energy deposition occurs can be elongated for non-refractory metal of lower initial electrical resistivity.

Another inference drawn from radial profile of self-emitted light expansion is that sound velocity (Table 5.1) in specific metal, which is highest for Al and lowest for Au, seems to govern radial expansion of these channels in these metals (Fig. 5.3).

5.1.1.2 Refractory Metals and Palladium

As can be inferred from the Fig. 5.1, the rate of change in voltage especially from melting to time up to burst and its peak value in metals of this group is smaller than that for the metals of non-refractory group.

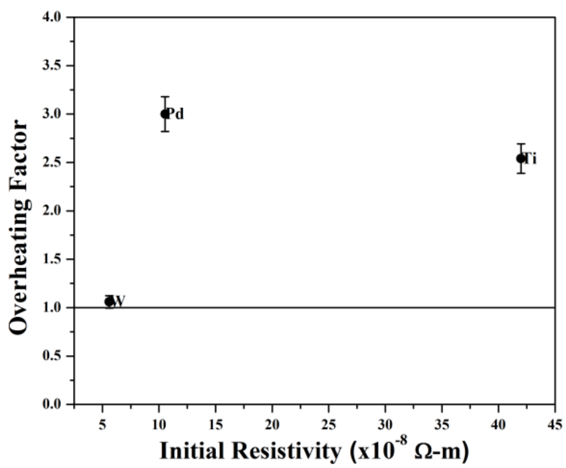

(a)

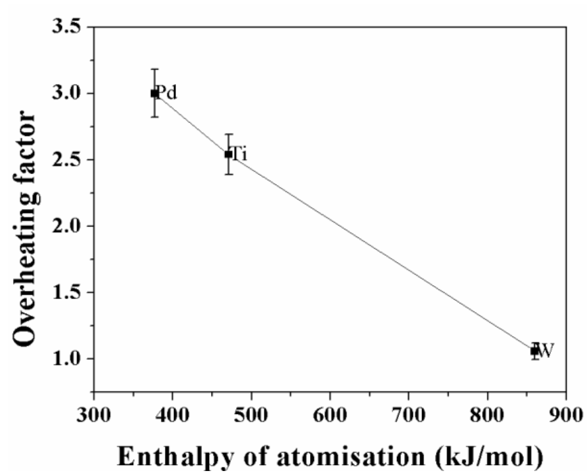

(b)

Fig. 5.4: Comparison of experimentally observed overheating factor with (a) initial resistivity and (b) Enthalpy of atomisation in Pd, Ti and W for EEW in air.

In contrast to non-refractory metals, in these metals, no consistent trend is found in time of burst, specific energy deposited up to burst, and overheating with initial resistivity of metals (Fig. 5.4 (a)).

Metals of this group seem to follow a trend of inverse relationship with enthalpy of atomisation as shown in Fig. 5.4 (b). This behaviour can be understood by the processes which can influence the process of energy deposition. These metals have relatively higher resistances and higher melting and boiling temperatures as compared to the non-refractory metals. The higher melting and boiling temperatures with comparative values of work function of these metals make them suitable for relatively higher surface thermionic emission of electrons than other metals (non-refractory metals). All these factors along with presence of significant desorbed gases can be a cause for earlier breakdown and diversion of energy from wire core. This leads to lesser energy deposition till burst hence relatively lower value of overheating is expected in these metals than that for non-refractory metals.

Further it may be noticed that the overheating in Pd is found to be little higher than that for the two non-refectory metals Au and Al as well the two refractory metals W and Ti. The W has least value of overheating among these metals. Possible reasons for lesser energy deposition in Ti and W than Pd among these metals could be as follows:

1. Since W has highest melting point among these three metals so it is more likely to expect earlier breakdown and current diversion in outer ionised parallel channels in comparison to other two metals.
2. Since behaviour of resistivity is anomalous in Pd and Ti where resistivity decreases with temperature during liquid heating [85], so it is expected that current would continue to flow through cores of these metal wires for duration longer than that for W.

Unlike that for the non-refractory metals, the experimentally observed trend for time taken for start of optical emission as inferred from the temporal profiles (Fig. 5.3) of these metals also does not exhibit any correlation with initial resistivity.

This optical emission appears to be arising due to ionisation of desorbed gases around the heated wire. In case of surrounding mediums like air or vacuum, expansion of metal vapours or desorbed gases from wire surface can result in formation of weaker parallel conducting channels in its surroundings. Apart from general conventional mechanisms of corona formation due to desorbed gases, other possible mechanisms of current diversion are also reported [67], [114] recently. These mechanisms indicate novel possibilities viz. breakdown in ambient gas compressed by shock waves [114] and role of metastable expanded liquid [67] in formation of corona and shunting channels in outer region of wire.

As weaker optical emission starts almost at same time instants in these three metals, therefore, it is difficult to correlate differences in specific energy deposition up to burst for these three metals from optical emission profiles. Further, it may be noted that the behaviour of radial expansion of light emission for Pd is similar to that of non-refractory metals whereas that for W and Ti, it differs significantly with no saturation and continuous expansion even after burst indicating the diversion of electrical energy to outer ionised channels.

5.1.2 Electrical Explosion in Vacuum

Experimentally observed voltage profiles for all metal wires exploded in vacuum are shown in Fig. 5.5 and various parameters obtained from the experiments are listed in Table 5.3. One common feature observed for all the metals for parameters related to energy deposited up to burst from Table 5.2 and Table 5.3 is that theses quantities are somewhat smaller for explosion in vacuum than those for explosion in air.

Other experimental outcomes for metals of two groups are discussed separately as follows:

5.1.2.1 Non-refractory Metals

Voltage profiles shown in Fig. 5.5 indicate that non-refractory metals show similar voltage profiles as observed for explosion in air with sharp single peaks but time duration for melting to burst is reduced considerably for explosion in vacuum (Table 5.2 and Table 5.3).

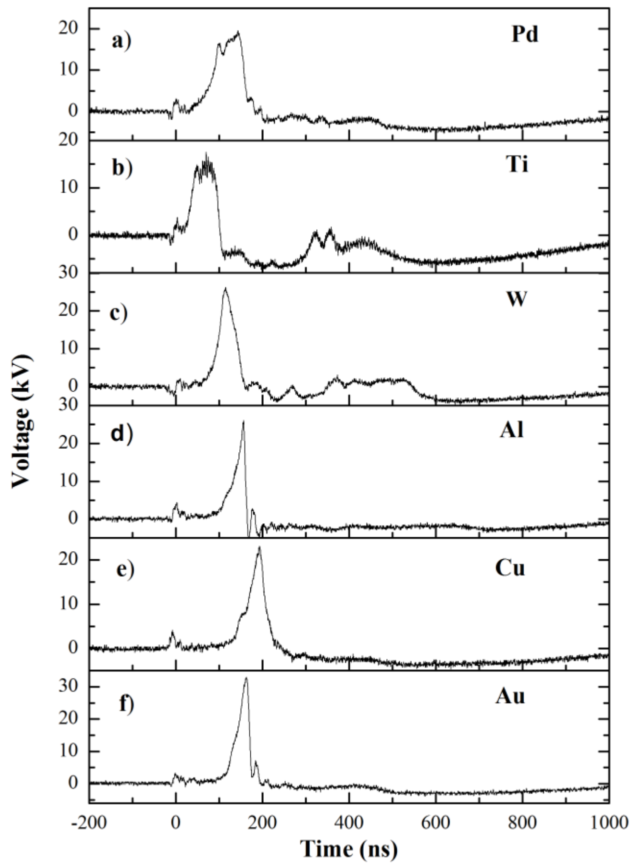

Fig. 5.5: Voltage profiles of a) Pd, refractory metals: b) Ti& c) W and non-refractory metals: d) Al e) Cu f) Au in vacuum.

Though the trend of time of burst is similar to that observed in air i.e. it is largest for Cu followed by Au and then Al but this is not true for energy deposition (Fig. 5.6 (a)). Unlike that for the explosion in air, the specific energy deposition in this case is largest in Au followed by Cu and then Al. Also, the value this quantity for all the three metals decreased significantly by changing surrounding medium from air to vacuum.

Further, earlier reported work [84] on electrical explosion of wires in vacuum indicate that overheating up to burst in metals of both the groups is inversely proportional to enthalpy of atomisation for slow (20A/ns) as well as fast (120A/ns) explosions. However, this is not found to be true for present case (Fig. 5.6 (b)) where current rate is of ~90A/ns. As may be noticed from Table 5.1 and Table 5.3 that though the enthalpy of atomisation of Cu and Al does not differ significantly, the overheating is significantly larger for Cu than that for Al (Fig. 5.6 (b)).

Table 5.3: Observed experimental parameters for electrical explosion of various metal wires in Vacuum

Metal	t_b[1] (ns) [±5 ns]	V_p[2] (kV) [± 3%]	I_b[3] (kA) [± 3%]	E_b[4] (J) [± 6%]	E_{sb}[5] (kJ/mol) [± 6%]	E_p[6] (1x 10^{-3} eV/ atom/ns)	K factor [± 6%]	t_m-t_o (ns) [± 0.8 ns]	t_b-t_m (ns) [± 0.8 ns]	t_{so}[7] (ns) [± 2 ns]
Non-Refractory metals										
Cu	210	24	21	14.24	416	20	1.2	179	33	153
Au	170	34	18	12.30	512.2	31	1.4	154	20	135
Al	160	23	18	0.86	35.1	22	0.1	134	27	>84
Refractory metals and Palladium										
W	120	27	11	6.16	239.2	21	0.3	-*	-*	90
Pd	152	18	13	12.05	434.6	30	1.1	-	-	92
Ti	83	15	7	2.66	115.2	14	0.2	-	-	>80

1. t_b : Time of burst
2. V_p : Peak Resistive Voltage
3. I_b: Burst Current
4. E_b: Energy Deposited up to burst
5. E_{sb} : Specific Energy Deposited up to burst
6. E_p : Time averaged energy deposited per atom up to burst
7. t_{so} : Time of start of optical Emission

*: Time instant corresponding to melting, is not observed distinctly

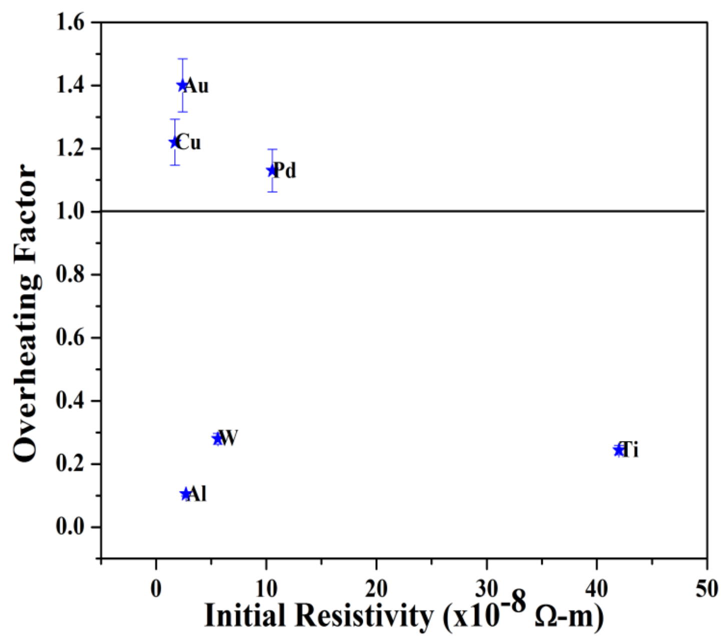

(a)

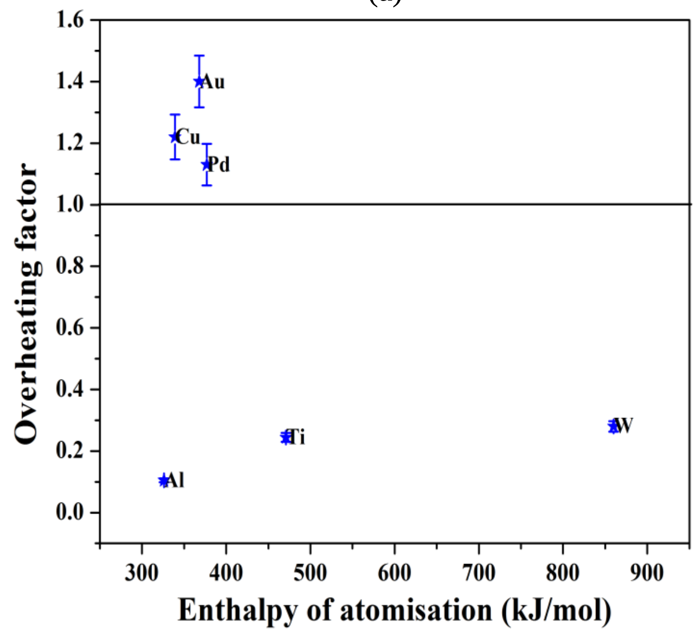

(b)

Fig. 5.6: Comparison of experimentally observed overheating factor with a) Initial Resistivity and b) enthalpy of atomisation for all metal wires electrically exploded in vacuum

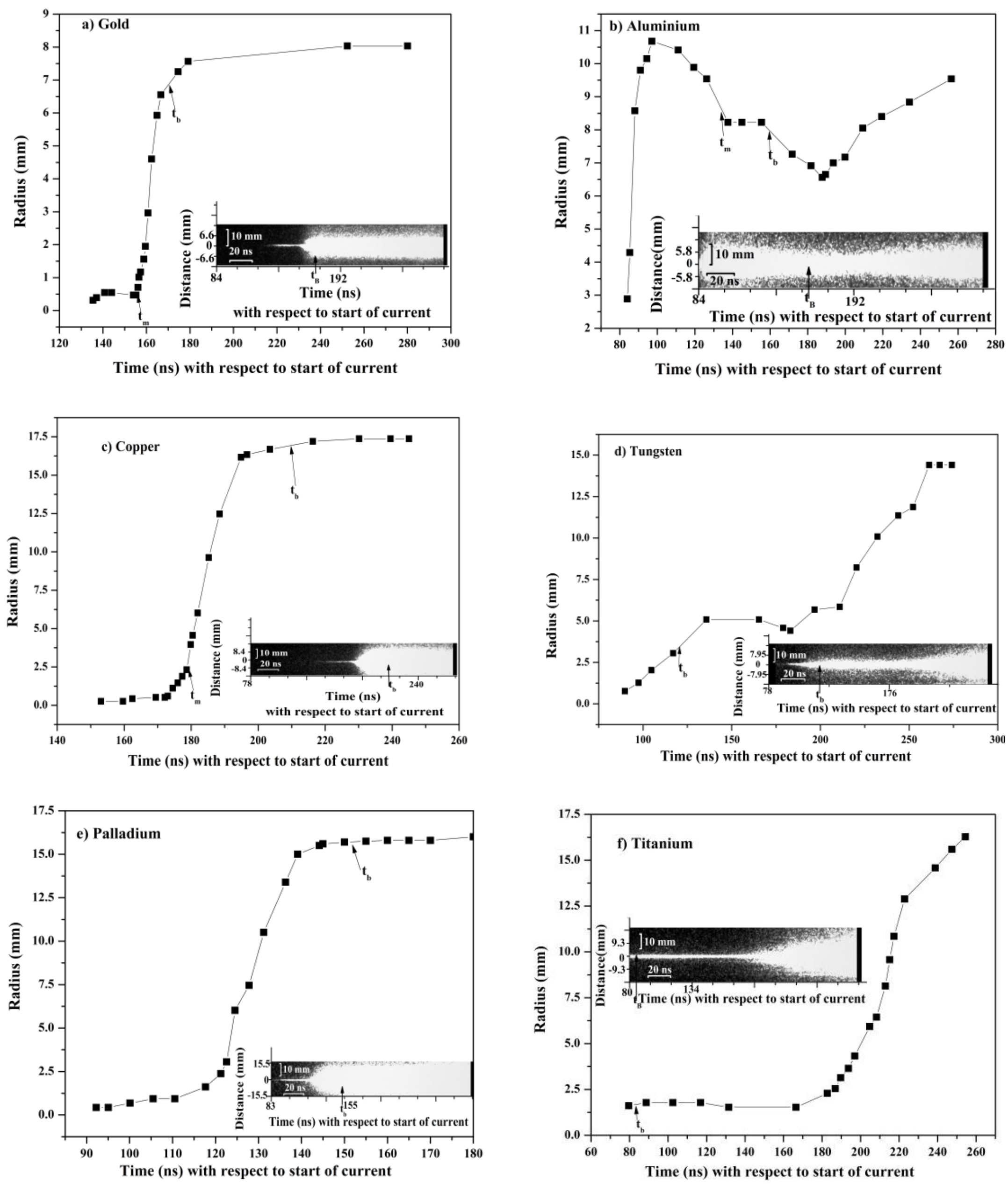

Fig. 5.7: Radial expansion of light emitted and Streak photographs of optical emission from EEW in vacuum a) Gold, b) Aluminium, c) Copper, d) Tungsten, e) Palladium and (f) Titanium with sweep speed of 100 ns/cm; minimum spectral sensitivity of photocathode in camera used is 20 mA/W. Sensitivity of camera is kept same for all metal wires using same neutral density filter of optical density 0.5 in front of focussing lens.

Temporal optical emission profiles (Fig. 5.7) of these non-refractory metals are similar to that observed for explosion in air except additional feature seen in Al. In case of Al, decrease in radius of optical emission to a minimum is more significant in vacuum as compare to that in air and also this reduction in radius initiates even before time of burst. Time taken to start optical emission is smaller for metal with higher resistivity and expansion after burst appears to be correlated with speed of sound in specific metal as in the case of wire explosion in air. However, no correlation could be established between optical emission characteristics and energy deposition parameters which need to be probed further in future work with other diagnostics including imaging techniques.

5.1.2.2 Refractory Metals and Palladium

It can be noticed from voltage profiles shown in Fig. 5.5 that these metals exhibit quiet different behaviour if surrounding medium is changed from air to vacuum. In case of these metals, voltage does not remain at zero just after dropping down from peak but rather either rises again to another peak or remains constant at fixed value for some time period (~200-300 ns). This kind of second peak and a pause are observed in Ti and W, respectively, whereas for Pd the voltage peak is quiet broad.

Overheating seems to follow an inverse relation with speed of sound in these metals as observed for non-refractory metals in vacuum. However, exceptionally low overheating is found in W even after having speed of sound in between Pd and Ti. This behaviour could be due to its higher value of melting temperature leading to significant surface thermionic emission.

In W and Ti, overheating factor is less than one; indicating that the energy deposited in these metals is less than that required for burst. Further, the total specific energy deposited for W and Ti before the breakdown initiated is measured to be 239.2 kJ/mol and 115.2 kJ/mol, respectively, in present study, however, the same has been reported to be 724.2 kJ/mol and 358 kJ/mol, respectively, for W and Ti in literature [23]. Additionally, in the same literature [23] the specific energies required for various phase changes like for melting (117.2 kJ/mol for W and 58.5 kJ/mol for Ti) and for initiating vaporization (191.7 kJ/mol for W and 108.2 kJ/mol for Ti) have also been reported. The comparison of presently measured specific energy at burst with the reported [23] specific energy for initiation of vaporization indicates that the breakdown in present case starts just after initiation of vaporisation and much before the complete vaporization. This might be attributed to earlier breakdown in desorbed gases.

Temporal optical emission profiles (Fig. 5.7) exhibit similar behaviour for these metals as observed for explosion in air except for Ti in which light starts appearing much earlier than that for other two metals. Though radial expansion in W is similar to that in air but reduction in radius of this self-emitted light is relatively more profound. Parameters related with energy deposition (Specific energy, overheating factor and time of burst) do not seem to have any correlation with optical emission characteristics for explosion of these metals in vacuum as also noticed for explosion in air.

5.1.3 Comparative Analysis of Overall Aspects of Effect of Material in Air and Vacuum

Now it can be inferred from the experimental results and analysis reported in previous sections that formation of parallel discharge channel can influence the process of energy deposition up to burst. It depends largely on material and its surrounding medium which can support the occurrence of such energy diverting channels. Formation of these parallel ionised channels at early stage in the process of wire explosion influences the energy deposited up to burst. Earlier formation of corona or ionised channels are more probable in vacuum than that in denser surrounding medium due to unrestricted expansion of desorbed gases with possible formation of a density gradient from wire surface to surrounding vacuum region. This causes earlier shifting of current from wire core to low resistive outer ionised channels resulting in earlier burst and hence lesser energy deposition up to burst in vacuum. This is also observed in present work that all metals have higher values of overheating in air than in vacuum.

Formation of these parallel ionised channels is facilitated by availability of electrons. Since, desorption of gases and emission of electrons both are relatively more profound in refractory metals, so overall lesser energy deposition is expected in these metals than non-refractory metals.

Based on the overheating data plotted against the sound speed in these metals (Fig. 5.8), it appears that the relative decrease in overheating by changing surrounding media from air to vacuum could be governed by the speed of sound in a particular metal.

In case of vacuum, no correlation of metals with initial resistivity and enthalpy of atomisation have been observed. The reason for this difference can also be associated to the apparent inverse relation of overheating to the speed of sound in these metals (Fig. 5.8). Thus, difference in energy deposited up to burst can be attributed to differences in speed of sounds in these metals.

The role of speed of sound can be understood by considering following reasoning. Since expansion rate of metal can be related qualitatively to sound velocity after the start of phase explosion process. Impurities and metal vapours eject out from the wire surface due to increasing temperature of wire surface. Therefore, a boundary created between core and vapour acts as a piston [28] which drives the surrounding vapour-gases, leading to a density gradient which with time gets ionised and contributes in energy diversion process. Though, the value of sound velocity is expected to vary with time during explosion process due to varying temperature and pressure but still this variation can be related to its initial values at room temperature as per the semi-empirical relations reported in [118]. Estimation of spatial and temporal profile of energy deposition, temperature and pressure in different wire segments being a complicated process, the, initial sound velocity is considered as qualitative marker for present analysis. Thus, finally it appears that relatively higher value of sound velocity in a specific metal in vacuum contributes for faster switching of current to outer parallel ionised channel in vacuum in addition to all other properties responsible for formation of such channels in air. In case of Al, substantial decrease in overheating factor is observed in vacuum in comparison to that in air. Highest value of speed of sound among considered non-refractory metals make it more susceptible for development of ionization channels in surface evaporated metal vapour.

Finally the experimental outcomes can be outlined as:

1. Specific power, which takes into account the time of energy deposition (defined as time averaged energy deposited per atom up to burst) and overheating in all metals is observed to be reduced in vacuum as compared to that in air (Table 5.2 and Table 5.3).
2. In air as surrounding medium, specific power averaged over time of burst appears to be of same order for all metals from both groups (Table 5.2) but values of burst current are smaller in refractory metals except that for Pd. Three parameters which seem to be of considerable importance in generating high energy density plasma are overheating factor, burst current and specific power, respectively. These three parameters are larger for Cu and Au and least for W among the materials investigated here.
3. Au is found to be best among all metals here in both the media after considering above three important parameters (burst current, specific power and overheating factor) whereas Ti and W have least values of these parameters in vacuum and air, respectively.

4. Minimum value of specific energy deposition is found for Al with highest speed of sound.

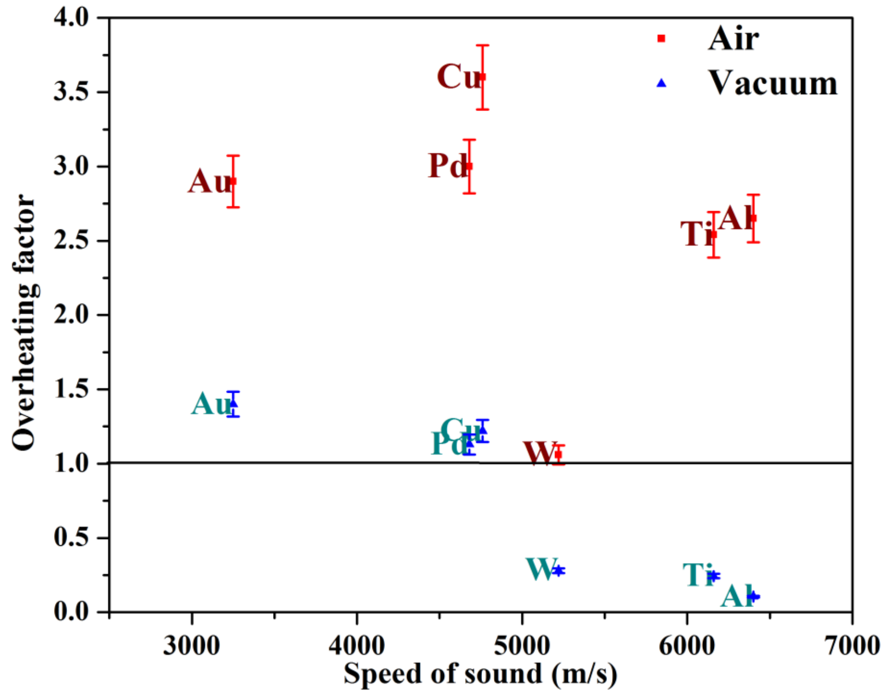

Fig. 5.8: Comparison of experimentally observed overheating factor with speed of sound in all metals in both mediums

5.2 Summary

Experimental study is carried out to look into the effect of material on fast electrical explosion characteristics in vacuum as well as in air. Experimentally observed behaviour is analysed and discussed in detail with possible causes. Metals from three groups; non-refractory metals (Cu, Au and Al) and refractory metals (Ti, W) and Pd are considered for this study. Since the trend in energy deposition parameters (Specific energy deposition, overheating factor and time of burst) for Pd is similar to that of W and Ti, so it has been discussed with refractory metals. Distinct behaviour is observed for overheating in non-refractory and refractory metals along with Pd; for former, it is seen to be dependent upon initial resistivity and for later, on enthalpy of atomisation; for explosion in air.

Temporal optical emission profiles of self- emitted light are also experimentally recorded which have been used to look into the formation of parallel outer ionised channels. Correlation of energy deposition parameters has been established with these profiles for non-refractory metals in air. Though similar characteristic behaviour for radial expansion profiles of all metals have been observed for explosion in vacuum also, but no correlation with energy deposition parameters has been seen for EEW in vacuum. Such behaviour of EEW in vacuum needs further detailed investigations.

An interesting and novel experimental outcome that is observed for explosion in vacuum is the importance of role of speed of sound in influencing the specific energy deposition and hence the overheating in specific metal till burst. In present study, speed of sound seems to be a dominating parameter in the process of formation of outer ionised channels in vacuum which indicates a distinct aspect which needs to be considered for responsible mechanisms of energy diversion.

Overall study concludes that Au is the most efficient among all the metals studied for energy coupling in electrical explosions under both the media for current rate of about 90 A/ns with present circuit parameters. These experimental results might be helpful in selection of metals and also in understanding the role of material properties in the process of wire explosion.

Chapter 6

Effect of Electrically Exploding Wire Configuration including X-pinches on Emission of X-rays

Experimental investigations to observe the effect of current rise rates, wire material, its diameter, and surrounding medium (air, vacuum and insulating medium) on electrically exploding wire behavior have been discussed in Chapter-4 and Chapter-5. These studies are useful in optimization of circuit parameters for efficient energy coupling in wire explosion process leading to enhancement in temperature of exploding wire plasma and hence in radiation emission. Earlier chapters were focused to a fixed and basic fundamental configuration viz. single exploding wire. This chapter presents effect of different wire configurations on X-rays radiation emission. First section describes all wire configurations which have been employed for present study. Since experimental study [73] as mentioned in chapter-4 suggests that insulating coating enhances specific energy to be deposited in single exploding wire. Therefore, after assessing the performance of different wire configurations, experiments have been carried out in X-pinch geometry; in which radiation emission is observed in X-rays range and the effect of insulation coating on X-rays yield has also been investigated. Experimental methodology, results and their analysis is discussed in different sections of this chapter. Finally, work is summarized in last.

6.1 Wire Configurations

Source of radiation emission in electrically exploding wire plasma column is interaction of charged particles with electric field [47], hot spots formation due to magnetohydrodynamic instabilities [46] and plasma compression or pinching [7], [9], [16], [17]. Apart from basic configuration of single wire in EEW, cylindrical wire arrays and X-pinches have been most commonly used as pulsed radiation sources. Cylindrical wire arrays are generally used in pulsed power systems with very high current rates (> 1kA/ns). For X-pinches also, a threshold value of current rate was reported in earlier studies [9], [95] which claimed that X-rays can only be emitted from X-pinches if current rise rate exceeds 1 kA/ns. However, X-rays have been observed in X-pinches with very lower values of current rising rate in some recent studies [86], [93]. Present study tries to investigate possibilities of radiation emission from various new geometries of EEW designed with the expectations of radiation emission by adding probable locations for formation of hot spots or also by enhancing the local magnetic field and by modifying conventional X-pinches.

For X-pinches, earlier reported experimental work [9], [10], [95] indicate its various stages which are responsible for emission of X-rays. Based upon these reported works, mechanism involved is discussed here in brief. At crossing point of X-pinches, current (I) from each of the wires add up in proportion to the number of wires i.e. total current of n x I for 'n' number of wires at crossing point in X-pinch. This enhanced current results in magnetic pressure which is proportion to the square of number of wires and becomes n^2 times to that of single wire. This enhanced magnetic pressure at crossing point compresses the plasma to create localized pinching (radial compression). This compressed narrow plasma column is prone to instabilities and regions of high density and high temperatures are formed. Formation of hot spots in this plasma column becomes the source of radiation emission. As this narrow pinching column disrupts, it results in formation of mini diode. In this mini diode, charged particles (ions and electrons) experience the electric field and hard X-rays are emitted.

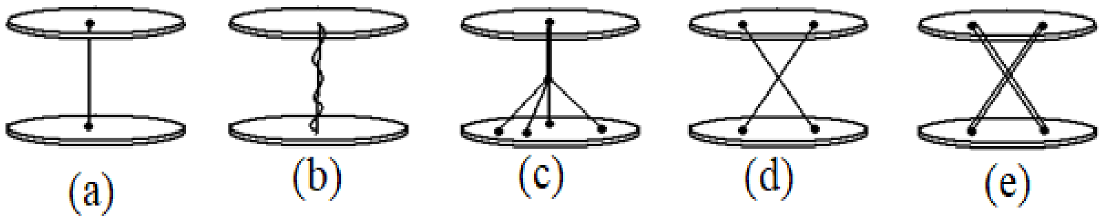

Fig. 6.1: Schematic of various wire configurations

Various configurations by placing wires in different geometries experimented in this work are shown in Fig. 6.1.

In Fig. 6.1(a), single wire of length 15 mm is considered for comparative study to other configurations (Fig. 6.1 (b)-(e)). Fig. 6.1(b) corresponds to a configuration in which two wires are twisted and aligned vertically straight in the load with same length as for single wire in Fig. 6.1(a). Design of this type of load (Fig. 6.1 (b)) was based upon anticipation of multiple points of sources of radiation which might develop due to instabilities at weaved crossing points. In Fig. 6.1 (c), two or four wires have been used. This configuration is attained by first soldering two ends of wires in diametrically opposite holes in one of the electrodes (Anode in present experiment; shown as lower plate in Fig. 6.1(b)); subsequently these wires are stretched by another single wire which is folded at centre and it's both ends are soldered in one hole of other electrode (here, Cathode) to form one half of X-pinch. Lengths of wires are chosen so that cross point comes at center of the gap between electrodes. This type of configuration which is like half X-pinch was designed to compare it with the radiation emission with normal symmetric X-pinch configuration because as per the suggested mechanisms involved in X-pinches [9], [119]; some fraction of radiation yield also is expected to come if hot spot formation take place by neck implosion at crossed point and outflow of matter in the axial direction in present configuration (Fig. 6.1(c)).

Fig. 6.1(d) is typical configuration used for X-pinches. In this study, two wires have been used initially. Further, the effect of increasing number of wires from two to four on radiation yield, have also been observed.

Design of Fig. 6.1(e) is another configuration of X-pinches with two wires is each arm (instead of single wire as in conventional X-pinches) of 'X' geometry. Though Fig. 6.1(e) corresponds to a similar configuration as that of X-pinches in equal mass at crossed point with four wires aligned in azimuthal symmetry but it differs in orientation of its arms. In present geometry, two wires passing from same hole are used in one arm and such two arms with four wires in total make cross point of X-pinch. In contrast to conventional configuration of four wire X-pinches (each wire from different hole), present configuration was designed to realize the significance of orientation of branches in X-pinches with same mass at crossed point. Gap between two plates (cathode and anode) is kept fixed at 15 mm. Angle between wires; which make arms of X-pinch based configurations; is kept fixed at around 86^o. Charging Voltage is also kept fixed at 38 kV to keep constant value of rate of rise of current of about 0.08 kA/ns for all configurations. Wire material in each configuration is also kept same viz. Mo for being high Z metal; suitable for X-rays emission. Though the comparison of radiation emission has been made for same metal wires of Mo but other metals like W and Cu are also experimented later in the configuration of X-pinches; in which significant X-rays emission has been observed. Effect of mixing of two different metals (each arm of different metal in X-pinch) on X-rays radiation emission is also experimentally observed. These experimental studies have been carried out in vacuum of 5-6 x 10^{-5} mbar range.

6.2 X-rays Detection Methodology

Si-PIN diodes along with filters are used to detect X-rays in different energy ranges. Its details along with the measurement technique for obtaining the radiation yield for a specific range of energy have already been discussed in detail in section 2.1 of chapter 2. Foils of different metals with varying thicknesses have been used as filters to estimate range of energies of emitted X-rays. Different filters used in this study are in-house designed using the foils of Al with thicknesses of 6.5 μm and 9 μm, Be and Ti with thicknesses of 50 μm and 12.5 μm respectively. Range of energy which can be detected using these filters are tabulated in Table 2.1 and shown in transmission curves [120] in Fig. 2.5 in chapter 2.

Qualitative comparison for intensity of emitted radiation for specific range of energy is carried out by using the output signals of PIN diodes mounted in front of specific filters.

6.3 Experimental Results and Analysis

Initially, PIN diode signals recorded in oscilloscope have been used as an indicative marker for studying the effect of configuration on emission of X-rays in specific range.

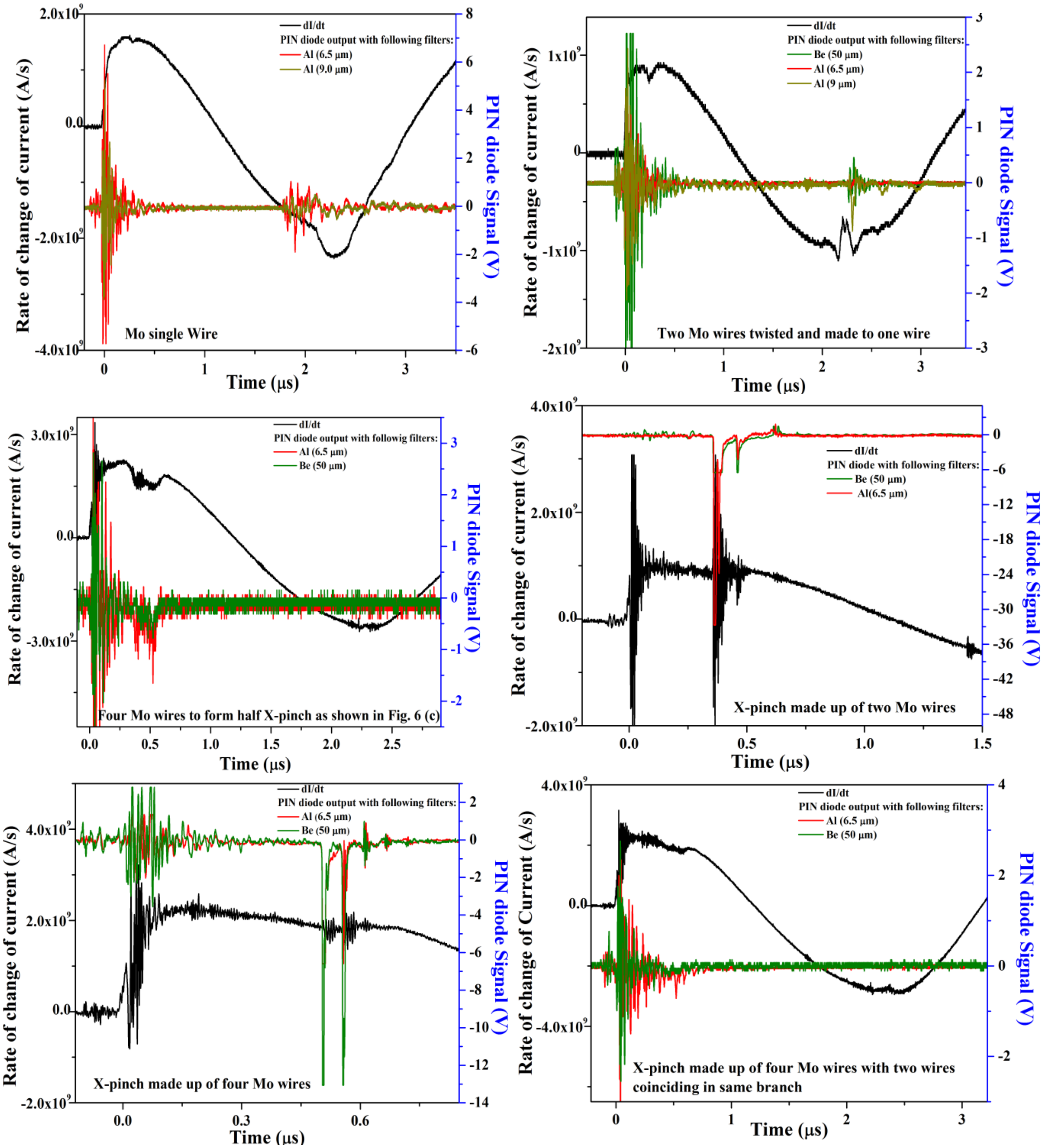

Fig. 6.2: PIN diode signals along with dI/dt signals for different configurations mentioned in each graph.

Table 6.1: Details of experimental circuit parameters and PIN diode signals

S.No.	Wire Material with diameter of 13 µm	Configuration of EEW load corresponding to following Figure	PIN diodes output (V) along with timing of emission (ns) with respect to start of current	Energy range (E) corresponding to PIN diode with filter output (keV)
1.	Mo	Fig. 6.1 (a)	-1.9 V @1.92 µs with filter of Al (6.5 µm)	1.7 >E>0.7 & E>2
2.	Mo	Fig. 6.1 (b)	-0.8 V @2.33µs with filter of Al (6.5 µm).	1.7>E>0.7 & E>2
3.	Mo	Fig. 6.1 (c)	No X-rays registered.	-------------
4.	Mo	Fig. 6.1 (d) (Two wires)	-7 V (Saturated) and 33.5 V (Saturated) @ 363 ns with filters of Be(50 µm) and Al(6.5 µm) respectively followed by -7 V and -4V @ 460 ns in filters of Be(50µm) and Al(6.5µm) respectively.	1.7>E>0.7 & E>2, E> 1.3
5.	Mo	Fig. 6.1 (d) (Four wires)	-13 V (Saturated) @ 522 ns and @572ns respectively with Be (50 µm)	1.7>E>0.7 & E>2, E> 1.3
6.	Mo	Fig. 6.1 (e)	No X-rays registered.	------------
7.	Al & Mo	Fig. 6.1 (d) (One Al and one Mo wire)	No X-rays registered.	------------
8.	Al & Mo	Fig. 6.1 (d) (Two Al & two Mo wires)	No X-rays registered.	------------

Since rate of change of current (dI/dt) can give clear and better indication for time of burst, thus dI/dt signals along with PIN diode signals are considered for qualitative examination of X-rays emission in different configurations of exploding wires as shown in Fig. 6.2. Noise in dI/dt signals at initial stage is caused by the electromagnetic interference associated with the closing of spark gap at higher charging voltages and also due to close vicinity of oscilloscope to experimental set-up. The corresponding experimental data along with details of wire material, its diameter, time of burst and filters used are tabulated in Table 6.1. Time of X-rays emission is different than the time of burst as can be inferred from PIN diode signals and also mentioned in Table 6.1.

It can be noticed from experimental results (Table 6.1) that the significant radiation output is obtained only for X-pinches (Fig.6.1 (d)) in contrast to other considered configurations.

By Further experimentation extended on X-pinches by making use of wires of dissimilar metals in present study, it has been inferred that X-pinches made up of wires of one metal only, could emit X-rays with present system. Different possibilities have been worked out. For example in one of the experiment, one wire of Al and other of Mo has been used to make an X-pinch of two wires. In another experiment, two Al wires and two Mo wires with same diameter have also been used to make an X-pinch of four wires. Results indicate that X-pinches made up of either two or four wires using two different metals viz. Mo and Al are not capable of generating X-rays (Fig. 6.2 and Table 6.1) with present circuit parameters. It appears that this type of study of using different metals in X-pinch requires more detailed investigations. However, X-pinches made up of two or four (same metal) Mo wires have always emitted radiation in X-rays range (Fig. 6.2).

Another inference in respect of number of wires from X-pinches is that X-pinch with only two wires is most efficient in radiation emission in comparison to X-pinches with higher number (Four or six) of wires (Fig. 6.2 and Table 6.1). Similar result has also been observed for W metal (Table 6.2). This might be because of lesser mass in case of two wires, at crossed point in X-pinches, which is more suitable to achieve compression with present rate of current rise.

X-pinches (Fig. 6.3) of W wires have also been found to be capable of generating significant X-rays yield (> 200 mJ) for E > 1.3 keV. In all cases of X-pinches in which significant X-rays yield has been noticed, are estimated and tabulated in Table 6.2.

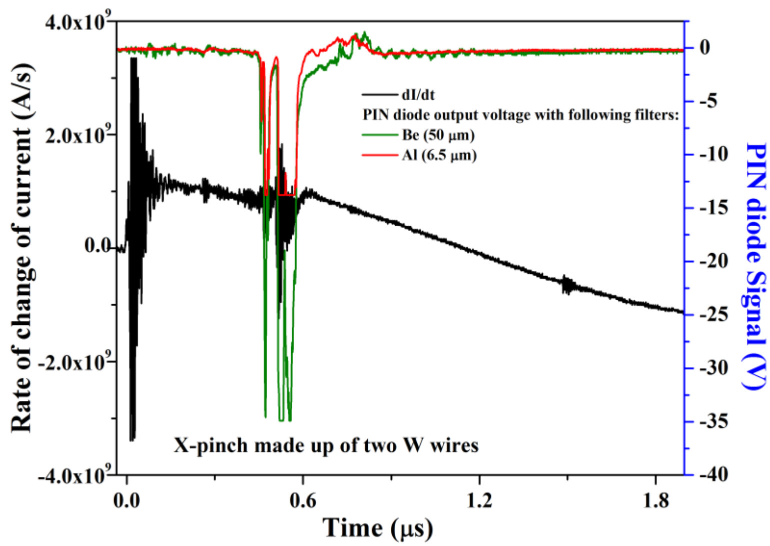

Fig. 6.3: dI/dt and PIN diode signals with different filters as mentioned in inset for X-pinches of two W wires

6.4 Effect of Insulation Coating on X-rays Yield of X-pinches

Efforts have been made to look into the effect of insulation coating on radiation emission in X-pinches. It is interesting to observe that X-pinches made up of two W wires overlaid with silicone-based lubricant resulted in significantly enhanced X-rays yield than X-pinches made of either two or four bare W wires.

Table 6.2: X-rays yield estimated using different types of X-pinches

X-pinch Configuration	Filters (Metal of foil and its thickness)	Source X-rays Yield (mJ)	Energy Range (keV)
Two bare 13 µm W wires	Be (50 µm)	240.82+2.4*	E>1.3
	Al (6.5 µm)	117.92+11.7*	1.7 >E>0.7 & E>2
Two coated 13 µm W wires	Be (50 µm)	313.98	E>1.3
	Ti (12.5 µm)	175.40	5 > E > 2.8
	Al (6.5 µm)	493.51	1.7 >E>0.7 & E>2
Two coated 13 µm W wires	Be (50 µm)	305.2	E>1.3
	Ti (12.5 µm)	85.5	5 > E > 2.8
	Al (6.5 µm)	231.6	1.7 >E>0.7 & E>2
Four bare Mo13 µm wires	Al (6.5 µm)	22.15	1.7 >E>0.7 & E>2
	Be (50 µm)	37.82	E>1.3
Two bare Mo 13 µm wires	Be (50 µm)	101.06	E>1.3
	Al (6.5 µm)	129.30	1.7 >E>0.7 & E>2
Two coated Cu 20 µm wires	Ti (12.5 µm)	50.25	5 > E > 2.8
	Al (6.5 µm)	677.48	1.7 >E>0.7 & E>2

*= Contribution in X-rays yield due to extrapolation

These shots have been repeated and, in each shot, experimentally observed signals for X-pinches of coated wires resulted in enhanced X-rays yield as compared to that of bare wires X-pinch. The comparative results for different wires are listed in Table 6.2 and oscilloscope signals for one experiment using two coated W wires is shown in Fig. 6.4.

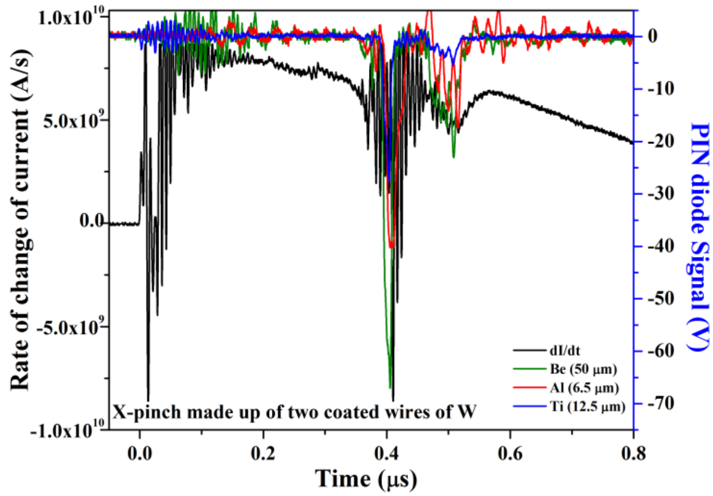

Fig. 6.4: Rate of change of current and two PIN diode signals observed in oscilloscope for X-pinch of two coated wires of W. Pin diode signals are truncated due to saturation of voltage range in oscilloscope.

6.5 Summary and Conclusion

Experimental study has been carried out to look into the effect of various wire configurations on X-rays yield. It has been observed that wire configurations in X-pinch geometry (made of wires of same metal (e.g. Cu, W and Mo) can yield significant X-rays with present setup of moderate current rise rate (~0.08 kA/ns). Another inference drawn from experiments on various designs of configurations is that arms of X-pinch are of significant relevance to contribute in the process of radiation emission. For instance, no X-rays have been observed in Fig.6.1 (c) and (e) in spite of having same mass at cross point (except the orientation of arms) as in X-pinches (Fig. 6.1 (d)) of four wires. This might be because of introduced asymmetry in configurations, which might have affected the magnetic field orientations at cross point and made the conditions unfavorable for pinching to occur and hence the formations of hot spots.

X-pinches of two wires yield more radiation in comparison to those of four wires. This might be because of lower mass at crossed point in X-pinch of two wires as compared to that for four wires, with present values of rate of rise of current, suited more for compression of plasma at crossed point in X-pinches. Efforts have also been made to observe the effect of coating on radiation yield because extra energy deposition till burst is seen for coated single wire in our earlier work as mentioned in chapter 4. Bare W wires of 13 µm were overlaid with silicone-based lubricant and it was interesting to observe that X-pinches made up of two coated wires resulted in enhanced yield of X-rays by approximately 1.3 times for energy of X-rays > 1.3 keV. This enhanced yield in X-pinches made up of coated wires might be because of limited expansion of exploding wire plasma.

Chapter 7

Conclusion and Future Scope of Studies

7.1 Conclusion

The present thesis reports the detailed investigations carried out to optimise the various experimental parameters for efficient energy coupling in EEWs. Experimental parameters which have been considered are rate of current rise (25-90 A/ns), wire diameter (20-233 μm), surrounding medium (insulating coating, air and vacuum), and wire material (Au, Cu, Al, W, Ti and Pd) for single wire explosion. Different geometrical configurations including single as well as multiple wires; as load; have also been experimentally probed to investigate the effect of geometry in wire's configurations on the probability of radiation emission in X-ray range using present compact pulsed power source of moderate current rise rate (~ 80 A/ns).

The experimental investigations have been carried out by employing various diagnostics, out of which some have been developed as a part of this work to measure electrical, optical and X-rays emission characteristics. Electrical diagnostics have been used to measure temporal profiles of current in circuit and voltage across the load. Current and voltage profiles are used for estimating temporal profiles of energy, and also to predict time instants for various stages of explosion viz. melting and burst. Experimental outcomes which have been considered for analysis and derived from estimated energy are specific energy, overheating factor and averaged specific power up to burst. Temporal profiles of optical self-emission, which have been registered using a streak camera, have also been considered for analysis to look into probable mechanisms involved in explosion characteristics of different metals.

To examine the effect of surrounding medium on explosion characteristics of different metals, experimental study is carried out for two surrounding mediums viz. air and vacuum.

Efforts have been made to establish a correlation of the quantities like specific energy, overheating factor and time of burst derived from electrical measurements and optical emission characteristics like time of start of optical emission, temporal profiles of expansion of outer most boundaries with a-priori known metal properties (initial electrical resistivity, enthalpy of atomisation and speed of sound).

Electron density profiles, being an important parameter to be considered to understand the dynamics involved in exploding wires, have been measured experimentally. Mach-Zehnder laser interferometer has been developed and implemented for measuring spatial as well as temporal electron density profiles in pulsed plasmas [96]. Further, to measure the ion flux, another useful parameter, Faraday cup has been designed and developed [98].

In initial experiments, single copper wire was examined to observe the effect of polyimide coating of around 36% of basic metal diameter for explosion in air. Specific energy is found to get enhanced in coated wire of diameter 136 μm (with the metal core diameter ~100 μm) by nearly 45-60% [73] in comparison to bare wire of 100 μm diameter for capacitor charging voltages in range of 16-40 kV. Thus, insulated copper wires (with coating of around 36% of basic diameter) have been characterized further for varying current rising rates (~25-90 A/ns) and wire diameters (20-233 μm).Experimental trend observed for specific energy and time of burst for varying diameter seems to support evaporation wave theory of wire explosion process for present experimental set-up. Evaporation wave theory for transforming conducting metal to non conducting vaporised state was proposed initially by Bennett [52] and later used by Tkachenko [30] et al. and Rakhel [53] which assume evaporation wave to initiate from surface of wire and travels to its core axis.

In this quest, it has been concluded that both the charging voltage and insulation coating can enhance specific energy for this range of circuit parameters (wire diameter, current rising rates) which might be due to their limited expansion (due to coating) and faster rate of energy deposition (higher current rising rates). This behaviour was more prominent especially for thinner wires with increasing charging voltage [73]. Further experiments were carried out to observe exploding wire behaviour of thinner wires (20-81μm) at enhanced current rates (72-96 A/ns). A distinct post burst feature or a pause has been marked in voltage profiles of these thinner wires for current rising rates beyond a threshold value which is specific to wire diameter. Though such kind of post burst feature has also been found to occur in voltage profiles of earlier reported works [31], [59], [67], [81] but it has not been pointed out and investigated in detail. This feature of pause has been found to be reproducible with specific circuit parameters and has been investigated experimentally as well as through numerical simulations. Based on our study, it has been inferred that the formation of a density front till burst is responsible for appearance of this signature in voltage profile. It is also concluded that time averaged specific energy which is also termed as "averaged specific power" is more important than specific energy for influencing the dynamics of exploding wire plasmas. It has been seen that this feature appears for shots in which averaged specific power exceeds a threshold value. For present case, this kink or pause after burst appeared in all those shots of copper wire explosion in air, in which averaged specific power exceeds a value of around 80 J/g/ns [80]. Efforts have also been made to measure spatial profiles of electron densities at different instants viz. before kink and after kink. It is observed that electron density remains around $10^{25}/m^3$ –10^{26} $/m^3$ and decreases from inner wire core to outer surface.

Another important outcome of the present experimental work is that the action integral which is generally taken as constant in predicting the time of burst for a specific diameter at first peak value of capacitor discharge current; varies with thickness of wire and current rising rates, in agreement with already reported theoretical work [50], [79].

After looking into detailed investigations on effect of coating, diameter, current rising rates on the explosion characteristics of a specific metal (copper), the effect of material covering low to high atomic number metals viz. Au, Cu, Al, Ti, Pd and W belonging to different groups (on the basis of their electrical explosion characteristics) on the explosion behaviour has been studied. Efforts have been made to establish a comparative qualitative criterion for efficient energy coupling in explosion process of different metals considering certain known thermo physical parameters of metals like initial resistivity, sound velocity in metals at room temperature, and enthalpy of atomization. However, while exploring the effect of properties of material in electrical explosion, the role of the surrounding medium being an important parameter has also been considered; to have a comparison on behaviour of different metals with respect to the media confining it, including vacuum. In this direction, a comparative study for wire explosion characteristics for different metals is carried out for explosion in air as well as in vacuum. The experimental data on electrical characteristics up to burst are analysed and their dependence on electrical and thermophysical properties of used materials is investigated. Additionally, the temporal profile of optical emission is also investigated to have an insight for probable mechanisms involved.

This type of comparative study for different materials in both; air and vacuum; as surrounding media is rarely reported. Some novel experimental outcomes reported for the first time to the best of author's knowledge in the present work are mentioned as follows.

i. The effect of material properties (initial resistivity and enthalpy of atomisation) on overheating of EEW in air
ii. Some unconventional behaviour of EEW of these metals in vacuum as indicated by present experimental data as compared to those reported in previous such works.
iii. Contribution of speed of sound in diverting energy deposition in different metals while changing surrounding medium from air to vacuum.

It has been found that despite displaying distinct dependency on material properties by two groups of metals (refractory and non-refractory) for explosion in air, the dependency on these in vacuum is more or less similar except that for W. Three parameters namely overheating factor, burst current and specific power plays an important role in generating high energy density plasma which have been found to be larger for Cu, Au and least for W among the materials investigated here for wire explosion in air. However, the same parameters for explosion in vacuum are highest for Au and least for Ti. Among these metals, overall behavior of Au has been found to be most favourable for efficient energy coupling irrespective of surrounding medium. The outcomes of this study are useful in selection of materials for a specific application depending upon energy deposited in wire exploded in a particular medium.

Finally, experiments are also carried out to observe the effect of configuration of wires for same capacitor bank parameters on X-rays yield. X-rays yield and their energy is measured using PIN diodes along with foil filters of various metals. Some new configurations along with typical configurations like single wire and X-pinches are also investigated. It has been found that at present range of moderate current rates (80-85A/ns), only conventional X-pinches can yield (>100 mJ) radiation in X-rays range (for energy>1.3 keV). Further, efforts have been made to enhance X-rays yield in X-pinch configuration by varying number of wires and using insulation coating on wires. It has been observed that the X-pinches with only two numbers of wires yield comparatively more radiation of X-rays than higher number of wires for present circuit parameters. Coating of silicone-based lubricant on W wires also helped in achieving significantly higher yield than X-pinches made up of bare wires.

7.2 Future Scope of Studies

Exploding wire has long been the topic of interest for high energy density physics research not only due to its wider range of applications but also due to involvement of intriguing dynamics. Due to dependencies on multiple intercorrelated parameters and involvement of various thermal as well as magnetohydrodynamic phenomena; understanding of mechanism of electrical explosion still needs more efforts. There is no uniform theory for explosion mechanisms but observation of transverse striations is typical in EEW. However, new advancement in instrumentation technology and theoretical simulations predict the density and temperature variation in axial direction resulting to formation of strata like structure in EEW [31], [59], [67], [121], [122].

In present work also, MHD simulation infer about non-uniformities in densities in radial direction which are dependent upon the rate of energy deposition till burst. Growth of the thermal instabilities in axial direction as per earlier reported theoretical work [121], [122] depends upon material properties like rate of change of resistivity with temperature or material density. The implementation of advanced diagnostic techniques such as shadowgraphy and schileren imaging could be quite helpful in understanding the physics involved in explosion dynamics. Recently reported [28], [67] hollow core (tubular) structure has also been a matter of investigation for probing the complicated core structures for variable range of experimental parameters. In future studies, experiments shall be carried out to correlate energy deposition characteristics with properties of metals accompanied by investigations using imaging diagnostics (shadowgraphy and schlieren) for the comprehensive analysis of thermal instabilities.

During the course of this work efforts have been made to understand the dependence of various interdependent parameters on energy deposition characteristics and various correlations have been established with some commonly known material properties. Even with simpler diagnostics, some interesting and new outcomes have been explored at pulse power system of moderate current rate. However, it has been found that detailed analysis of exploding wire dynamics can reveal many intriguing and interesting outcomes. Imaging techniques can prove to be more useful for further investigations on spatial and temporal density profiles in exploding wire plasma in two different mediums. Electron density measurement technique is to be improved further for enhancing fringe contrast and spatial resolution of fringe profiles to detect the fringe shift with better accuracies. Experimental results of present study may prove useful for efficient energy coupling not only in metal wires but also for deuterated polyethylene fibers, which can be used for generation of pulsed neutrons for different applications. Developed pulsed plasma diagnostic techniques like laser interferometer, faraday cup shall also be used for characterization of different pulsed and pinch plasmas like spark gap plasmas, electric discharges, EEW or X-pinches of metal wires, as well as of polyethene deuterated fibers.

In present work, X-rays yield has been observed for X-pinches at relatively much lower current rising rates (80 A/ns) as compared to that reported in most of the earlier experimental work [9], [95], [119]. This work shall be extended further for understanding the pinching mechanism and enhancing the yield of pulsed X-rays using easily configurable compact pulsed power systems.

References

[1] “Physics of High-Density Z-Pinch Plasmas”, Michael A. Liberman, S. De Groot John, Arthur Toor, Rick B. Spielman, Springer-Verlag **1999**, New York**,** USA.

[2] “Magnetically Self-Focussing Streams”, W. H. Bennett, *Phys. Rev.*, **1934***, 45, 12,* 890-897.

[3] “Self-Focusing Streams”, H. Bennett, Willard, *Phys. Rev.*, **1955***, 98, 6,* 1584-1593.

[4] “Exploding wires as an intense ultraviolet continuum excitation source with preliminary application to atomic fluorescence spectrometry”, D.W. Brinkman and R.D. Sacks, *Anal. Chem.*, **1975**, *47,8*, 1279-1285.

[5] “Optical Pumping of Lasers Using Exploding Wires”, C. H. Church, R. D. Haun, T. A. Osial, and E. V. Somers, *Appl. Opt.*, **1963**, *2, 4,* 451-452.

[6] “Intense pulsed plasma x-ray source for lithography”, D. H. Kalantar, D. A. Hammer, K. C. Mittal, and N. Qi, Vladimirsky Y.*, J. Vac. Sci. Technol. B: Microelectron Nanometer Struct. Process Meas. Phenom.,* **1991,** *9:6*, 3245-3249.

[7] “Pinch plasmas as intense EUV sources for laboratory applications”, R. Lebert, D. Rothweiler, A. Engel, K. Bergmann, W. Neff, *Opt. Quant. Electron.*, **1996**, *28*, *3*, 241–259.

[8] Extreme Ultraviolet Radiation from Pulsed Discharges: A New Access to “Nanoscopy” and “Nanolytics”, In: Knobloch H., Kaminorz Y. (eds) MicroNano Integration, R. Lebert, C. Wies, L. Juschkin, B. Jägle, W. Neff, J. Barthel, K. Walter, K. Bergmann, **2004**, VDI-Buch. Springer, Berlin, Heidelberg, 169-184.
https://doi.org/10.1007/978-3-642-18727-8_23.

[9] "Evolution of X-pinch loads for pulsed power generators with current from 50 to 5000 kA", T.A. Shelkovenko, S.A. Pikuz, I.N. Tilikin, M.D. Mitchell, S.N. Bland, D.A. Hammer, *Matter Radiat. Extremes,* **2018,** *3, 6,* 267-277.

[10] "Point-projection X-ray radiography using an X pinch as the radiation source", T.A. Shelkovenko, D.B. Sinars, S.A. Pikuz, K.M. Chandler, D.A. Hammer, *Rev. Sci. Instrum.*, **2001**, *72,1*, 667-670.

[11] "A review of projection radiography of plasma and biological objects in X-pinch radiation", T.A. Shelkovenko, S.A. Pikuz, D.A. Hammer, *Plasma Phys. Rep.*, **2016,** *42*, 226-268.

[12] "Physico-chemical factors influence beet (Beta vulgris L.) seed germination", A.G. Tailor, M.C. Goffinet, S.A. Pikuz, T.A. Shelkovenko, M.D. Mitchell, et al., *The biology of seeds: recent research advances,* CAB Int., Chapter 47, **2003**, 433.

[13] "Axial X-ray backlighting of wire-array Z-pinches using X pinches", I. C. Blesener, J. B. Greenly, S. A. Pikuz, T. A. Shelkovenko, S. Vishniakou, et al., *Rev. Sci. Instrum.*, **2009**, *80, 12,* 123505-1-5.

[14] "Multiple wire array load for high power pulsed generators", C. Stallings, K. Nielson and R. Schneider, *Appl. Phys. Lett*., **1976**, *29,7*, 404-406

[15] "Improved Symmetry Greatly Increases X-Ray Power from Wire-Array Z-Pinches", T. W. L. Sanford et al, *Phys. Rev. Lett.*, **1996**, *77, 25*, 5063-5066.

[16] "Enhancement of X-Ray Power from a Z Pinch Using Nested-Wire Arrays", C. Deeney, M.R. Douglas, B. Spielman Rick et al., *Phys. Rev. Lett.,* **1998,** *81, 22,* 4883-4886, DOI: 10.1103/PhysRevLett.81.4883.

[17] "Z pinches as intense X-ray sources for high-energy density physics applications", M. Keith Matzen, *Phys. Plasmas*, **1997**, *4, 5*, 1519-1527, doi: 10.1063/1.872323.

[18] "Dynamics of a Z-pinch x-ray source for heating inertial confinement-fusion relevant hohlraums to 120–160 eV", T. W. L. Sanford, R. E. Olson, R. C. Mock, G. A. Chandler, R. J. Leeper, T. J. Nash, L. E. Ruggles, W. W. Simpson, and K. W. Struve, *Phys. Plasmas*, **2000**, *7, 11*, 4669-4682.

[19] "Imploding argon plasma experiments", C. Stallings et al., *Appl. Phys. Lett.*, **1979,** *3*, *7*, 524-526.

[20] "Z-pinches-A historical view", R. B. Spielman and J. S. De Groot, *Laser Part. Beams*, *19*, *4*, **2001**, 509-525. DOI: https://doi.org/10.1017/S0263034601194012

[21] "Investigation of Radial Wire Arrays for Inertial Confinement Fusion and Radiation Effects Science", David J. Ampleford, Christopher A. Jennings, Simon N. Bland, Sergey V. Lebedev, Jeremy, P. Chittenden, Gareth N. Hall, Francisco Suzuki-Vidal, Michael E. Cuneo, T. J Rogers, Monica Cleveland, Ryan D. McBride, Jason D. Serrano, Brad Peyton, Christine A. Coverdale, Michael C. Jones, Brent M. Jones, *Sandia Report*, **2010**, SAND2010-0833, 1-56.

[22] "Z pinch-generated X-rays demonstrate potential for indirect-drive ICF experiments", T. W. L. Sanford, R. E. Olson, R. L. Bowers, G. A. Chandler, M. S. Derzon, D. E. Hebron, R. J. Leeper, R. C. Mock, T. J. Nash, D. L. Peterson, L. E. Ruggles, W. W. Simpson, K. W. Struve, and R. A. Vesey, *Phys. Rev. Lett.*, **1999**, *83*, 5511–5514.

[23] "EBW1: A Computer code for the prediction of the behaviour of electrical circuits containing exploding wire elements", T. J. Tucker and R. P. Toth, Report SAND -75-0041, Sandia Laboratories, **1975**, *15*, 1-85.

[24] "Metals during rapid heating by dense currents", S. V. Lebedev and A. I. Savvatimskii, *Sov. Phys. Usp.*, Oct. **1984**, *27*, *10*, 749-771. http://dx.doi.org/10.1070/PU1984v027n10ABEH004128

[25] "Temporal evolution of the hydrodynamic instability of the boundary between the dense core and the plasma corona during nanosecond explosion of wires", S. Y. Gus'kov, G. V. Ivanenkov, A.R. Mingaleev *et al.*, *JETP Lett.*, **1998**, *67*, 559–566. https://doi.org/10.1134/1.567726

[26] "Study of the core-corona structure formed during the explosion of an aluminum wire in vacuum", S. I. Tkachenko, A.R. Mingaleev, S. A. Pikuz *et al.*, *Plasma Phys. Rep.*, **2012,** *38*, 1–11. https://doi.org/10.1134/S1063780X11120105

[27] "Thermodynamical calculation of metal heating in nanosecond exploding wire and foil experiments", G. S. Sarkisov, S. E. Rosenthal and K. W. Struve, *Rev. Sci. Instrum*., **2007**, *78*, *043505*, 1-5.

[28] "Distribution of Matter in the Current Carrying Plasma and Dense Core of the Discharge Channel Formed upon Electrical Wire Explosion", S. I. Tkachenko, A. R. Mingaleev, V. M. Romanova, A. E. Ter-Oganes'yan, T. A. Shelkovenko, S. A. Pikuz, *Plasma Phys. Rep.*, **2009**, *35*, 734-753.

[29] "Experimental study to investigate effect of thermophysical properties of various metals on electrical explosion of wire in air and vacuum", Jigyasa Batra, Alok K. Saxena, Ashutosh C. Jaiswar, Rajashri R. Valvi, K.D. Joshi and T.C. Kaushik; *IEEE Trans. Plasma Sci*., **2021**, *49, 9*, 2866-2877. doi: 10.1109/TPS.2021.3099899.

[30] "Dynamics of phase transitions at electrical explosion of wire", S. I. Tkachenko and N. I. Kuskova, *J. Phys.: Condens. Matter,* **1999**, *11*, *10,* 2223–2232.

[31] "Wire explosion in vacuum: Simulation of a striation appearance", V.I. Oreshkin, R.B. Baksht, N.A. Ratakhin, and A.V. Shishlov, *Phys. Plasmas*, **2004**, *11*, *10*, 4771-4776.

[32] "Electrical resistivity model of metals", T. J. Burgess, presented at the *4th International Conference on Megagauss Magnetic Field Generation and Related Topics,* Santa Fe, NM, USA, **1986**, 307-317.

[33] "Electric explosion of wires as a method for preparation of nanopowders", Yu. A. Kotov, *J. Nanopart. Res.*, **2003,** *5*, 539-550.

[34] "Exploding wire research 1774-1963", J. R. McGrawth, U.S NRL, Washington, DC, USA, NRL Memo. Rep. 1698, **1966,** 1-17.

[35] "Equilibrium Characteristics of a Pinched Gas Discharge Cooled by Bremsstrahlung Radiation", R. S. Pease, *Proc. Phys. Soc. Lond. Section B,* **1957,** *70*, *11*, 11-23.

[36] "A simple derivation of the Pease-Braginskii current", Nino R. Pereira, *Phys. Fluids B: Plasma Physics,* **1990**, *2*, *3*, 677-678.

[37] "Exploding Wires as a Source of X-Rays", I. M. Vitkovitsky, P. P. Bey, W. R. Faust, R. Fulper, G. E. Leavitt, J. D. Shipman, **1962,** In: W. G. Chace, H. K. Moore (eds) *Exploding Wires*. Springer, Boston, MA. **DOI:** https://doi.org/10.1007/978-1-4684-7505-0_8.

[38] "Exploding Wires Vol. 2", W. G. Chace and H. K. Moore, **1962,** *1st ed.,* New York, NY, USA: Plenum. (Collected papers of the second conference on Exploding wire phenomenon, Boston, 1961)

[39] "Exploding Wires Vol. 1", W. G. Chace and H. K. Moore, **1959,** *1st ed.,* New York, NY, USA: Plenum. (Collected papers of the conference on Exploding wire phenomenon, Boston, 1959)

[40] "Exploding Wires Vol. 3", W. G. Chace and H. K. Moore, **1964,** *1st ed.,* New York, NY, USA: Plenum. (Collected papers of the third conference on Exploding wire phenomenon, Boston, 1964)

[41] "Exploding Wires Vol. 4", W. G. Chace and H. K. Moore, **1968,** *1st ed.,* New York, NY, USA: Plenum. (Collected papers of the fourth conference on Exploding wire phenomenon, Boston, 1967)

[42] "A Bibliography of the Electrically Exploded Conductor Phenomenon", W. G. Chace, E. M. Watson, *Air Force Cambridge Research Laboratories*, **1967**, *Special Reports, Fourth Edition*, *68,* AFCRL.67.0556.

[43] "Classification of wire explosions", W. G. Chace and M. A. Levine, *J. Appl. Phys.*, **1960,** *31, 7,* 1298.

[44] "Liquid Behavior of Exploding Wires", W.G. Chace, *Phys. Fluids,* **1959,** *2*, 230-235.

[45] "Phase explosion of a metastable fluid", M. M. Martynyuk, *Combust. Explos. Shock Waves,* **1997,** *13***,** *2*, 178–191. doi:10.1007/BF00754998.

[46] "X-radiation from high-energy-density exploded-wire discharges," D. Mosher, S. J. Stephanakis, I. M. Vitkovitsky, C. M. Dozier, L. S. Levine, and D. J. Nagel, *Appl. Phys. Lett.*, **1973** *23*, *8*, 429–430.

[47] "Effect of Wire Parameters on the Emission of Hard X-Rays from Exploding Wires", B. Stenerhag, S. K. Händel, and B. Göhle, *J. Appl. Phys.* , **1971,** *42*, *5*, 1876-1882. https://doi.org/10.1063/1.1660461.

[48] "Use of action integral in EW studies", G. W. Anderson and F. W. Neilson, *Sandia Corporation*, **1959,** *SCR-94,* 1-13**.** ; https://www.osti.gov/servlets/purl/4230868

[49] "The electrical behavior of fine wires exploded by a coaxial cable discharge system", T. J. Tucker and F. W. Neilson, in "*Exploding Wires Vol. 1*", W. G. Chace and H. K. Moore, **1959,** New York, NY, USA: Plenum, 73–81.

[50] "The integral of specific current action and the specific energy input under fast electrical explosion", L. I. Chemezova, G. A. Mesyats, V. S. Sedoi, B. N. Semin, and V. V. Valevich, in *Proc. ISDEIV: IEEE 18th Int. Symp. Discharges Elect. Insul. Vac.*, Eindhoven, The Netherlands, August 17-21 **1998**, 48–51. [Online Available: https://ieeexplore.ieee.org/document/740570]

[51] "A computational model of exploding metallic fuses for multimegajoule Switching", Irvin R. Lindemuth, John H. Brownell, Arthur E. Greene, George H. Nickel, Thomas A. Oliphant et al., *J. Appl. Phys.*, **1985,** *57*, 4447-4460. doi: 10.1063/1.334569.

[52] "Vaporization waves as a general property of high temperature matter," F. D. Bennett, *Phys. Fluids*, **1965,** *8*, *8*, 1425–1427.

[53] "Evaporation of metals by high-density (10^7A· cm^{-2}) electrical currents," A. D. Rakhel, *Int. J. Thermophys.*, **1996,** *17, 5*, 1011–1024.

[54] "The current density and the specific energy input in fast electrical explosion," V. S. Sedoi, G. A. Mesyats, V. I. Oreshkin, V. V. Valevich and L. I. Chemezova in *IEEE Trans. Plasma Sci.*, **1999,** *27*, *4*, 845-850.

[55] "The nucleation mechanism of wire explosion", S. I. Tkachenko, V. S. Vorob'ev, and S. P. Malyshenko, *J. Phys. D: Appl. Phys.*, **2004**, *37*, *3*, 495-500.

[56] "A review of the dense Z-pinch", M. G. Haines, *Plasma Phys. Control. Fusion* **2011**, *53, 9, 093001*, 1-168. doi: 10.1088/0741-3335/53/9/093001

[57] “Universal diagram for regimes of *Z*-pinch stability”, M. G. Haines and M. Coppins, *Phys. Rev. Lett.*, **1991,** *66*, *11*, 1462-1465.

[58] “Resistive stability of the z-pinch revisited”, M. Coppins and I. D. Culverwell, **1997,** *Dense Z-pinches: AIP Conf. Proc. 409:1,* 589-592. https://doi.org/10.1063/1.53928

[59] “MHD instabilities developing in a conductor exploding in the skin effect mode”, V. I. Oreshkin, S. A. Chaikovsky, I. M. Datsko, N. A. Labetskaya, G. A. Mesyats, E. V. Oreshkin, N. A. Ratakhin, and D. V. Rybka, *Phys. Plasmas*, **2016**, *23*, 122107-1-8.

[60] “Observation of a stable dense core within an unstable coronal plasma in wire-initiated dense *Z*-pinch experiments”, D. H. Kalantar and D. A. Hammer, *Phys. Rev. Lett.*, **1993,** *71, 23*, 3806-3809.

[61] “Temporal evolution of the hydrodynamic instability of the boundary between the dense core and the plasma corona during nanosecond explosion of wires”, S. Y. Gus’kov, G. V. Ivanenkov, A. R. Mingaleev et al., *JETP Lett.*, **1998**, *67*, 559–566. https://doi.org/10.1134/1.567726

[62] “Dynamics of thin exploded-wire plasma with a cold dense core”, G.V. Ivanenkov, A. R. Mingaleev, S. A. Pikuz *et al.*, *J. Exp. Theor. Phys.*, **1998**, *87*, 663–671. https://doi.org/10.1134/1.558708.

[63] “Multiphase Foamlike Structure of Exploding Wire Cores”, S. A. Pikuz, T. A. Shelkovenko, D. B. Sinars, J. B. Greenly, Y. S. Dimant, and D. A. Hammer, *Phys. Rev. Lett.*, **1999**, *83*, 4313-4316.

[64] “Exploding aluminum wire expansion rate with 1–4.5 kA per wire”, D. B. Sinars, T. A. Shelkovenko, S. A. Pikuz, J. B. Greenly, and D. A. Hammer, *Phys. Plasmas*, **2000**, *7*, 1555-1563. https://doi.org/10.1063/1.873975.

[65] “Experiments measuring the initial energy deposition, expansion rates and morphology of exploding wires with about 1 kA/wire”, D. B. Sinars, Min Hu, K. M. Chandler, T. A. Shelkovenko, S. A. Pikuz, J. B. Greenly, D. A. Hammer, *and* B. R. Kusse, *Phys. Plasmas,* **2001**, *8*, *1*, 216-230. https://doi.org/10.1063/1.1323759

[66] “Analysis of the discharge channel structure upon nanosecond electrical explosion of wires”, S. I. Tkachenko, D. V. Barishpoltsev, G. V. Ivanenkov, V. M. Romanova, A. E. Ter-Oganesyan, A. R. Mingaleev, T. A. Shelkovenko, and S. A. Pikuz, *Phys. Plasmas*, **2007,** *14, 123502*, 1-10.

[67] “Electric explosion of fine wires: Three group of materials”, V.M. Romanova, G.V. Ivanenkov, A.R. Mingaleev, A.E. Ter-Oganesyan, T.A. Shelkovenko, S.A. Pikuz, *Plasma Phys. Rep*., **2015,** *41*, *8*, 617–636.

[68] “Core structure and secondary breakdown of an exploding wire in the current-pause regime”, V. M. Romanova, A. R. Mingaleev, A. E. Ter-Oganesyan, T. A. Shelkovenko, G. V. Ivanenkov, and S. A. Pikuz, *Matter Radiat. Extremes,* **2019**, *4, 2,* 026401-1-9. https://doi.org/10.1063/1.5085487.

[69] “Factors affecting energy deposition and expansion in single wire low current experiments”, P. U. Duselis, J. A. Vaughan, and B. R. Kusse, *Phys. Plasmas,* **2004**, *11, 8,* 4025-4031.

[70] Effect of current rate on energy deposition into exploding metal wires in vacuum”, G. S. Sarkisov, K. W. Struve and D. H. McDaniel, *Phys. plasmas,* **2004**, *11, 10,* 4573-4581.

[71] "Polarity effect for exploding wire in a vacuum", G. S. Sarkisov, P. V. Sasorov, K. W. Struve, D. H. McDaniel, A. N. Gribov, and G. M. Oleinik, *Phys. Rev.* E, **2002,** *66*, 046413-1-6.

[72] "The effect of insulating coatings on exploding wire plasma formation", D. B. Sinars, T. A. Shelkovenko, S. A. Pikuz, Min Hu, V. M. Romanova, K. M. Chandler, J. B. Greenly, D. A. Hammer, and B. R. Kusse, *Phys. Plasmas*, **2000**, *7, 2*, 429-432.

[73] "Experimental investigations on specific energy deposition and burst characteristics in electrically exploded single copper wires," J. Batra, A. C. Jaiswar, R. Valvi, and T. C. Kaushik, *IEEE Trans. Plasma Sci.*, **2019**, *47, 1*, 596–602.

[74] "Temporal shock wave analysis produced by copper exploding wires in air at atmospheric pressure", M. Barbaglia and G. R. Prieto, *Phys. Plasmas*, **2016,** *23*, 102706-1-5.

[75] "Visualization of copper wire explosion in atmospheric pressure air", J. Jadidian, S. Mohseni, M. Jebeli-Javan, E. Hashemi, A. A. Shayegani, K. Niayesh, *IEEE Trans. Plasma Sci.*, **2011**, *39, 11*, 2842 – 2843.

[76] "Interpreting experimental data on the electric explosion of thin wires in air", S. A. Pikuz, S. I. Tkachenko, D. V. Barishpol'tsev, G. V. Ivanenkov, A. R. Mingaleev, V. M. Romanova, A. E. Ter-Oganes'yan, T. A. Shelkovenko, *Tech. Phys. Lett.*, **2007**, *33,* 8, 651–654.

[77] "Electrical characteristics of microsecond electrical explosion of Cu wires in air under various parameters", G. Yin, X. Li, and S. Jia, *IEEE Trans. Plasma Sci.*, **2018**, *46,* 4, 972-981.

[78] "Experimental Study on Critical Length of Electrically Exploding Wire", Jigyasa Batra, Ashutosh Jaiswar and T. C. Kaushik, *32nd National Symposium on Plasma Science & Technology,* Gandhinagar, India, November 7-10, **2017**, 284.

[79] "Numerical calculations of the current specific action integral at the electrical explosion of wires", V. I. Oreshkin, S. A. Barengol'ts, S. A. Chaikovsky, *Tech. Phys.*, **2007**, *52*, 5, 642-650.

[80] "Experimental and Numerical Analysis of Post Burst Dynamics in Electrically Exploding Single Copper Wire", Jigyasa Batra, Alok K. Saxena, Ashutosh C. Jaiswar, Rajashri Valvi and Trilok C. Kaushik, *IEEE Trans. Plasma Sci.*, **2020**, *48,* 6, 2187-2194.

[81] "Multi frame synchrotron radiography of pulsed power driven underwater single wire explosions", D. Yanuka, A. Rososhek, S. Theocharous, S. N. Bland, Y. E. Krasik, M. P. Olbinado, and A. Rac, *J. Appl. Phys.*, **2018**, *124*, 153301-1-9.

[82] "Electrical Exploding Nickel and Tungsten Wires in Air and Water", G. B. Vunni, *Army Research Laboratory Report*, **2009**, *ARL-CR- 619*, U.S, 1-22.

[83] "Electrical Explosion of Metal Wires", I. F. Kvarkhtsava, A. A. Pliutto, A. A. Chernov and V.V. Bondarenko, *Sov. Phys. JETP.*, **1956**, *8, 1*, 40-51.

[84] "Joule Energy Deposition in exploding Wire Experiments", G. S. Sarkisov, S. E. Rosenthal, K. W. Struve, D. H McDaniel, E. M. Waisman and P. V. Sasorov, *American Institute of Physics; Dense Z-pinches: 5th International Conference on Dense Z-Pinches*, presented in *14th International Conference on High-Power Particle Beams (BEAMS)*, Albuquerque, NM, USA, June 23-28, **2002**, 213-216.

[85] "Circuit simulation of the behaviour of exploding wires for nano-powder production", Z. Mao, X. Zou, X. Wang, X. Liu and W. Jiang, *Laser Part. Beams*, **2009**, *27*, 49-55.

[86] "Study of X-pinch dynamics using a low current (25 kA) and slower current (400 ns) pulse", G. W. Collins IV, M. P. Valdivia, T. Zick, R. E. Madden, M. G. Haines, and F. N. Beg, *Phys. Plasmas*, **2013**, *20*, 042704-1-9.

[87] "Warm-dense-matter studies using pulse-powered wire discharges in water", T. Saski, Y. Yano, M. Nakajima, T. Kawamura, & K. Horioka, *Laser Part. Beams*, **2006**, *24, 3*, 371-380. doi:10.1017/S0263034606060538.

[88] "Simple high-performance exploding wire opening switch," B. M. Novac, I. R. Smith, P. Sarkar, and G. Louverdis, presented at the *16th IEEE Int. Pulsed Power Conf.*, Albuquerque, NM, June 17-22, **2007**, 1004-1007. [Online Available: https://ieeexplore.ieee.org/document/4652359].

[89] "Measurement Techniques in Pulsed Discharges", D.C. Pande, **2010**, In: Pulsed Power School Lecture Book *"Pulse Power Technology; Theme: Pulsed Electron Beams and Their Applications"*, by *Power Beam Society of India*, Bhabha Atomic Research Center, Mumbai, India, 244.

[90] "Foundations of Pulsed Power Technology", Jane Lehr and Pralhad Ron, **2017,** *1st ed.*, The Institute of Electrical and Electronics Engineers, New York, USA: John Wiley & Sons, Chapter 10, 493-545.

[91] "Coaxial capacitive voltage divider with high division ratio for high voltage pulses with very fast rise times", T. Hobejogi and J. Biela, *2011 IEEE Pulsed Power Conference*, Chicago, IL, June 19-23, **2011**, 313-318, doi: 10.1109/PPC.2011.6191436.

[92] "Introduction to High Power Pulsed Technology", S.T. Pai, Q.I. Jhang, *Advanced Series in Electrical and Computer Engineering - Vol. 10*, Singapore: World Scientific Publishing Co. Pte. Ltd, **1995,** 279-285.

[93] "Investigations on slow current driven X-pinch as soft X-ray source for radiographic applications", S.C. Andola, J. Batra, A.C. Jaiswar, A.K. Saxena, T.C. Kaushik, *High Energy Density Physics*, **2020**, 35, 100732, https://doi.org/10.1016/j.hedp.2019.100732-1-7.

[94] "X-ray interactions, photo absorption, scattering, transmission, and reflection at E= 50-30,000 eV, Z= 1-92", B.L. Henke, E.M. Gullikson, J.C. Davis, *At. Data Nucl. Data Tables*, **1993**, 54, 181–342.

[95] "X-pinch. Part I", S. A. Pikuz, T. A. Shelkovenko and D. A. Hammer, *Plasma Phys. Rep.*, **2015**, 41, *4*, 291–342.

[96] "Interferometer for Electron Density Measurement in Exploding Wire Plasmas", Jigyasa Batra, Ashutosh Jaiswar and T.C Kaushik, BARC/2016/E/018, BARC Report **2016**, 1-31**.**

[97] "Abel inversion of a holographic interferogram for determination of the density profile of a sheared-flow Z pinch", S. L. Jacksona and U. Shumlak, *Rev. Sci. Ins.*, **2006**, 77, 083502-1-10.

[98] "Low and high energy deuterium ions emission in a 4.7 kJ plasma focus device and its variation with gas filling pressure", Jigyasa Batra, Ashutosh Jaiswar, Rohit Srivastava, Ram Niranjan, R.K. Rout and T.C Kaushik, *Indian J Pure Ap Phy*, **2014**, 52, 246-250.

[99] "Shock experiments and numerical simulations on low energy portable electrically exploding foil accelerators", A. K. Saxena, T. C. Kaushik and S. C. Gupta, *Rev. Sci. Instrum.*, **2010,** *81*, 033508-1-9.

[100] "An analytical formulation of equation of state", D. J. McCloskey, Report RM-3905-PR, Rand Corp., Santa Monica, CA, USA, **1964,** 1-106.

[101] "Semiempirical wide-range conductivity model with exploding wire verification", J. Stephens, J, Dickens and A. Neuber, **2014,** *Phys. Rev. E*, *89*, *5*, 053102-1-5.

[102] "Difference methods for initial value problems", R. D. Richtmyer and K.W. Morton **1967,** 2nd ed., New York: Interscience.

[103] "A Method for the Numerical Calculation of Hydrodynamic Shocks", J. VonNeumann and R.D. Richtmyer, *J. Appl. Phys.*, **1950**, *21*, 232-237.

[104] "Numerical study of the impedance mismatch effect in laser irradiated layered targets", T. C. Kaushik and B. K. Godwal, *J. Appl. Phys.,* **1988,** *64*, *10*, 4889-4895.

[105] "Underwater Electrical Wire Explosion and Its Applications", Yakov E. Krasik, Alon Grinenko, Arkady Sayapin, Sergey Efimov, Alexander Fedotov, Viktor Z. Gurovich, Vladimir I. Oreshkin, *IEEE Trans. Plasma Sci.,***2008**, *36*, *2*, 423-434.

[106] "Temporal distribution of the electrical energy on an exploding wire", G. Rodriguez Prieto, L. Bilbao and M. Milanese, *Laser Part. Beams*, **2016**, *34*, 263-269.

[107] "A comparative study of exploding wires in air and water," H. D. Edelson and T. Korneff, *J. Appl. Phys.*, **1966**, *37*, *5*, 2166–2168.

[108] "Review of effects of dielectric coatings on electrical exploding wires and *Z* pinches," J. Wu, X. Li, M. Li, Y. Li, and A. Qiu, *J. Phys. D: Appl. Phys.*, **2017**, *50*, *40*, 1–15.

[109] “High-temperature exploding wires,” F. D. Bennett, In: *Progress in High Temperature Physics and Chemistry Vol. 1*, C. A. Rouse, **1969**, *1st ed.*, Ed. London, U.K.: Pergamon Press.2–63.

[110] “Prediction of conditions for a single pulse discharge,” P. M. Sherman, *J. Appl. Phys.*, **1977**, *48*, *1*, 143–144.

[111] “Characteristics of a magnetic energy storage system using exploding foils,” J. N. DiMarco and L. C. Burkhardt, *J. Appl. Phys.*, **1970**, *41*, *9*, 3894–3899.

[112] “The Relationship Between Exploding Wire Expansion Rates and Wire Material Properties Near the Boiling Temperature”, K. M. Chandler, D. A. Hammer, D. B. Sinars, S. A. Pikuz, and T. A. Shelkovenko, *IEEE Trans. Plasma Sci.*, **2002**, *30*, *2*, 577-587.

[113] “Web Elements”, Mark Winter, The University of Sheffield, **1993**, U.K. Available online: https://www.webelements.com/.

[114] “LASL Shock Hugoniot Data”, S. P. Marsh, University of California Press, London, **1980**, U.K..

[115] “CODATA Key Values for Thermodynamics”, J. D. Cox, D. D. Wagman, and V. A. Medvedev, **1989,** Hemisphere Publishing Corp., New York. Available online: http://www.codata.info/resources/databases/key1.html

[116] “Current Shunting and Formation of Stationary Shock Waves during Electric Explosions of Metal Wires in Air”, G.V. Ivanenkov, S. Yu. Gus’kov, and D.V. barishpol’tsev, *Plasma Phys. Rep.*, **2010**, *36*, *1*, 67-76.

[117] “Experimental investigations on energy deposition and morphology of exploding aluminum wires in argon gas", Haoyu Liu, Junping Zhao, Zhicheng Wu, Lisong Zhang, and Qiaogen Zhang, *J. Appl. Phys.*, **2019**, *125*, 103301-1-13.

[118] "Sound Velocities at High Pressure and Temperature and Their Geophysical Implications", S. Duffy Thomas, and J. Ahrens Thomas, *J. Geophys. Res.*, **1992,** *97, B4*, 4503-4520.

[119] "X-pinch dynamics: Neck formation and implosion", V. I. Oreshkin, S. A. Chaikovsky, A. P. Artyomov, N. A. Labetskaya, A. V. Fedunin, A. G. Rousskikh, and A. S. Zhigalin, *Phys. Plasmas*, **2014**, *21*, 102711-1-9.

[120] https://henke.lbl.gov/optical_constants/filter2.html

[121] "Strata formation at fast electrical explosion of cylindrical conductors", V. I. Oreshkin, K. V. Khishchenko, P. R. Levashov, A. G. Rousskikh and S. A. Chaikovskii, *High Temp.*, **2012**, *50*, 584-595.

[122] "The effect of the metal phase state on the growth of thermal instabilities in an electrically exploding conductor", V. I. Oreshkin, K. V. Khishchenko, E. V. Oreshkin and A. G. Rousskikh, *Plasma Res. Express, **2019**, 1, 3, 035006-1-14.*